Structure and Stable Isotopic Biogeochemistry of Organic Sulfur in the Geosphere: Application of Bulk and Compound-Specific Sulfur Isotope Analysis to Modern and Ancient Euxinic Systems

by

Molly Darlene O'Beirne

BSci Chemistry – Biochemistry, Bemidji State University, 2009

MSci Water Resources Science – Limnology and Oceanography, University of Minnesota, 2013

Submitted to the Graduate Faculty of

the Dietrich School of Arts and Sciences in partial fulfillment

of the requirements for the degree of

Doctor of Philosophy

University of Pittsburgh

2018

UNIVERSITY OF PITTSBURGH

DIETRICH SCHOOL OF ARTS AND SCIENCES

This dissertation was presented

by

Molly Darlene O'Beirne

It was defended on

November 30, 2018

and approved by

Charles E. Jones, Senior Lecturer, Department of Geology and Environmental Science, University of Pittsburgh

Emily M. Elliott, Associate Professor, Department of Geology and Environmental Science, University of Pittsburgh

Daniel J. Bain, Assistant Professor, Department of Geology and Environmental Science, University of Pittsburgh

William P. Gilhooly III, Associate Professor, Department of Earth Sciences, Indiana University-Purdue University Indianapolis

Dissertation Director: Josef P. Werne, Professor, Department of Geology and Environmental Science, University of Pittsburgh

Structure and Stable Isotopic Biogeochemistry of Organic Sulfur in the Geosphere: Application of Bulk and Compound-Specific Sulfur Isotope Analysis to Modern and Ancient Euxinic Systems

Molly Darlene O'Beirne, PhD

University of Pittsburgh, 2018

Organic sulfur (OS) is the second largest pool of reduced sulfur in the environment after pyrite and is a topic of interest as it has considerable connections to petroleum formation; the global biogeochemical cycles of sulfur, carbon, oxygen, and iron; microbial activity; and organic matter preservation through geologic time. Despite these connections, our understanding of OS formation and occurrence is limited and therefore, interpretations of the geologic record based on changes in the relative abundances of inorganic, organic, and elemental sulfur are also limited. The research presented here is one of the first to use measured variations in the stable sulfur isotope composition ($\delta^{34}S$) of inorganic sulfur species and OS (at the bulk and molecular level) to investigate OS formation on multiple timescales in both the laboratory and natural environment. Results of this research are multifold.

First, we demonstrate the ability to measure polysulfide speciation via gas chromatography (GC) at sub-micromolar levels and with good precision in both laboratory and environmental samples. With a bit more refinement, our method of analysis can be used for direct compound-specific sulfur isotope analysis (CSSIA) of individual polysulfide species using a GC coupled to a multi-collector ICP-MS (GC/MC-ICP-MS). Such measurements could provide valuable information on the role polysulfides play in the natural environment.

Second, detailed structural (i.e. FT-IR and online pyrolysis) and $\delta^{34}S$ analysis of reaction products from laboratory experiments involving the abiotic sulfurization of carbohydrates and natural dissolved organic matter provides experimental evidence for the structural and sulfur isotopic relationships between reactive inorganic sulfur species and OS in the geosphere.

Lastly, we show the utility of paired pyrite and OS isotope records in reconstructing paleoenvironmental conditions. $\delta^{34}S$ values of pyrite and OS from the Jurassic aged Blackstone Band of the Kimmeridge Clay Formation display dynamic fluctuations that are related to variations in microbial sulfate reduction rates, which may be influenced by the formation of macromolecular OS during times of increased organic carbon burial. CSSIA of bitumen and kerogen-pyrolysates reveals more complex dynamics, where bitumen compounds record a sulfur source unrelated to bulk OS and kerogen compounds reflect the $\delta^{34}S$ of bulk OS.

Table of Contents

List of Tables

List of Figures

List of Equations

1.0 Introduction to Organic Sulfur Occurrence and Sulfur Isotope Systematics

1.1 Introduction

Organic sulfur is a topic of great interest as it has considerable connections to petroleum formation; the global biogeochemical cycles of sulfur, carbon, oxygen, and iron; microbial activity; and organic matter preservation through geologic time. In fact, organic sulfur is the second largest pool of reduced sulfur in the environment after pyrite. Despite its relevance, our understanding of organic sulfur formation and occurrence is limited and therefore, interpretations of the geologic record based on changes in the relative abundances of inorganic, organic, and elemental sulfur are limited. The limitations associated with the organic sulfur record stem from both the wide variety of organic sulfur compounds (OSC) found in the environment, as well as the complexity of biological and abiological sulfur cycling which include a number of reactive sulfur intermediates (readily formed via oxidation and reduction reactions) with valence states ranging from +6 to -2.

Reactive sulfur intermediates (e.g. bisulfides, polysulfides, elemental sulfur, thiosulfate, polythionates, and sulfite) are incorporated into organic compounds via a range of mechanisms, leading to myriad OSC being formed in the natural environment. For instance, after initial sulfur attack and S-C bond formation the resulting thiol (in the case of bisulfide sulfurization) or dianion (in the case of polysulfide sulfurization), may undergo additional reaction with another functional group on the same molecule, forming a ring (intramolecular addition), or on a different molecule, forming a (poly)sulfide bridge (intermolecular addition). In fact, more than 1500 novel OSC were identified during the 1980s alone and their geochemical significance has been previously discussed (see Sinninghe Damsté and de Leeuw 1990 for a thorough review).

Currently, it is uncertain whether the sulfur that is incorporated into organic compounds is derived from pore-water sulfide, some other pool of reduced sulfur, such as polysulfides or elemental sulfur, or a mixture of different sources. Likewise, the timing of formation of OSC remains unclear

– whether they are formed in the water column, at the sediment-water interface, in the uppermost sediments, or on longer timescales. Different types of OSC are likely formed on varying timescales and via different sulfur intermediates – characterizing such intricacies has the potential to lead to far richer interpretations of (paleo)environmental conditions and nutrient cycling dynamics. Yet, traditional bulk measurements of organic and inorganic sulfur species do not provide sufficient detail to distinguish specific mechanisms and pathways of formation of OSC. One way to disentangle these complexities is by measuring variations in stable sulfur isotope compositions (i.e. $^{34}S/^{32}S$ ratios, expressed as $\delta^{34}S$ values, see section 1.2 below) at the molecular level. Recent technological advances, specifically the coupling of a gas chromatograph (GC) to a multicollector inductively coupled plasma mass spectrometer (MC-ICP-MS), have made the measurement of compound specific $\delta^{34}S$ values possible with great precision and at natural abundance (Amrani et al. 2009).

The overarching goal of this dissertation is to develop an interpretive framework for the organic sulfur record, as well as to discuss implications for the evolution of the Earth and connected biogeochemical systems. In order to accomplish this rather daunting task, bulk measurements of the stable sulfur isotope compositions of organic and inorganic sulfur species were made in conjunction with compound specific sulfur isotope measurements from the same sample(s). Analyses include measurements of bulk and compound-specific stable sulfur isotopes from laboratory sulfurized organic compounds (i.e. glucose and dissolved organic matter), as well as the Jurassic aged Blackstone Band of the Kimmeridge Clay Formation.

1.1.1 The global sulfur cycle

Sulfur, being a period three/group sixteen element, has a valence electron structure of $3s^2\ 3p^4$. Accordingly, sulfur will occur in +6 and -2 oxidation states. In addition to S^{6+} and S^{2-}, sulfur also occurs as S^{4+}, S^{2+}, and S^0.[a] Transformations among the many oxidation states of sulfur, commonly

[a] Although balanced reactions can be written in terms of the monomer, S^0, in reality the sulfur reactant is S_8. Individual sulfur atoms, represented as S^0, do not exist practically in aqueous solutions. Elemental sulfur is normally

microbially mediated, drive the global S cycle. The global cycle of sulfur can be regarded as having two primary components – geologic and biologic, in which sulfur influences the oxidation state of systems and interacts with the biogeochemical cycling of other elements such as C, O, and Fe.

1.1.1.1 Geologic cycle

Geologic cycling of sulfur consists of the transfer of sulfur from the mantle to the Earth's surface and oceans. The atmosphere, although characterized by large fluxes of sulfur, does not have a major impact on the long-term cycle of sulfur, as no sulfur gas is a long-lived or major constituent of the atmosphere. There are three significant long-term pathways involved in the transfer of sulfur from the Earth's mantle, including (1) volcanic outgassing of SO_2 and H_2S, (2) release of H_2S during hydrothermal circulation, and (3) the weathering of igneous sulfides during the hydrothermal circulation of oxic seawater. The dominant reservoirs of sulfur on Earth's surface are as sulfide (e.g. pyrite – FeS_2) and sulfate (e.g. gypsum – $CaSO_4 \cdot 2H_2O$) minerals in various sedimentary rocks. These sulfide and sulfate minerals are then weathered on land and eventually delivered to the oceans in the form of the sulfate ion (SO_4^{2-}). Upon reaching the oceans sulfate may be formed into sulfide during sulfate reduction, or precipitated in evaporite basins. Sulfate concentration in the ocean thus reflects a balance between incoming (source) sulfate and the burial (sink) of reduced sulfur in sediments as mineral sulfides (i.e. pyrite) and to a lesser extent organic sulfur and the deposition of sulfate as marine evaporites. The subduction of sediments containing sulfide and sulfate represent return fluxes back into the mantle. The rates of exchange and therefore balance between the mantle, surface environment, and ocean reservoirs fix the size of the global sulfur inventory – their dynamics and magnitudes have changed throughout geologic time.

1.1.1.2 Biologic cycle

Over geological timescales, biogeochemical cycling of sulfur is closely tied to the redox state of the Earth through the burial of oxidized (sulfate) and reduced (sulfide) sulfur species. Microbial metabolic processes (e.g. sulfate reduction, disproportionation, and sulfide oxidation; Table 1) play

---

orthorhombic α-S_8 in most natural and laboratory environments. IUPAC nomenclature is octathiocane, but elemental sulfur is also informally referred to as octasulfur, cyclo-S_8, and/or cyclooctaatomic sulfur.

an intimate role in this cycle by regulating the oxidation state of sulfur. These metabolic processes have distinct sulfur isotope fractionations (discussed in section 1.2.1.2), that are recorded in the geologic record as the stable sulfur isotopic offset between sulfur-bearing phases – predominantly sulfate minerals and sulfides, particularly pyrite. Thus, the sulfur isotopic records of sulfate and pyrite are often used to reconstruct ocean chemistry at the time of deposition, constrain the activity of sulfur metabolizing organisms, as well as to determine diagenetic processes in marine depositional environments (Claypool et al. 1980, Canfield and Teske 1996, Canfield 2004, Johnston et al. 2005, Fike et al. 2006, Gill et al. 2007, Fike and Grotzinger, 2008, Hurtgen et al. 2009, Halevy et al. 2012, Jones and Fike 2013, Leavitt et al. 2013).

Ultimately, sulfide is formed from sulfate either by assimilatory sulfate reduction (anabolism – formation of sulfur-containing amino acids) or through dissimilatory sulfate reduction (catabolism – energy gain). Assimilatory sulfate reduction is a unidirectional process that requires energy to transport sulfate across the cell membrane, reduce sulfate to sulfide and then incorporates this sulfide into principal organic sulfur compounds within the cell (e.g. amino acids and proteins). Dissimilatory sulfate reduction (or microbial sulfate reduction – MSR) is conducted by a large group of bacteria and archaea that have a broad ecological tolerance. Collectively these microorganisms are referred to as sulfate reducers. Sulfate reducers gain energy for their growth by catalyzing exergonic chemical reactions in which organic carbon or hydrogen is oxidized, while sulfate is reduced. In coastal marine sediments 90% or more of the sulfide produced via MSR is re-oxidized to sulfate (Canfield and Teske 1996). The pathways of sulfide oxidation are poorly known, but include biological (e.g. phototrophic sulfide oxidation) and abiological (e.g. reactions with oxygen, and Fe and Mn oxides) oxidation to sulfate and other intermediate compounds (Jørgensen 1990, Thamdrup et al. 1994, Fry et al. 1988). Examples of intermediate compounds include sulfite (SO_3^{2-}), elemental sulfur (S_8), thiosulfate ($S_2O_3^{2-}$), and polythionates ($S_xO_y^{2-}$). These intermediate compounds do not generally accumulate in the environment and are instead readily transformed either by common oxidation and reduction reactions or via disproportionation (Canfield et al. 1998). Disproportionation is a specific type of redox reaction in which a species is simultaneously reduced and oxidized to form two different products. In this case, bacteria disproportionate sulfur intermediates directly to sulfide and sulfate without an external electron donor or electron acceptor.

1.1.2 Interactions with the biogeochemical cycles of C, O, and Fe

1.1.2.1 Carbon

As seen in Table 1, the cycles of carbon and sulfur are linked through common metabolic pathways. Anoxygenic phototrophs (i.e. photosynthetic green and purple sulfur bacteria) play an important role in carbon fixation by taking up CO_2 and converting it into biomass (organic matter) during photosynthesis. In some environments, anoxygenic phototrophs contribute up to 83% of total productivity, as is the case in Fayetteville Green Lake, NY, USA. On a global scale, MSR is arguably the most important metabolic pathway coupling the oxidation of organic matter to the production of sulfide and often accounts for one half of total carbon oxidation in coastal marine sediments (Jørgensen and Nelson 2004). Additionally, reactions between organic matter and reduced inorganic sulfur species lead to complex mixtures of low and high molecular weight organic sulfur compounds in the environment. These reactions often result in the formation of macromolecules (organic compounds bound via (poly)sulfide cross-linking) which prevent or at least significantly hinder microbial attack and degradation of labile organic matter. The sulfurization of organic matter thereby acts as a preservation mechanism (net sink) of carbon – an important process during times of widespread oceanic anoxia or euxinia (i.e. anoxic and sulfidic) in Earth's history.

Table 1. Important microbial sulfur metabolisms

$\mathbf{SO_4^{2-} + 2CH_2O \rightarrow H_2S + 2HCO_3^-}$	**Sulfate reduction**
$\mathbf{2SO_3^{2-} + 3CH_2O + H^+ \rightarrow 2H_2S + 3HCO_3^-}$	Sulfite reduction
$\mathbf{4S^0 + 4H_2O \rightarrow 3H_2S + SO_4^{2-} + 2H^+}$	Sulfur disproportionation
$\mathbf{4SO_3^{2-} + 2H^+ \rightarrow H_2S + 3SO_4^{2-}}$	Sulfite disproportionation
$\mathbf{S_2O_3^{2-} + H_2O \rightarrow H_2S + SO_4^{2-}}$	Thiosulfate disproportionation
$\mathbf{H_2S + CO_2 \rightarrow CH_2O + H_2O + 2S^0}$	Phototrophic sulfide oxidation to sulfur
$\mathbf{H_2S + 2CO_2 + H_2O \rightarrow 2CH_2O + SO_4^{2-} + 2H^+}$	Phototrophic sulfide oxidation to sulfate
$\mathbf{2S^0 + 3CO_2 + 5H_2O \rightarrow 3CH_2O + 2SO_4^{2-} + 4H^+}$	Phototrophic sulfur oxidation to sulfate

1.1.2.2 Oxygen

Like with carbon, the link between the sulfur and oxygen cycles is made through a series of oxidation-reduction reactions beginning with the production of organic matter and oxygen through photosynthesis. The next reaction that links the cycles is the reduction of sulfate (via sulfate reducers) while oxidizing organic matter and producing hydrogen sulfide (H_2S) as a waste product. Subsequent reaction of H_2S with iron oxides and other iron phases yields pyrite. The net result of pyrite formation and its subsequent burial is an increase in atmospheric oxygen. Likewise, the burial of organic matter equates to net photosynthesis, with a corresponding gain in atmospheric O_2. Thus, the O_2 content of the atmosphere reflects the net burial versus oxidation of both pyrite and organic matter on geologic timescales. By deductive reasoning, if more sulfur is buried as organic sulfur instead of as pyrite, this would change the traditional estimates of atmospheric oxygen concentrations (and CO_2 concentrations), such that past atmospheric concentrations during periods of prolonged organic sulfur burial (e.g. during oceanic anoxic events - OAEs) may have been considerably larger (Werne et al. 2004, Raven et al. 2018).

1.1.2.3 Iron

The iron cycle is inextricably linked to the sulfur cycle via the formation of pyrite (FeS_2) and thereby the cycles of carbon and oxygen. Degree of pyritization (DOP - the ratio of pyrite Fe to reactive Fe) is an iron-based paleoredox proxy for euxinia (Berner 1970, Raiswell et al. 1988, reviewed by Lyons and Severmann 2006). Additionally, the balance between sulfidic (euxinic or H_2S-containing) and ferruginous (Fe^{2+}-containing) anoxic ocean waters during the Proterozoic (2.4 to 0.54 billion years ago) shaped early ocean chemistry and the beginning of life on earth (Canfield 2005, Lyons 2008, Lyons et al. 2009).

1.1.2.4 Chemical equations linking S, C, O, and Fe cycles

Relevant equations are shown below:

<u>PHOTOSYNTHESIS</u>

$CO_2 + H_2O \Leftrightarrow CH_2O + O_2$

<u>PYRITE FORMATION</u>

$$4Fe(OH)_2 + 8SO_4^{2-} + 15CH_2O + O_2 \Leftrightarrow 4FeS_2 + 15\ HCO_3^- + 11H_2O + 5OH^- + 15O_2$$

ORGANIC SULFUR FORMATION

$$SO_4^{2-} + 3CH_2O \Leftrightarrow CH_2S + 2HCO_3^- + H_2O$$

1.2 Sulfur isotope geochemistry

The terrestrial abundances of the four naturally occurring stable isotopes of sulfur, ^{32}S, ^{34}S, ^{33}S, ^{36}S, are 95.04%, 4.20%, 0.75%, and 0.01%, respectively (De Laeter et al. 2003). Stable isotope geochemistry is primarily concerned with the relative partitioning of stable isotopes among substances (i.e. changes in the ratios of isotopes), rather than their absolute abundances. The difference in the partitioning behavior of various isotopes (i.e. fractionation) is due to equilibrium and kinetically controlled physical, chemical, and biological processes. In general, heavier isotopes form more stable bonds and molecules of different masses react at different rates (O'Neil, 1986). In stable isotope studies, the ratio of the less abundant isotope (e.g. ^{34}S or ^{33}S) to the more abundant isotope (e.g. ^{32}S) in a sample is expressed in delta (δ) notation as the deviation in parts per thousand (per mil, ‰) relative to the same ratio in a reference standard, example shown below for $\delta^{34}S$:

$$\delta^{34}S = [(^{34}S/^{32}S_{sample})/(^{34}S/^{32}S_{ref.std.}) - 1] \times 1000\ (‰).$$

Samples with positive $\delta^{34}S$ values have a higher $^{34}S/^{32}S$ ratio than the reference standard, while those with negative $\delta^{34}S$ values have a lower $^{34}S/^{32}S$ ratio than the standard. Historically, the reference standard commonly referred to is sulfur from troilite (FeS) of the Canyon Diablo iron meteorite (CDT). The current agreed upon reference for sulfur is Vienna Canyon Diablo Troilite (VCDT), because CDT has been shown to be isotopically inhomogeneous (Beaudoin et al. 1994).

1.2.1 Isotope fractionation processes.

Two types of fractionation processes are responsible for the naturally occurring sulfur isotope variations[b]: (1) chemical exchange reactions between various inorganic sulfur species resulting in equilibrium isotope distributions, and (2) kinetic isotope effects during microbial processes. Microorganisms have long been known to fractionate isotopes during their sulfur metabolism, particularly during dissimilatory sulfate reduction, which produces the largest fractionations in the sulfur cycle.

1.2.1.1 Equilibrium processes

Equilibrium processes include isotope mixing or isotope exchange reactions that redistribute isotopes among different substances, between phases, or between individual molecules. This process is also referred to as equilibrium isotope distribution. Isotope distributions rely on the properties of the equilibrating substances but do not depend on the particular pathways or mechanisms involved in attaining equilibrium (there is no net reaction). Distributions are related to the effect of atomic mass on bonding, which is to say molecules containing a heavier isotope are more stable than those containing a lighter isotope in a system at equilibrium (Bigeleisen 1965). Temperature also exerts an influence on the vibrational energies of substances. The temperature-dependence of sulfur isotope partitioning between sulfide mineral pairs formed in equilibrium with one another is the basis of sulfur isotope geothermometry, but is not further discussed here (see review by Ohmoto and Rye 1979).

1.2.1.2 Microbial Sulfate Reduction (MSR)

The fractionations associated with sulfur assimilation are small, 0.9 to 2.8‰ (Kaplan and Rittenberg 1964). Dissimilatory MSR yields sulfide that is ^{34}S-depleted relative to the source sulfate. The fractionation imparted during dissimilatory MSR is highly variable, but is commonly between 19‰ and 66‰ with values as low as 2‰ observed in the laboratory (Habicht and

[b] Sulfur mass-independent fractionation (S-MIF), is not considered here as it has only been observed in ancient sediments before the Great Oxidation Event, ca. 2.45 million years ago.

Canfield, 1997, 2001; Detmers et al., 2001; Brüchert et al., 2001; Sim et al., 2011). The magnitude of isotope fractionation depends on the rate of sulfate reduction with the highest fractionation at low rates and the lowest fractionation at high rates. The rates of sulfate reduction are controlled by the availability of dissolved organic compounds (used as an energy source), sulfate concentration, and temperature - insofar as it regulates natural microbial populations and enzymatic kinetics (Kaplan and Rittenberg 1964, Brüchert et al. 2001, Canfield et al. 2006). More recent studies (Sim et al. 2011, Leavitt et al. 2013, Wing and Halevy 2014) found that the type of organic electron donor is essential in controlling the magnitude of sulfur isotope fractionations of pure culture sulfate reducing bacteria, with complex substrates leading to sulfur isotope discrimination exceeding 50‰.

Most sulfide formed in nature is re-oxidized, through light-mediated photosynthetic pathways or through inorganic reactions (e.g. abiological reactions with oxygen, and Fe and Mn oxides). Numerous sulfur intermediate compounds (sulfite, thiosulfate, elemental sulfur, polythionates) may be formed during these processes, and these may be oxidized, reduced, or in many cases disproportionated to sulfide and sulfate (discussed in section 1.1.2). The fractionations associated with microbial sulfide oxidation are generally small (± 5‰) (Fry et al. 1986, Zerkle, 2009), while those associated with microbial disproportionation can be up to 37‰ (Canfield et al. 1998b; Habicht et al., 1998; Cypionka et al. 1998). Thus, it has been suggested that a repeated cycle of sulfide oxidation to sulfur intermediates and subsequent disproportionation is responsible for producing offsets up to 65‰ between the $\delta^{34}S$ values of sulfate and sulfide (Canfield and Thamdrup, 1994).

1.2.1.3 Thermochemical Sulfate Reduction (TSR)

In contrast to MSR, thermochemical sulfate reduction (TSR) is an abiotic process where sulfate is reduced to sulfide via the oxidation of hydrocarbons under the influence of heat (> 100°C) rather than bacteria (Trudinger et al. 1985, Krouse et al. 1988). TSR can alter the $\delta^{34}S$ record of both sulfide and sulfate minerals, and by connection the organic sulfur record, thereby biasing interpretations of paleo-S records. In general, fractionations during TSR are smaller than during MSR. Several studies (e.g. Kiyosu 1980, Kiyosu and Krouse 1993, Amrani et al. 2011) have

reported fractionations of 10–20‰ between the $\delta^{34}S$ values of sulfate and sulfide in the temperature range of 200–100°C in the laboratory and field settings. TSR in oil reservoirs is thought to produce ^{34}S-enriched H_2S close to its parent gypsum or anhydrite $\delta^{34}S$ value (Machel 2001), whereas MSR produces ^{34}S-depleted H_2S (discussed above). It has been suggested that thermally and chemically stable OSC (e.g. dibenzothiophenes) preserve their original, non-TSR-altered $\delta^{34}S$ values (Amrani et al. 2012, Meshoulam et al. 2016, Cai et al. 2016). Such compounds can be used to detect TSR alterations and also provide a unique way to look at sulfur cycling in paleo-records that would otherwise be obscured.

1.2.2 Compound-specific $\delta^{34}S$ analysis

Compound-specific sulfur isotope analysis of sedimentary organic matter is a valuable tool for determining past and ongoing processes, similar to those obtained from other light isotopes (e.g. ^{2}H and ^{13}C). Measuring $\delta^{34}S$ values in individual compounds can help unravel some of the complexities within the dynamic organic-inorganic S cycle, beyond what is obtained from traditional bulk organic sulfur measurements made via Elemental Analysis - Isotope Ratio Mass Spectrometry (EA-IRMS). Recently developed instrumentation and methods, specifically the coupling of a gas chromatograph (GC) to a multicollector inductively coupled plasma mass spectrometer (MC-ICP-MS), have made the measurement of compound specific $\delta^{34}S$ values possible with great precision and at natural abundance (nanomolar concentrations of sulfur; Amrani et al. 2009). This technique has been useful for the analysis of volatile OSC in seawater and associated aerosols (e.g. Amrani et al. 2012, 2013; Said-Ahmad and Amrani 2013), sediment extracts (e.g. Raven et al. 2013), crude oils and rock extracts (e.g. Amrani et al. 2012). For a full review of the development and initial applications of compound-specific $\delta^{34}S$ the reader is referred to Amrani (2014) and Greenwood et al. (2015).

1.3 Origin and significance of organic sulfur in the geosphere

Sulfur is an essential element for all living organisms because it plays a critical role in energy transduction, enzymatic reactions, and biosynthesis (Clark, 1981). Given that organic sulfur species synthesized by biota occur in chemically labile forms (e.g. amino acids and proteins) and are thus thought to be rapidly mineralized, it is expected that this form of organic sulfur will decrease during the course of diagenesis (Tissot and Welte 1984). Yet, in several sedimentary environments this is not the case and the sulfur content bound in organic matter increases beyond the expected original biomass sulfur content of ca. 0.5-1 cell wt%. This phenomenon has been documented in the Cariaco Basin, where the sulfur-to-carbon or S/C ratio increases with sediment depth from ca. 0.05 to 0.12 (Werne et al. 2003), as well as in the Peru Margin, where the S/C ratio increases from 0.03 to 0.15 (Mossman et al. 1991). Additionally, the organic sulfur content in older, more mature deposits can reach up to 14 wt% in some oils (Orr and Sinninghe Damsté 1990) and up to 80 wt% of total reduced sulfur in black shales (e.g. the Miocene Monterey Formation; Zaback and Pratt 1992). Moreover, the structures of OSC found in sediments, oils, bitumens, and coals are very different from those biosynthesized (Sinninghe Damsté and de Leeuw 1990). For instance, the sulfur atoms in OSC are located at specific positions, where they replace functional groups such as double bonds or hydroxyl groups. Also, the bulk isotope composition of organic sulfur in sediments is ^{34}S-depleted relative to primary biological sulfur (Adam et al. 1998, Filley et al. 2002, Werne et al. 2003) and isotopic mass balance calculations show that at least 75–90% of sedimentary organic sulfur is not primary biological sulfur (Anderson and Pratt 1995). Therefore, a major part of sulfur bound in organic matter within sediments is produced via reactions of functionalized organic compounds with inorganic sulfur (a process termed sulfurization and/or natural vulcanization; Sinninghe Damsté and de Leeuw 1990), rather than the sedimentation and preservation of primary biological sulfur compounds.

Despite having lower concentrations than HS^-, polysulfides likely play an important role in the sulfurization of organic matter as suggested by several studies (Aizenshtat et al. 1983; Francois 1987; Mossmann et al. 1991; Vairavamurthy et al. 1992, 1995; Werne et al. 2003). It is now generally accepted that reactive reduced sulfur species, hydrogen sulfide (H_2S; though at

physiological pH, hydrogen sulfide is usually fully ionized to bisulfide or HS^-), elemental sulfur (S_8), thiosulfate ($S_2O_3^{2-}$), polythionates (S_xO_y), sulfite (SO_3^{2-}), and/or polysulfides[c] (S_x^{2-}), are the sulfur donors in sulfurization reactions (Orr 1978, Tissot and Welte 1984, Aizenshtat and Amrani 2004a, 2004b). Bisulfide anions and polysulfides, both strong nucleophiles, are the main sulfurizing agents in conditions present in marine environments (Krein, 1993), but polysulfides have been shown to be the more reactive species both theoretically and experimentally (Lalonde et al. 1987; Vairavamurthy and Mopper 1989; Loch et al. 2002). Elemental S is a rather poor nucleophile with low solubility in pure water (30 ± 10nmol L^{-1} at 25°C; Kamyshny 2009) as well as in seawater (60% of its solubility in pure water; Kamyshny 2009), which makes it an unlikely candidate for reaction with organic matter under marine conditions – slightly basic to neutral pH and low temperature (Krein 1993). Thiosulfate and sulfite have been suggested as the likely inorganic S species that form sulfonates in sediments near the oxic-anoxic interface, although results in the study were equivocal (Vairavamurthy et al. 1994).

Sulfurization of organic matter has played a significant role in the preservation of organic matter through geologic time. Biological molecules with reactive functional groups (i.e. proteins, carbohydrates, lipids, and nucleic acids) are highly labile and subject to rapid microbial degradation and mineralization (Hedges and Keil, 1995; Burdige, 2007; Vandenbroucke and Largeau, 2007). Reaction of these functional groups with reduced sulfur species during diagenesis can lead to crosslinking of molecules that results in a highly polymerized, high molecular weight, stable structure that is more resistant to low-temperature degradation (Aizenshtat et al., 1983; Kohnen et al., 1991a; Adam et al., 1993, 2000). Indeed, the sulfurization of carbohydrates has been invoked to explain the very high total organic carbon (TOC) content of not only organic-rich sedimentary rocks, such as those from the Kimmeridge Clay Formation (van Kaam-Peters et al.

[c] Polysulfides are formed through oxidation of HS^- at the interface between oxic and anoxic zones, through oxidation of HS^- with iron or dissolved organic matter, or through reaction of HS^- with S_8 at ambient temperatures. They can also be derived from cyclic sulfur species via bacterial enzymatic cleavage of S-S bonds with membrane bound thiol groups or glutathione, as postulated for *Acidithiobacillus thiooxidans* (formerly, *Thiobacillus thiooxidans*) which oxidizes solid elemental sulfur (Suzuki 1965). The most abundant polysulfide species under marine conditions are S_4^{2-}, S_5^{2-}, S_6^{2-}, as well as hydropolysulfide (HS_2^{2-}; Kamyshny et al. 2004, 2008).

1998, van Dongen et al. 2006), but also more recent sediments from the Cariaco Basin (Aycard et al. 2003, Raven et al. 2016). Sulfurization of organic matter has largely been overlooked in discussions of the carbon cycle and associated processes (e.g. nutrient sequestration, surface redox balance, and oxidation of the atmosphere) but is a fundamental aspect of the connections between sulfur and carbon throughout geologic time (cf. Fike et al. 2015 and Raven et al. 2018).

1.3.1 Environmental conditions required for organic sulfur formation

Two main factors are required in order for organic sulfur formation to occur in the environment. First, the environmental conditions must be conducive to MSR in the water column and/or sediments. MSR is dependent on (i) the presence of anoxia – typically in euxinic (anoxic and sulfidic) basins and anoxic sediments, (ii) the adequate supply of sulfate – the grand majority of sulfide and thus reduced S species are derived from sulfate reduction, and (iii) the amount and reactivity of organic matter – organic matter is used as a carbon (energy) source by sulfate reducing bacteria during sulfate reduction. Additionally, reactive organic matter (i.e. organic matter containing organic compounds with functional groups such as double bonds, aldehyde, and/or ketone groups) can react directly with reduced sulfur species to form OSC. Second, concentrations of metal ions, especially reactive or available iron, must be low. Reduced sulfur species react more readily with iron than organic matter when an excess of reactive iron relative to the amount of reduced sulfur species is the controlling factor (Hartgers et al. 1997). If reactive iron (iron oxides and oxyhydroxides) is present in excess, more than 90% of sulfur in sediments is in the form of iron sulfides (e.g. pyrite). While both processes, pyrite formation and organic matter sulfurization, can occur simultaneously in sedimentary environments (Brüchert and Pratt, 1996; Werne et al., 2003; Shawar et al. 2018), this likely reflects a subset of organic compounds that are more reactive than the bulk of organic matter. To summarize, the sulfurization of organic matter is most likely to occur in environments favorable to MSR, which receive high amounts of reactive organic matter and where the concentration of reactive iron is exceeded by the amount of reduced sulfur species.

1.3.2 General model of sulfur incorporation into organic matter

A general model for the incorporation of sulfur into organic matter was originally proposed by Sinninghe Damsté et al. 1989 and was based on a number of observations involving OSC and their precursor molecules in the environment. Briefly, after initial nucleophilic sulfur attack and S-C bond formation the resulting thiol (in the case of bisulfide sulfurization) or dianion (in the case of polysulfide sulfurization), may undergo additional reaction with another functional group or double bond on the same molecule, forming a ring (*intramolecular* sulfur addition), or on a different molecule, forming a (poly)sulfide bridge (*intermolecular* sulfur addition). Sedimentary compounds with one or many double bonds (or other reactive functionalities) are not likely to serve as a precursor for OSC. Instead they are more likely to undergo intermolecular S addition, where they become linked via C-S_x-C bonds into a macromolecular matrix forming sulfur-rich, high molecular weight substances (e.g. resins, asphaltenes, and/or kerogen). Sulfur incorporation into organic compounds with two double bonds (or other reactive functionalities) in a favorable position (i.e. not separated by more than three C-C bonds) will undergo intramolecular addition by forming thiolane, thiane, and/or thiophene structures and thus yield low molecular weight OSC (MW < 800). Since this general sulfurization scheme was first proposed it has been corroborated by a number of laboratory and environmental studies. Evidence for intermolecular sulfur addition abounds (e.g. Adam et al. 1993, Kohnen 1991b, Riboulleau et al. 2000, Kok et al. 2000, van Kaam-Peters et al. 1998, van Dongen et al. 2003; 2006, Amrani et al. 2007), as does evidence for intramolecular sulfur addition (e.g. de Graaf et al. 1992, Schouten et al. 1994, 1995, Amrani and Aizenshtat 2004a, 2004b, Werne et al. 2008).

1.3.3 Organic sulfur isotope composition

The sulfur isotope composition of bulk sedimentary organic sulfur is dependent on the sulfur isotope composition of the sulfur source, which carries the isotopic history of MSR, sulfide oxidation, and disproportionation, and any isotopic fractionation(s) associated with sulfur incorporation into organic compounds. At the molecular level, $\delta^{34}S$ values of individual OSC will also reflect multiple contributing factors, including (1) inorganic sulfur source, (2) pathway of

formation, (3) environmental conditions, (4) timing of sulfurization, and (5) diagenetic overprinting, including that from microbial sulfur cycling. The ranges of fractionation(s) associated with said processes (1-5) have yet to be fully evaluated in the natural environment.

1.4 Scope and framework of thesis

The general objective of this dissertation is to provide more detailed evidence for the timing and pathway(s) of formation of organic sulfur in the geosphere. To reach this goal a combined bulk, molecular, and isotopic approach was used, aiming at the structural and isotopic elucidation of organic sulfur compounds and sulfur-containing moieties from laboratory sulfurization experiments, as well as those from geologic samples.

Chapter 2 addresses the determination of inorganic polysulfide speciation in euxinic water column samples using gas chromatography. We show the ability to measure polysulfide speciation (up to dimethylpentasulfide) via GC FID/FPD and GC/MS at sub-micromolar levels and with good precision in both laboratory and natural samples. Additionally, we determine the storage conditions required for accurate analysis of derivatized polysulfides. With improvement, our method of analysis can be used for direct compound-specific sulfur isotope analysis (CSSIA) of individual polysulfide species at concentrations present in natural samples using GC/MC-ICP-MS. Such measurements are expected to provide valuable information on the role polysulfides play in the natural environment [(e.g. sulfurization of organic matter (Aizenshtat et al. 1995), pyrite formation (Luther 1991), metal precipitation (Chadwell et al. 1999), and formation of volatile sulfur compounds (Ginzburg et al. 1999, Heitz et al. 2000, Kamyshny et al. 2003)].

Detailed structural and stable sulfur isotope analysis associated with abiotic sulfur incorporation into carbohydrates and natural dissolved organic matter under controlled conditions is presented in **Chapters 3 and 4**. Glucose and Pahokee Peat (a humic acid standard) were sulfurized under laboratory conditions at room temperature (24°C) using three commercially available sulfides, each mixed with elemental sulfur to produce (poly)sulfide solutions. The reaction products were analyzed using FT-IR and online pyrolysis, which revealed structural differences among the

products formed via the three sulfide reactants. Samples from both modern (Mahoney Lake, British Colombia, Canada) and ancient (Jurassic aged Blackstone Band from the Kimmeridge Clay Formation, Dorset, United Kingdom) euxinic systems were also analyzed via FT-IR for comparison to laboratory samples. Our results show that (1) the degree of sulfur incorporation is dependent on reaction conditions, (2) the hydroxyl group plays an important role during sulfur incorporation into organic matter, and (3) the production of alkylthiophenes during pyrolysis of sulfurized glucose is not universal, rather, it depends of reaction conditions. The structural nature of sulfurized organic matter in the geosphere is similar to laboratory sulfurized organic matter, demonstrating that similar reaction mechanisms are followed. We analyzed the bulk sulfur isotope compositions of reactants and products to determine the fractionation(s) associated with abiotic sulfur incorporation into organic matter. We show that sulfur isotopic fractionation varies (-2.05 to +1.61‰) during sulfur incorporation into organic substrates (i.e. glucose and Pahokee Peat). Our results provide experimental evidence for sulfur isotopic relationships between reactive inorganic reduced sulfur species and sulfurized organic matter in the geosphere.

Paired pyrite and organic sulfur isotope records from the Jurassic aged Blackstone Band of the Kimmeridge Clay Formation are presented in **Chapter 5**. Measurements of bulk sulfur species, show dynamic fluctuations that are related to environmental conditions during deposition. We find that pyrite isotope values record variations in MSR rates that are influenced by the availability of metabolizable organic carbon. We show the importance of macromolecular organic sulfur formation in potentially limiting the availability of metabolizable carbon for MSR during times of increased organic carbon burial. Additionally, ^{34}S-enrichment of organic sulfur relative to pyrite, outside of what can be accounted for by known fractionations associated with organic sulfur formation, reflects contributions of primary biosulfur and its subsequent preservation in the geologic record. Compound-specific sulfur isotope analysis (CSSIA) of benzothiophenes (BTs) and dibenzothiophenes (DBTs) from bitumen (solvent-extractable organics) and kerogen (non-solvent extractable organics) pyrolysates reveals more complex dynamics. Sulfur incorporated into bitumen compounds is unrelated to the sulfur source responsible for the formation of both bulk organic sulfur and kerogen compounds. Kerogen compounds, on the other hand, reflect the sulfur isotopic composition of bulk organic sulfur, which may be useful in reconstructions where measurements of bulk organic sulfur may be influenced by pyrite relicts.

2.0 Determination of inorganic polysulfide speciation in euxinic water column samples using gas chromatography

2.1 Introduction

Inorganic polysulfides (S_n^{2-}) are important reactive intermediates in the sulfur cycle. They exist in basic (pH ≥ 7) aqueous systems as chains of sulfur atoms (S_2^{2-} to S_8^{2-}) with longer chain lengths favored at higher pH. Polysulfides result from various processes including the oxidation of hydrogen sulfide, the reaction of hydrogen sulfide and zerovalent sulfur, and the disproportionation of thiosulfate. Despite their low concentrations in most natural environments, polysulfides may play a significant role in environmentally relevant processes [e.g. sulfurization of organic matter (Aizenshtat et al. 1983; 1995, Francois 1987, Mossmann et al. 1991, Vairavamurthy et al. 1992; 1995, Werne et al. 2003), pyrite formation (Luther 1991), metal precipitation (Chadwell et al. 1999), and formation of volatile sulfur compounds (Ginzburg et al. 1999, Heitz et al. 2000, Kamyshny et al. 2003)]. Their redox reactivity, nucleophilic tendencies, and thermal instability make determining polysulfide speciation challenging, and published measurements of polysulfide speciation derived from natural samples are limited.

Published methods range in complexity from UV absorbance (Giggenbach et al. 1972, Danielsson et al. 1996), to electrochemical methods (Luther et al. 1985;1994, Rozan et al. 2000), as well as gas and liquid chromatography-based techniques (Clarke et al. 1985, Stuedal et al. 1989, Heitz et al. 2000, Kristiana et al. 2010). Each method has its limitations, but many of the methods are optimized for the determination of total polysulfide concentrations rather than individual speciation, abundance and distribution – which is critical for determining the role polysulfides play in the natural environment (see Kamyshny et al 2006 for a brief review). The most promising method for determining individual polysulfide speciation involves derivatization of labile polysulfides to stable dimethylpolysulfanes using methyl trifluoromethanesulfonate (methyl triflate - MeOTf; $CF_3SO_3CH_3$) and subsequent analysis via high-performance liquid chromatography (HPLC) (Kamyshny et al. 2004;2006). This rapid derivatization method, carried

out in a methanol-water medium, preserves the original distribution of inorganic polysulfides (S_3^{2-} to S_7^{2-}), with detection limits in the nM range. The method has been validated for the determination of inorganic polysulfide species under environmentally relevant conditions (Kamyshny et al 2006). To reach the lowest detection limits, however, requires harsh sample treatment involving large sample volumes, and multiple liquid-liquid extractions with complete solvent evaporation and redissolution, which can result in a loss of some of the species (e.g. S_3^{2-}). Additionally, the method is not validated for the detection and quantification of the shortest polysulfide species (S_2^{2-}).

The goals of this study were to optimize protocols for sampling, derivatization, storage, extraction and GC analysis of dimethylpolysulfanes. We then applied our optimized method to polysulfide-rich water column samples from euxinic Mahoney Lake, British Colombia, Canada. Mahoney Lake is a small, shallow (maximum depth of ca. 15 m), saline kettle basin with high sulfate concentrations (approaching 500 mM), which promotes vigorous sulfate reduction below a prominent chemocline at ca. 7 m water depth. The vigorous sulfate reduction leads to high concentrations of sulfide (exceeding 30 mM) and subsequent production of polysulfides via various reaction mechanisms (e.g. oxidation of hydrogen sulfide, reaction of hydrogen sulfide and zerovalent sulfur, and/or the disproportionation of thiosulfate).

Our on-going refinement of earlier methods used to determine polysulfide speciation in artificial and natural samples allows for future direct measurements of the sulfur isotopic compositions of each polysulfide species (S_2^{2-} to S_7^{2-}) at concentrations present in natural samples using a GC coupled to a multi-collector ICP-MS (GC/MC-ICP-MS). Such measurements can ultimately provide context for further defining the role polysulfides play in the natural environment.

2.2 Experimental

2.2.1 Chemicals and materials

Ammonium sulfide ($[NH_4]_2S$; 20% aqueous solution) and methyl trifluoromethanesulfonate (98%) were obtained from Sigma-Aldrich. Elemental sulfur (99%), anhydrous sodium sulfate (99%),

potassium phosphate monobasic (99%) and dibasic (98%), as well as Optima grade (99.9%) methanol and *n*-hexane were obtained from Fisher Scientific.

2.2.2 (Poly)sulfide solution preparation, derivatization, and extraction

In a glovebox under nitrogen atmosphere (0.3% O_2) ammonium sulfide ($[NH_4]_2S$; 20% aqueous solution) was mixed with elemental sulfur in a 1:1 stoichiometric ratio with the following concentrations 0.0001 M, 0.005 M, 0.05 M, 0.3 M, and 2.9 M. The resulting solution was stirred for one hour to reach equilibrium (Amrani and Aizenshtat 2004). After 1 hour, the (poly)sulfide solution was filtered through a 0.2 µm regenerated cellulose syringe filter to remove colloidal elemental sulfur and/or particulates (if present, as in the case of natural samples). Derivatization (methylation) of labile polysulfides to stable dimethylpolysulfanes was completed using methyl triflate (MeOTf; chemical reaction shown in Figure 1), following procedures modified from Kamyshyny et al. 2004; 2006. In brief, the following were added consecutively (under 5 seconds) to a 100 mL amber flask containing 40 mL deaerated (sparged for 30 min with 99.999% N_2) methanol under vigorous stirring (i) 5 mL of 50 mM phosphate buffer (sparged for 30 min with 99.999% N_2) within 0.25 pH units of the polysulfide solution; (ii) 5 mL filtered polysulfide solution; and (iii) 250-300 µL methyl triflate. The resulting mixture was allowed to react for 5 min while being stirred vigorously under nitrogen atmosphere (0.3% O_2). After the 5 minutes, the derivatization mixture was removed from the glovebox and transferred to a 250 mL separatory funnel for extraction. 80 mL of 375 mM sodium sulfate (Na_2SO_4) solution was added to the separatory funnel to assist in salting out dimethylpolysulfanes from the derivatization mixture (Kamyshyny et al. 2006). The dimethylpolysulfanes were then extracted using three consecutive 1 mL volumes of *n*-hexane for the most concentrated solution (2.9 M) and two consecutive 1 mL volumes for the remaining less concentrated solutions. An aliquot (10 ul) of the 2.9 M dimethylpolysulfanes in *n*-hexane was further diluted in 90 µL pure *n*-hexane (100 µL total volume) in preparation for GC analysis. The less concentrated solutions (0.0001 M, 0.005 M, 0.05 M, 0.3 M) were run directly on the GC in the 2 mL hexane extraction volume. An internal standard (decane) was also added for quantification. The total time from extraction of dimethylpolysulfanes to injection on the GC was less than 10 min.

2.2.3 Storing derivatized solutions

In order to determine the stability of derivatized polysulfides (i.e. dimethylpolysulfanes), derivatized solutions of 2.9 M, 0.3 M and 0.0001 M were stored in the refrigerator at 4°C and in the freezer at -20°C for 3 to 17 days for 2.9 M solutions and one- and two-weeks in the case of the 0.3 M and 0.0001 M (dilute) solutions. For the dilute samples, six replicates (three from the refrigerator and three from the freezer) at each concentration (12 total samples) were extracted and analyzed via GC-FID/FPD and GC-MS at the one- and two-week mark.

2.2.4 Sample collection and preparation

Lake water column samples were taken from the depths of euxinic Mahoney Lake (British Columbia, Canada) in August 2015 using trace metal clean tubing and a dialysis pump. Clean (ashed at 450°C for 4 hours) 20 mL scintillation vials were flushed with at least 2 volumes of water before being filled to overflow and capped without headspace. The cap was secured with electrical tape and vials were kept cool (close to the water temperature the sample was taken) and in the dark for transport back to shore. Three replicates were taken per water depth. Once back at the field station, the samples were derivatized in a glovebag under nitrogen atmosphere using the same procedure as was done for the polysulfide solutions. The samples were derivatized within 2 hours of collection. The derivatized sample mixtures were stored in PTFE septa-sealed amber bottles, and kept cool on dry ice and in the dark for transport back to the University of Pittsburgh. Within one week the samples were extracted as described for the polysulfide solutions, except two consecutive 1mL volumes of *n*-hexane were used for extraction (as was the case for the less concentrated laboratory polysulfide solutions). The dimethylpolysulfanes in *n*-hexane (2 mL total volume) were analyzed via GC with decane added as an internal standard. The total time from extraction of dimethylpolysulfanes to injection on the GC was less than 10 min.

2.2.5 Quantification and identification using gas chromatography flame ionization detection/flame photometric detection and mass spectrometry (GC-FID/FPD and GC-MS).

Derivatized samples were quantified using a Thermo Trace 1310 gas chromatograph with both flame ionization and flame photometric detectors. Aliquots (1 μL) of each sample were introduced via a PTV injector operated at constant temperature (70°C) and in splitless mode. The gas chromatograph was programmed from 70°C (2 min) to 300°C (5 min) at a rate of 5°C min^{-1}. Separation was achieved using a SUPELCO SPB®-1 SULFUR Capillary GC Column (L 30 m × I.D. 0.32 mm, d_f 4.00 μm) with a helium flowrate of 2 mL min^{-1}. Dimethylpolysulfanes were identified using a Thermo ISQ QD single quadrupole mass spectrometer connected to a Thermo Trace 1310 gas chromatograph. Injector and GC operating conditions were the same as described above. The mass spectrometer transfer line was held at 320°C and ion source at 275°C. Compounds were ionized at 70 eV and mass analyzed over a range of m/z 50-600. Dimethylpolysulfanes were identified on the basis of relative retention time and on the basis of mass spectral data in comparison with literature data.

2.2.6 Analytical method validation

Following optimization of the GC operating conditions for analysis of the dimethylpolysulfanes, precision, sensitivity, and linearity of the method was evaluated over four orders of magnitude. This was completed by analyzing three replicate solutions (12 total) at each of the following concentrations 0.3 M, 0.05 M, 0.005 M and 0.0001 M.

2.3 Results and discussion

2.3.1 Optimization of GC operating conditions

In order to optimize the GC operating conditions, we used repeated analysis of dimethylpolysulfanes (dimethyldisulfide- DM2S, dimethyltrisulfide – DM3S, dimethyltetrasulfide – DM4S, dimethylpentasulfide – DM5S; structures shown in Figure 1) from the most concentrated solution (2.9 M).

Injector – A programmed temperature vaporizing injector (PTV), operated in splitless mode and maintained at low temperature (70°C) was used to minimize potential degradation of dimethylpolysulfanes at high temperatures during injection. Higher (up to 290°C) temperatures were also tested. At temperatures above 200°C, significant degradation of dimethylpolysulfanes took place. We also tested several temperature programs for the injector, but none improved the vaporization/degradation of the dimethylpolysulfanes over maintaining the injector at a constant temperature of 70°C.

Column – Three GC capillary columns were tested, a Thermo TG-SQC (L 15 m x I.D. 0.25 mm x df 0.25 µm), an Agilent J&W DB-5 (L 30 m x I.D. 0.32 mm x d_f 0.25 µm), and a SUPELCO SPB®-1 SULFUR Capillary GC Column (L 30 m × I.D. 0.32 mm, d_f 4.00 µm). The SUPELCO SPB®-1 SULFUR capillary was determined to be the best column that maintained peak shape, separation, and reasonable elution times. Additionally, the greater film thickness of the SUPELCO SPB®-1 SULFUR capillary column allowed for the potential of larger injection volumes for low concentration samples. An example of peak shape from each of the columns tested is shown in Figure 2.

Oven temperature ramp and flowrate – We found that the dimethylpolysulfanes (DM2S to DM5S) were baseline separated, with gaussian peak shapes using a flowrate of 2 mL min^{-1} and a temperature ramp of 5°C min^{-1} from 70°C (hold 2 min) to 300°C (hold 5 min).

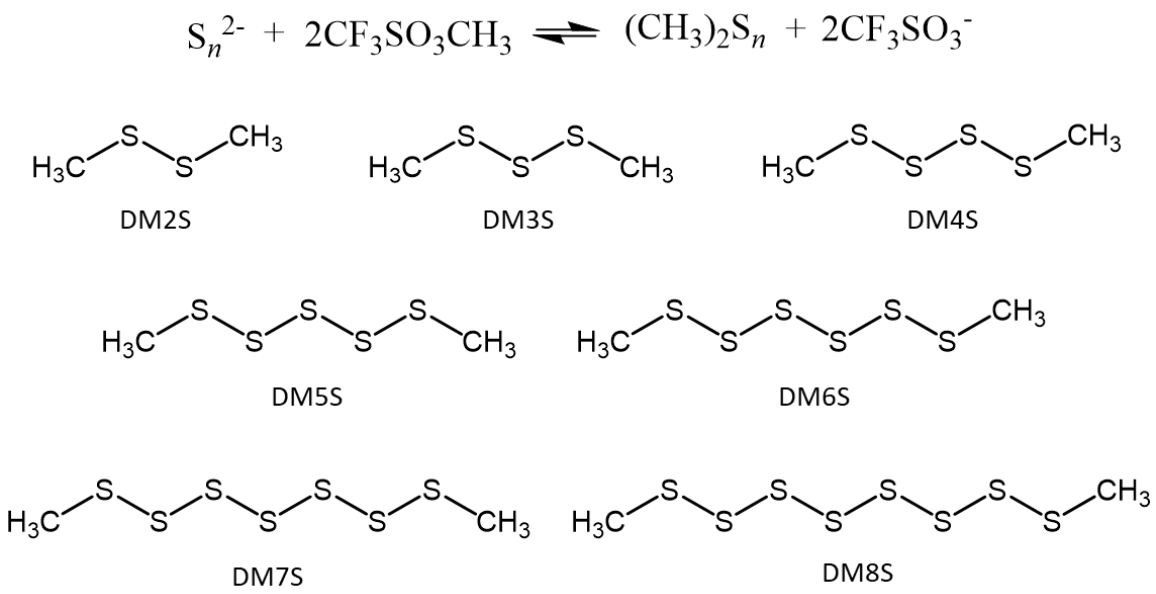

Figure 1. Equation for polysulfide derivatization and resulting dimethylpolysulfane structures. Labile polysulfide species (S_n^{2-}) react with methyl triflate ($CF_3SO_3CH_3$) to form stable dimethylpolysulfanes of varying sulfur chain lengths ($n \geq 8$); dimethyldisulfide (DM2S), dimethyltrisulfide (DM3S), dimethyltetrasulfide (DM4S), dimethylpentasulfide (DM5S), dimethylhexasulfide (DM6S), dimethylheptasulfide (DM7S), and dimethyloctasulfide (DM8S).

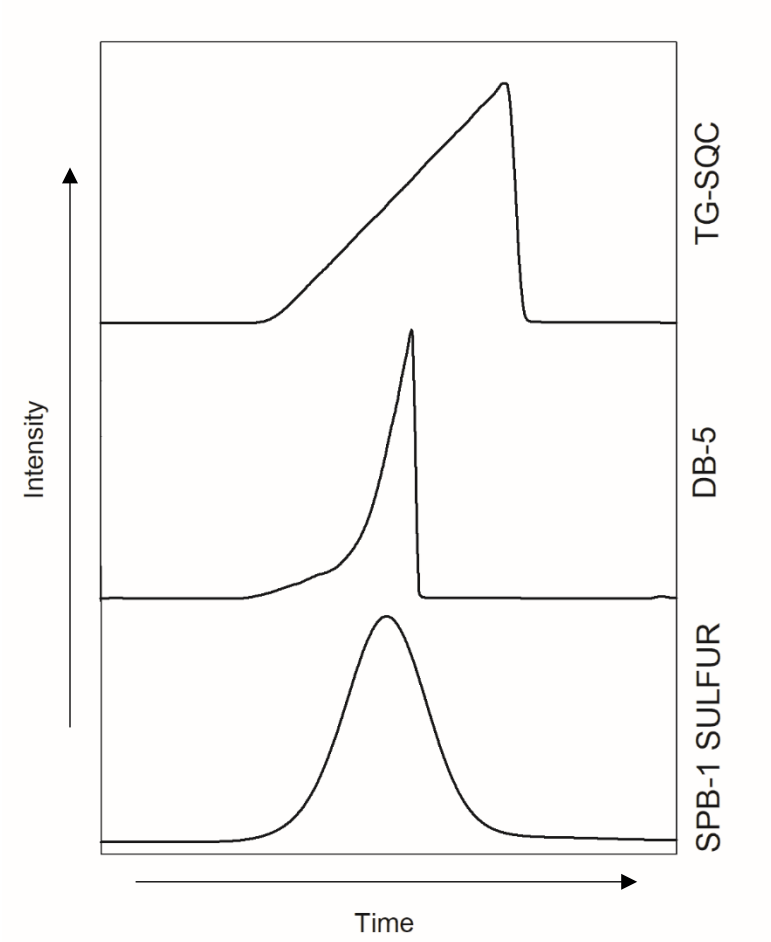

Figure 2. GC capillary column comparison. Three capillary GC columns were tested during the current study. Supelco's SPB-1 SULFUR column performed the best, with gaussian peak shapes and good peak separation with short run times.

2.3.2 Method validation – precision, sensitivity, and linearity

We were able to detect dimethylpolysulfanes at all concentrations. Within pure (undiluted with deaerated water) 2.9 M solutions we were able to analyze dimethylpolysulfanes from DM2S to DM5S consistently. That said, the samples would degrade to ca. 20% of the peak area from the first injection within 90 minutes (data not shown), so we were unable to test the actual precision of replicate measurements for the 2.9M solutions. The pure solution was diluted with deaerated water, step-wise, to the following concentrations 0.3 M, 0.05 M, 0.005 M, and 0.0001 M. Within the dilute solutions we were able to analyze DM3S and DM5S consistently, and only sometimes DM4S. Curiously, dilution of the pure solution altered peak resolvability within the FPD chromatograms compared to the pure solution, where the later eluting dimethylpolysulfanes (DM4S and up) were no longer identifiable as distinct peaks in the FPD chromatogram (Figure 3). Along with this observation, GC/MS analysis of the dilute samples showed interference of ammonia/ammonium polysulfides along with other nitrogen-sulfur compounds, these same compounds were not observed in the concentrated (2.9 M) derivatized solutions also analyzed via GC/MS. This leads us to surmise that there are competing reactions with ammonia/ammonium in the formation of polysulfides when water is added. The addition of water and subsequent reaction with the ammonium sulfide solution likely affected the distributions of polysulfide species and assisted in their breakdown. With these complications in mind, the precision of replicate measurements of the dilute solutions was not optimal and detection of the polysulfide species suffered, especially at 0.05 M and 0.005 M concentrations. Despite these complications, we were able to measure concentrations of polysulfide species at sub-micromolar levels in the solutions with good precision and with even better precision at the lowest concentrations (Figure 4).

We also calculated the theoretical concentrations of each polysulfide species which are based on previously reported thermodynamic values (Kamyshyny et al. 2004). The thermodynamic constants used for the calculation are based on equilibrium and saturated conditions with respect to sulfur, additionally the predicted thermodynamic constants have a sizable degree of uncertainty [ca. 31 (48), 6 (25), and 5 (24) % for tri- to pentasulfide at 25°C (4°C), respectively]. The solutions are not saturated solutions, so were not expected to necessarily match theoretical calculations, but

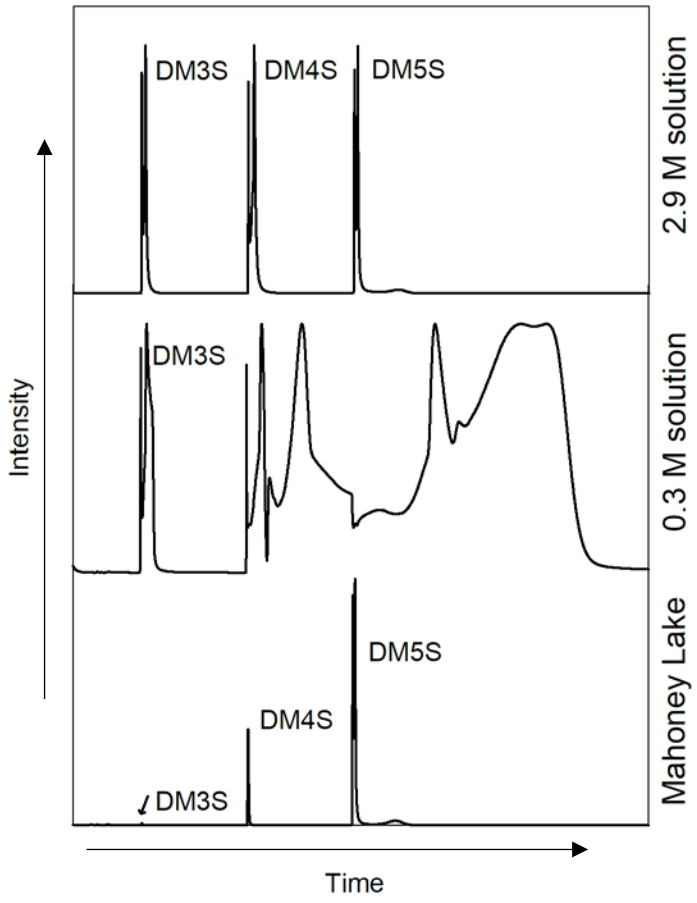

Figure 3. FPD chromatogram comparison. Dilution of the 2.9 M solution (top) to 0.3 M (middle) resulted in side reactions of ammonia/ammonium, which complicated the resolvability of the longer dimethylpolysulfanes in the 0.3 M solution. The bottom plot is of dimethylpolysulfanes from Mahoney Lake.

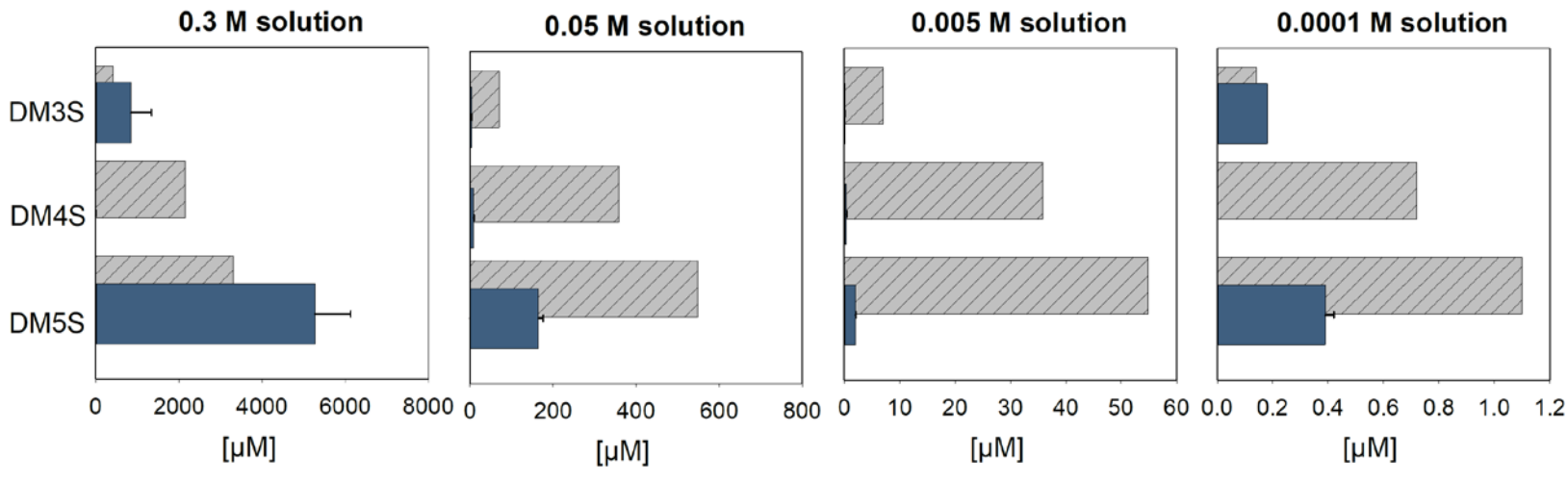

Figure 4. Method validation over four orders of magnitude. Measured concentrations are offset from the thermodynamic theoretical concentrations. The greater disparity between measured and theoretical concentrations observed in the 0.05 M and 0.0005 M solutions is a likely result of ammonia/ammonium side reactions (additionally discussed in section 2.3.2.). Despite the difference between measured and theoretical concentrations, the precision of replicate sample analysis is quite good, and especially so at the lower concentrations.

are shown for comparison since true values are not available (Figure 4). As discussed previously, for the more dilute samples, ammonia/ammonium competition/reactions in the formation of nitrogen-sulfur compounds likely affected the concentrations of the dimethylpolysulfanes, resulting in an additional factor affecting the offset between the measured and theoretical values of the polysulfides.

2.3.3 Derivatization, extraction and storage

Volume of derivatization agent – This was determined from the equation proposed by Kamyshyny et al. 2006 (shown below) and was not further tested in the current study.

$V_{MeOTf} = 0.91pH - 1.37$

where V_{MeOTf} denotes the volume in microliters (µL) of methyl triflate per mL of sample-methanol derivatization mixture. For our solutions and natural samples, the pH ranged from 7-9 and the total volume of the derivatization mixture (mL sample + mL buffer + mL methanol) was 50 mL, thus we used volumes between 250-300 µL of methyl triflate for derivatization.

Extraction solvent and volume – Dodecane was initially used as the extraction solvent as per Kamyshyny et al. 2006. However, we found that the temperature needed for complete vaporization of dodecane caused thermal degradation and loss of dimethylpolysulfane species during injection on the GC. We instead used *n*-hexane as our extraction solvent, which allowed for a lower vaporization temperature. There is concern that dimethylpolysulfanes longer than DM5S are not sufficiently extracted using organic solvents of carbon chain lengths less than 10 (Kamyshyny et al. 2006). Our choice of solvent may have affected the recovery of longer sulfur chain lengths of dimethylpolysulfanes, as we were not able to detect them. That said, it is more probable that they thermally degraded within the GC (Kamyshyny et al. 2004), as Amrani et al. 2006 used pentane for extraction of dimethylpolysulfanes with subsequent LC/MS detection of sulfur chain lengths up to DM6S and isolation for sulfur isotopic analysis via EA-IRMS. For the 2.9 M solutions, extraction volumes of 3 mL were necessary for recovery of the dimethylpolysulfanes, whereas for the dilute solutions 2 mL extraction volumes could be used. This was based on analysis of

subsequent 1 mL extraction volumes, where in the fourth (-third) 1 mL hexane extraction no dimethylpolysulfanes were detectable in the 2.9 M (-dilute) solution(s).

Drying down extraction volumes – After extraction, the extraction solvent was dried down under a gentle stream of N_2 in order to concentrate the sample to analyze low concentration samples. Solvent dry down, whether to dryness, leaving a small amount of hexane, or adding a higher-boiling point keeper solvent (i.e. dodecane) resulted in the variable loss of all dimethylpolysulfane species (data not shown).

To test the stability of the dimethylpolysulfanes we derivatized and stored pure and dilute solutions in the refrigerator (4°C) and freezer (-20°C) for up to two weeks (17 days for pure solutions) before extraction and analysis.

Pure solutions – Pure (undiluted with deaerated water) 2.9 M solutions were mixed, derivatized and stored in the refrigerator (4°C) and freezer (-20°C) for 3 to 17 days from their initial derivatization date before being extracted and analyzed. The pure solution peak areas after storage were compared to the peak areas of the initial solution analyzed (initial refers to the solution which was mixed, derivatized, extracted, and analyzed immediately without being stored). Peak areas were compared instead of calculated concentrations because the standard we used co-eluted with the S_8 peak. Results show that storage temperature and length of storage affects the concentrations of the dimethylpolysulfanes (Figure 5). For the most part, solutions stored in the refrigerator were more consistent, maintaining ca. 70-80% of the initial peak areas, than those stored in the freezer, which were highly variable, maintaining ca. 50-180% of the initial peak areas. The effects of storage temperature and length of storage were evenly distributed among dimethylpolysulfanes (i.e. short chain lengths were not more affected than longer chain lengths and vice versa).

Dilute solutions – Solutions at 0.3 M and 0.0001 M were stored in the refrigerator (4°C) and freezer (-20°C) for one- and two-week periods from their initial derivatization date. Peak areas of the dimethylpolysulfanes were converted to concentrations using an internal standard (decane) of known concentration. Overall the storage conditions affected the solutions differently depending on the concentration (Figure 6). The more dilute solution (0.0001 M) was more stable in regards to dimethylpolysulfane concentrations. The 0.3 M solutions showed slight variability in the concentration of DM3S, but measurements were within the calculated error of one another. DM5S

concentrations increased over time, with lower temperatures yielding more DM5S in the 0.3 M solutions (Figure 6). DM3S measured in the 0.0001 M solution varied slightly with storage, whereas DM5S showed a slight increasing trend with storage time, but measurements were within error of one another (Figure 6).

2.3.4 Analysis of natural samples

Results from the analysis of dimethylpolysulfanes from Mahoney Lake's water column are shown in Figure 7. We were able to detect polysulfide species as their dimethylpolysulfane derivatives DM3S, DM4S, and DM5S at micromolar concentrations throughout the euxinic portion of the water column (below 6.5 m water depth) and with high precision among replicate samples. The concentrations increase with depth, following the trend in sulfide concentrations. Dimethylpolysulfane distributions also show the same trends as the theoretical calculations, but the absolute concentrations are offset by an order of magnitude (Figure 7). This is likely due to the fact that the samples from Mahoney Lake are not saturated with respect to sulfur, as is a condition of the theoretical calculations, as well as the uncertainty associated with the reported thermodynamic constants (> 51% depending on polysulfide chain length and temperature; Kamyshyny et al. 2004). Other explanations for the offset likely include slight degradation during storage before extraction and analysis, and the potential that polysulfides are reacting in the water column, so their abundance is lower than the theoretical measurement. Despite this, our method of analysis does allow for the determination of polysulfide species in natural samples at micromolar concentrations and shows promise for determining subsequent reactions of polysulfides in Mahoney Lake (e.g. reaction with organic matter, forming organic sulfur compounds and/or reaction with iron, forming iron monosulfides and pyrite).

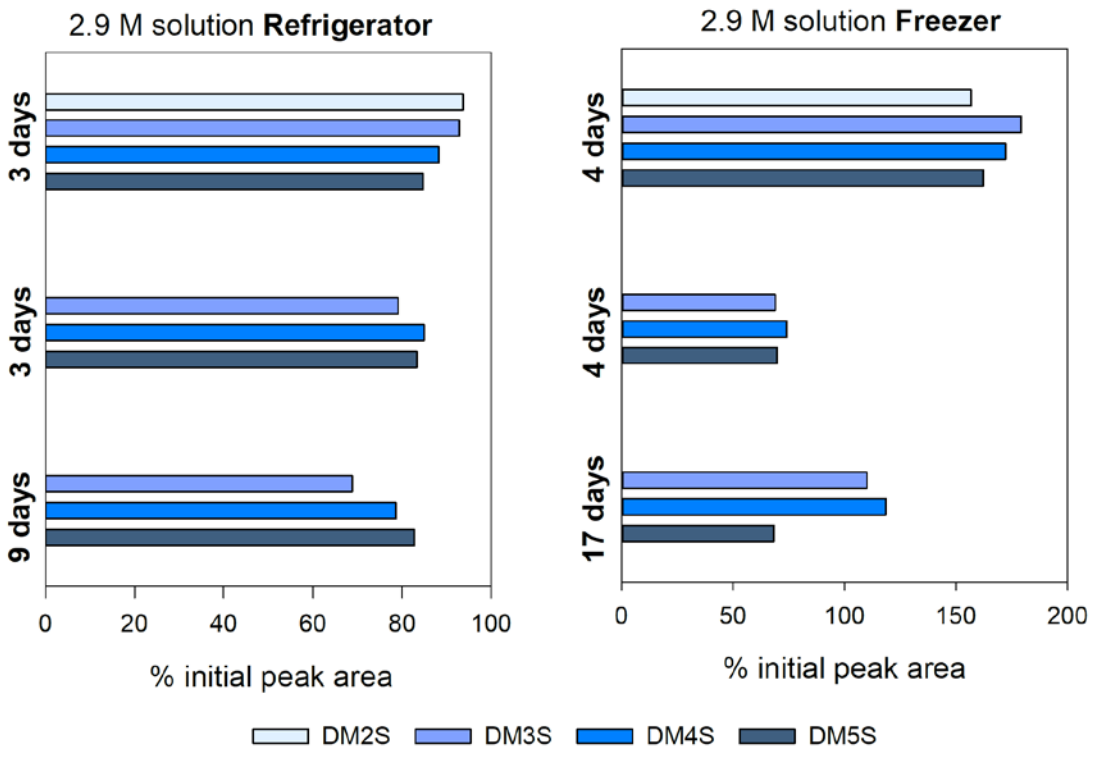

Figure 5. Effects of storage conditions on polysulfide concentration and distribution from the pure (2.9 M) solution. Peak areas from each analysis were compared to the peak areas of the initial solution analyzed (initial refers to the solution which was mixed, derivatized, extracted, and analyzed immediately without being stored) and are represented as % of the initial peak area. Storage at 4°C (refrigerator) results in less variability, while maintaining > 70% of the initial concentrations. Storage at -20°C (freezer) is highly variable, with peak concentrations > 100% of the initial concentrations.

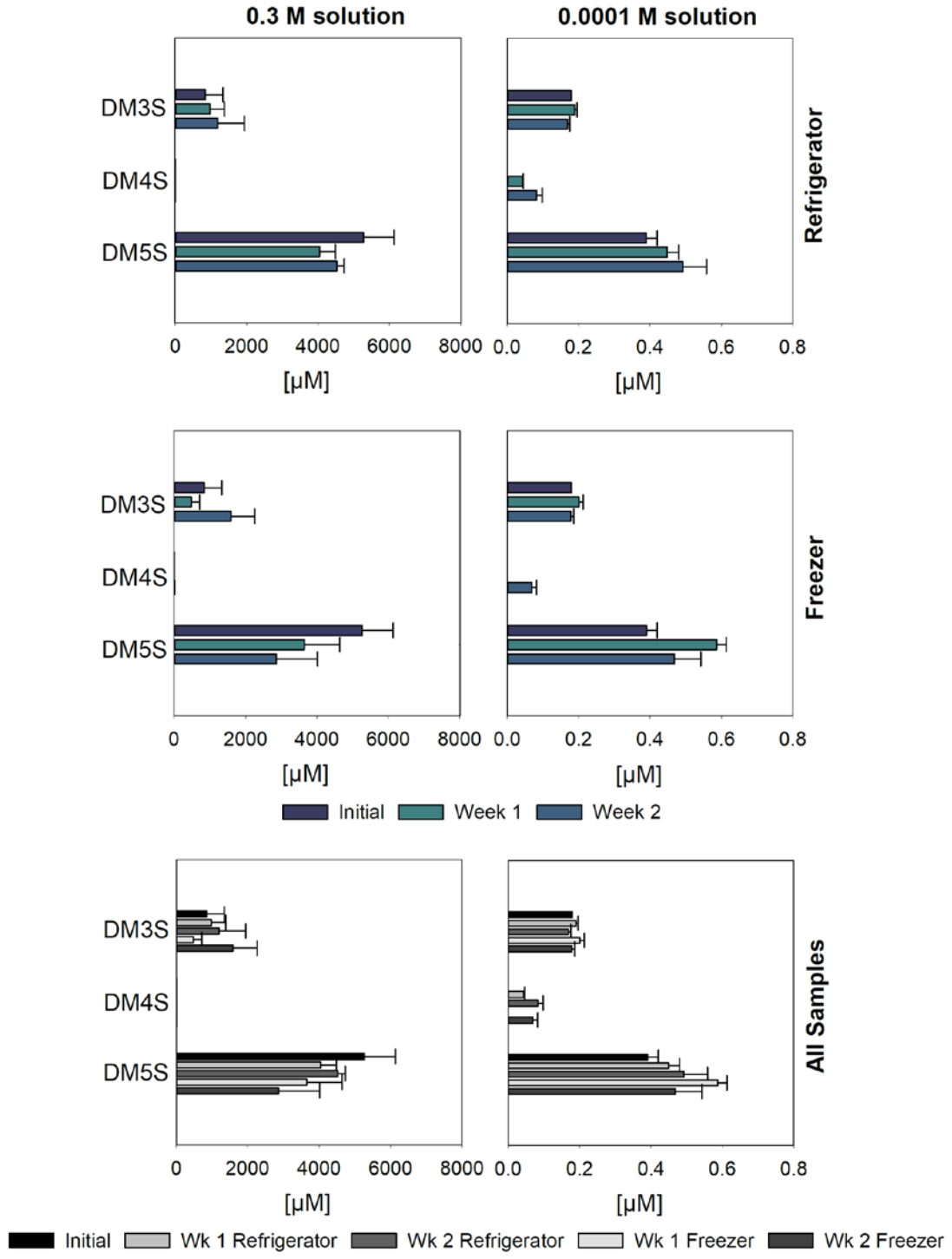

Figure 6. Effects of storage conditions on polysulfide concentration and distribution from the dilute, 0.3M and 0.0001M, solutions. Peak areas were converted to concentrations using an internal standard (decane) of known concentration. The more dilute solution (0.0001 M) show less variability through storage time and temperature. The longer sulfur chain length polysulfide (DM5S) shows greater variability than the shorter sulfur chain length polysulfide (DM3S), indicating that the shorter chain length is more stable.

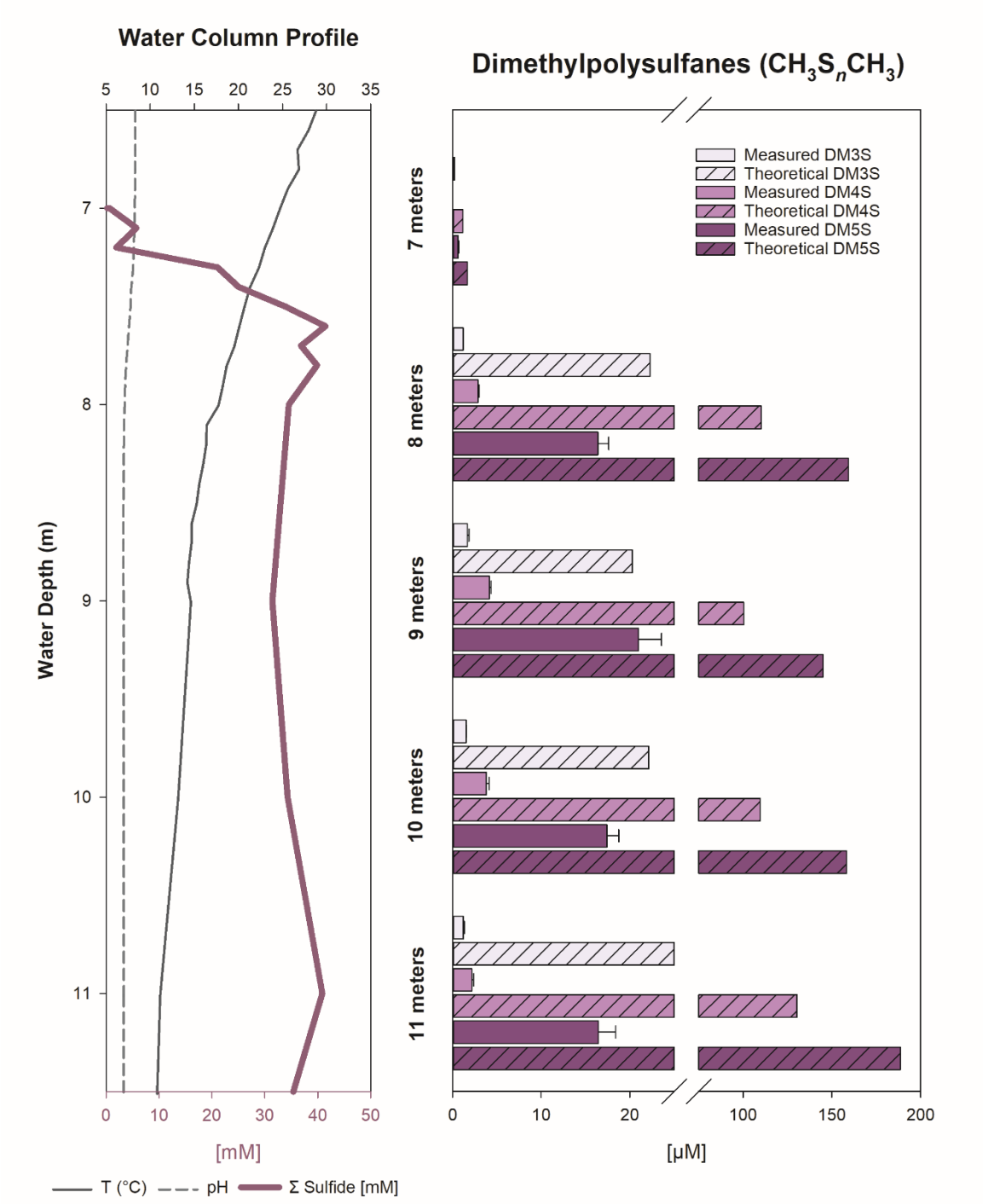

Figure 7. Mahoney Lake water column profile, polysulfide species distribution and concentrations. Water column measurements of pH and temperature are from August 2015 and Σ sulfide concentrations are from July 2008. Micromolar concentrations of polysulfides are detectable just below the chemocline (ca. 7 m) in Mahoney Lake. Polysulfide concentrations increase with depth similar to sulfide concentrations. Note break in scale from 25-75 µM, with a change in scale after the break.

2.4 Future directions and recommendations

Here we have shown the ability to measure polysulfide speciation (up to DM5S) via GC FID/FPD and GC/MS at sub-micromolar levels and with good precision in both laboratory and natural samples, despite complications within laboratory synthesized solutions. The main direction for future optimization and validation of the method presented in the current study is to apply our method to a polysulfide solution synthesized from elemental sulfur mixed with sodium sulfide (Na_2S) and/or to a solution of K_2S_5 dissolved in phosphate buffer as in Kamyshyny et al. 2004;2006, thereby eliminating interference from ammonia/ammonium side reactions.

Additionally, we have shown the importance of storage conditions in analyzing polysulfides after derivatization. We recommend that derivatized polysulfide samples be stored at 4°C and analyzed within one week, to avoid substantial degradation and/or rearrangement of dimethylpolysulfanes.

We are confident that with further optimization and validation, this method of analysis can be used for direct compound-specific sulfur isotope analysis (CSSIA) of individual polysulfide species at concentrations present in natural samples using a GC coupled to a multi-collector ICP-MS (GC/MC-ICP-MS). Such measurements could ultimately provide valuable information on the role polysulfides play in the natural environment [(e.g. sulfurization of organic matter (Aizenshtat et al. 1983; 1995, Francois 1987, Mossmann et al. 1991, Vairavamurthy et al. 1992; 1995, Werne et al. 2003), pyrite formation Luther 1991), metal precipitation (Chadwell et al. 1999), and formation of volatile sulfur compounds (Ginzburg et al. 1999, Heitz et al. 2000, Kamyshny et al. 2003)].

3.0 Laboratory low-temperature sulfurization of carbohydrates and dissolved organic matter using different sulfides. Part I: Structural characteristics

3.1 Introduction

Characterization of organic sulfur compounds (OSC) is an important topic of geochemical interest as OSC can provide paleoenvironmental information, information on the timing and preservation of organic matter (OM), as well as petroleum quality (Stock et al. 1989, Orr and Sinninghe Damsté 1990, Sinninghe Damsté et al. 1999). A myriad of OSC have been identified (for a review see Sinninghe Damsté and de Leeuw 1990). Since the earliest studies, OSC have been found in the water column of euxinic basins, both modern and ancient sediments, as well as in petroleum (Sinninghe Damsté et al. 1989, Sinninghe Damsté and de Leeuw 1989, Aizenshtat et al. 1995, Krein and Aizenshtat 1995, Werne et al. 2008, Raven et al. 2015;2016). It is now accepted that OSC form during early diagenesis through the incorporation of inorganic sulfur species into functionalized lipids (de Graaf et al. 1992, Rowland et al. 1993, Krein and Aizenshtat 1993;1994, Schouten et al. 1994) forming low-molecular weight (LMW) OSC. More recent studies have shown that, in addition to functionalized lipids, carbohydrates can also be preserved through inorganic sulfur incorporation (Moers et al. 1989, Kok et al. 2000, van Dongen et al. 2003). In general, carbohydrates are considered to be preferentially degraded during early diagenesis and as such, are not extensively preserved in the sedimentary record (e.g. Arnosti et al. 1994, Arnosti and Repeta 1994, Arnosti 1995). That said, several studies have shown that carbohydrates survive early diagenesis in water columns and sediments, and are preserved in the sedimentary record (Swain 1969, Hernes et al. 1996, Cowie et al., 1995, Jensen et al. 2005). Preservation of carbohydrates over geologic timescales has been linked to sulfur incorporation during early diagenesis (Sinninghe Damsté et al. 1998, van Kaam-Peters et al. 1998, van Dongen et al. 2006), which can result in a sulfur-rich high-molecular weight (HMW) macromolecular matrix resistant to heterotrophic reworking and remineralization. Even though LMW OSC have been the most studied, due to ease of analysis, they constitute a comparatively smaller portion of sulfurized OM in the environment. HMW OSC, by contrast, make up the larger proportion of kerogen (solvent

insoluble macromolecular OM) – which is not only the largest pool of OM on Earth, but also the least well understood in terms of formation mechanisms and structural components.

Laboratory studies, the majority focused on the sulfurization of lipids, have demonstrated that sulfur incorporation into OM can occur readily under relatively mild conditions. The reaction conditions applied and sulfurization agents used vary considerably among the different studies, with most reaction conditions being atypical of those found in modern sediments. Elemental sulfur, hydrogen sulfide gas, and (poly)sulfides (from mixtures of elemental sulfur and ammonium sulfide, sodium sulfide, and/or sodium hydrosulfide) have been used as the inorganic sulfur source (Mango 1983, Lalonde et al. 1987, de Graaf et al. 1992, Rowland et al. 1993, Schouten et al. 1994, Moers et al. 1989, Kok et al. 2000, van Dongen et al. 2003, Amrani and Aizenshtat 2004a;b). Other differences are associated with the reaction medium employed, e.g., (sea) water, a two-phase system of ethyl acetate and water or pure dimethyl formamide (Fukushima et al., 1992; de Graaf et al., 1992, 1995; Schouten et al., 1993, 1994). Sometimes, a base or a phase transfer catalyst was added to the reaction mixture (Krein and Aizenshtat, 1993, 1994; Rowland et al., 1993). Despite the use of the same lipid substrate in the studies, differences in reaction conditions resulted in the formation of different sulfurized reaction products (c.f. Schouten et al. 1994, Amrani and Aizenshtat 2004). Most recently, Amrani and Aizenshtat (2004a;b) conducted sulfurization experiments on lipids under conditions that more closely resemble those in the natural environment. They were able to show that reaction rates are controlled by the concentration of both (poly)sulfides and the substrate, and also revealed the importance of the sulfide cation (e.g., sodium vs. ammonium), pH conditions, and functional group (e.g. carbonyl groups), as controlling factors for sulfur incorporation into functionalized lipids.

Comparative laboratory studies focused on the sulfurization of carbohydrates, on the other hand, are fewer (Mango 1983, Moers et al. 1998, Kok et al. 2000, van Dongen et al. 2003) and have not been as extensive as those for lipids. Mango (1983) showed the formation of OSC (thiophenes, sulfides, and sulfones) from the interaction of carbohydrates with hydrogen sulfide at elevated temperatures (140-200°C); however, the reaction conditions used were not comparable to those in the natural environment (e.g. elevated temperatures and non-aqueous). Moers et al. (1998) reacted glucose and cellulose with hydrogen sulfide and (poly)sulfides at ambient temperatures in an

aqueous environment. Analysis of the reaction products revealed that OSC were formed produced several thiophenes upon pyrolysis. Kok et al. (2000) used a (poly)sulfide mixture in seawater to sulfurize a phytoplankton concentrate (i.e., cell material of the prymnesiophyte alga *Phaeocystis*), as well as pure glucose. Sulfurization, in the case of the cell material, resulted in the loss of labile carbohydrate components through the formation of HMW sulfur-rich macromolecules. The resulting macromolecular structure was composed of (poly)sulfide cross-linked carbohydrate skeletons, which upon pyrolysis produced short-chain alkylthiophenes – with distributions similar to those found in pyrolysates of type II-S kerogens. Sulfurization of glucose under similar conditions also resulted in the formation of a macromolecular structure, which also produced short-chain alkylthiophenes upon pyrolysis. Most recently, van Dongen et al. (2003) expanded upon the previous studies by sulfurizing a number of different monosaccharides (C_4-C_6 monosaccharides) and focused on the mechanisms involved in the formation of the sulfurized material, as well as the effect of the original structure of the monosaccharide on the sulfurization process. Pyrolysis of the reaction products once again revealed the formation of alkylthiophenes, while NMR showed the importance of the carbonyl functionality in the sulfurization process. It is apparent that understanding the formation and structure of sulfur-rich macromolecular matter derived from sulfur incorporation into carbohydrates could lead to a better understanding of the formation and structural nature of kerogen.

In the present study, we add to the understanding of kerogen formation and structure by sulfurizing glucose and humic acid under environmentally relevant conditions (e.g., aqueous mixtures of (poly)sulfides, under inert atmosphere, and at 24°C). We prepared (poly)sulfide solutions using modified versions of previously published methods (van Dongen et al., 2003; Amrani and Aizenshtat, 2004) in order to determine differences in reaction conditions. We then analyzed the reaction products formed from each of the methods and also those formed from mixtures of elemental sulfur and various sulfides (ammonium $[NH_4]_2S$, sodium sulfide $[Na_2S]$, sodium hydrosulfide [NaHS]) in order to elucidate the influence of sulfide cation on the sulfurization process and the product(s) formed.

3.2 Experimental

3.2.1 Substrates

Glucose, a C_6 monosaccharide, was obtained from Sigma-Aldrich as D-(+)-GLUCOSE. Pahokee Peat Humic Acid Standard (1S103H) was obtained from the International Humic Substances Society (IHSS).

3.2.2 Preparation of (poly)sulfide solutions and sulfurization procedures

Ammonium sulfide ($[NH_4]_2S$; 20% aqueous solution), sodium sulfide (Na_2S), sodium hydrosulfide (NaHS), and elemental sulfur were obtained from Sigma-Aldrich. Sulfurization of the substrates was based on several previously published methods (outlined below). In order to elucidate any differences among the different (poly)sulfide solutions, as well as the various published methods reaction conditions we prepared (poly)sulfide solutions as outlined below.

3.2.2.1 Method 1: modified from van Dongen et al. (2003) - glucose sulfurization

Sulfurization of glucose followed the procedure of van Dongen et al. (2003), which was based on Kok et al. (2000). Briefly, glucose (ca. 200mg) was dissolved in 6 ml of solvent extracted, 18mΩ water, and magnetically stirred while being heated at 50°C under nitrogen atmosphere for four weeks after the addition of 560mg NaHS and 16mg elemental sulfur (10mmol:0.5mmol:1.0mmol; sulfide:elemental sulfur:glucose; ca. 1.6 M sulfide solution). After the reaction time ended, aliquots of each solution were taken for bulk sulfur stable isotope analysis (outlined in Chapter 4) and then residual elemental sulfur was removed by passing the solutions through a separatory funnel filled with activated (reduced) copper beads several times until no additional color change of the copper was observed. Next, the solutions were freeze dried to obtain the reaction product/sulfurized glucose. The sulfurized glucose was then homogenized by grinding in an agate mortar and pestle, flushed with N_2 and stored in the freezer until analysis.

3.2.2.2 Method 2: modified from Amrani and Aizenshtat (2004) - glucose and Pahokee Peat sulfurization

In a glovebox under nitrogen atmosphere (0.3% O_2) the (poly)sulfide solutions were prepared in serum bottles in a 1:1 stoichiometric ratio of sulfide to elemental sulfur and mixed with solvent extracted, nitrogen purged (deaerated) 18mΩ water to a concentration of ca. 0.3 M. The ammonium sulfide solution was mixed with simulated seawater (35 ppt. NaCl in solvent extracted, nitrogen purged/deaerated 18mΩ water) instead of pure 18mΩ water. The ammonium sulfide solutions were naturally buffered at pH 8-9, whereas the sodium sulfide and sodium hydrosulfide solutions were not buffered and maintained a pH between 11-12 (as determined before and after the experiment). After the initial mixing, the serum bottles were sealed under nitrogen atmosphere and removed from the glovebox. The solutions were then left to mix at room temperature (24°C) on an orbital shaker table for 30 days without any substrate addition to allow for full isotopic mixing between the sulfides and elemental sulfur.

At 30 days, glucose (ca. 200mg; molar ratio of 29mmol:29mmol:1.6mmol sulfide:elemental sulfur:glucose) was added to duplicate (poly)sulfide solutions and Pahokee Peat (ca. 1.00g) was added to a sodium sulfide solution only. Addition of substrates took place under a nitrogen atmosphere (in a glovebox with 0.3% O_2), after which the serum bottles were re-sealed under nitrogen atmosphere and removed from the glovebox. The solutions were then allowed to mix for an additional four weeks at room temperature (24°C) on an orbital shaker table. After the reaction time ended, aliquots of each solution were taken for bulk sulfur stable isotope analysis (outlined in Chapter 4) and then residual elemental sulfur was removed by passing the solutions through a separatory funnel filled with activated (reduced) copper beads several times, until no additional color change of the copper was observed. Next, the solutions were freeze dried to obtain the reaction products (sulfurized glucose and Pahokee Peat). The reaction products were then homogenized by grinding in an agate mortar and pestle, flushed with N_2 and stored in the freezer until analysis. A split of the sulfurized Pahokee Peat was additionally solvent (DCM:MeOH; 2:1, vol./vol.) extracted before analysis to remove extractable material (e.g. lipids) in order to more accurately represent non-extractable/macromolecular organic matter in environmental samples (e.g. solvent extracted residues from Mahoney Lake sediments and KCF rock samples).

3.2.3 Environmental samples

Mahoney Lake, BC, Canada is a small, shallow (maximum depth of ca. 15 m), saline kettle basin that has maintained water column euxinia (anoxic and sulfidic conditions) since its formation (ca. 11,000 YBP; Overmann et al., 1993; Heinrichs et al., 1997; Coolen and Overmann, 1998). Such modern euxinic environments serve as analogues to ancient water columns and their associated sedimentary basins, though Mahoney Lake represents an extreme end-member of euxinia. Sedimentary organic sulfur concentrations in Mahoney Lake average ca. 0.5 to 1.5 %TOS. The Jurassic aged Blackstone Band of the Kimmeridge Clay Formation, Dorset, UK was deposited under water column euxinia (van Kaam-Peters et al. 1998; van Dongen et al. 2006). Sedimentary organic sulfur concentrations within the Blackstone Band average ca. 0.3 to 2.5 %TOS. Solvent extracted sediment residues from Mahoney Lake and solvent extracted rock residues from the Blackstone Band of the Kimmeridge Clay Formation were thus analyzed comparison to laboratory sulfurized substrates. The environmental sediment and rock residues constitute HMW non-extractable/macromolecular OM found in the environment.

3.2.4 Fourier Transform Infrared Spectroscopy (FT-IR)

Freeze-dried, homogenized, glucose reaction products as well as solvent extracted sulfurized Pahokee Peat, Mahoney Lake sediments and KCF rock samples were analyzed at the University of Manchester using a PerkinElmer® Frontier™ 400 FT-IR/NIR spectrometer equipped with a Universal Attenuated Total Reflectance (UATR) sampling accessory. Sample spectra were obtained in the mid infrared region (MIR) with a scan resolution of 4 cm^{-1} and with 16 scans in the range of 4000-650 cm^{-1}. Background was measured and removed before each spectrum collection. A very small amount of sample was loaded onto the UATR plate and pressed to a thin film after which sample spectra were collected. Spectra were collected in duplicate and those shown are the averaged spectra. Peak assignment and identification of functional groups were based on comparison to literature data (Bruno and Svoronos 2005).

3.2.5 Derivatization of glucose and sulfurized reaction products

To check reaction products for the presence of unsulfurized glucose, portions of each were derivatized to their trimethylsylil esters using N, O-Bistrifluoroacetamide (BSTFA). Approximately 100 mg of sulfurized reaction product was weighed into a vial, 100 uL BSTFA and 100 uL of pyridine were then added. The vial was flushed with N_2, capped and allowed to react at 60°C for 45min. After the reaction time ended, residual BSTFA and pyridine were removed under a gentle stream of N_2. Pure glucose (ca. 100mg) was derivatized in the same manner described and used as an external standard. The samples were then dissolved in a known volume (1000 uL) ethyl acetate before GC/MS analysis.

3.2.6 GC/MS analysis of glucose and sulfurized reaction products

Derivatized samples were analyzed at the University of Pittsburgh using a Thermo ISQ QD single quadrupole mass spectrometer connected to a Thermo Trace 1310 gas chromatograph. Aliquots (1 uL) of each fraction were introduced via an SSL injector operated in splitless mode held at 300°C. The gas chromatograph was programmed from 70°C (1 min) to 130°C at a rate of 10°C min^{-1}, and then to 320°C (15 min) at a rate of 4°C min^{-1}. Separation was achieved using an Agilent J&W DB-5 (30m x 0.32mm x 0.25µm) capillary column with a helium flowrate of 2ml/min. The mass spectrometer transfer line was held at 320°C and ion source at 275°C. Compounds were ionized at 70 eV and mass analyzed over a range of m/z 50-600 with a scan rate of 4 scans per second. Compounds of interest were identified on the basis of relative retention time and on the basis of mass spectral data in comparison with literature data.

3.2.7 Online flash pyrolysis-gas chromatography/mass spectrometry (Py-GC/MS)

Py-GC/MS was conducted at the University of Manchester using an Agilent 5875C inert XL EI/CI MSD connected to an Agilent 7890A GC equipped with a CDS Analytical Pyroprobe 5000 series pyrolysis unit. Small amounts of the freeze-dried, homogenized glucose reaction products and

solvent extracted sulfurized Pahokee Peat were packed into pre-cleaned quartz glass tubes and introduced into the pyrolysis unit, where each sample was heated from 300°C (1 sec.) to 600°C (20 sec.) at a rate of 20°C/millisecond. The desorbed fragments were flushed into the capillary column using helium as a carrier gas. The gas chromatograph was programmed from 40°C (5 min) to 320°C (10 min) at a rate of 4°C min^{-1}. Separation was achieved using a Phenomenex Zebron™ ZB-5MS (30m x 0.25mm x 0.25µm) capillary column with a helium flowrate of 2ml min^{-1}. Compounds were ionized at 70 eV and mass analyzed over a range of m/z 50-650 with a cycle time of 1.8s (resolution 1000). Pyrolysates were identified by mass spectral comparison to literature values and normalized to the levoglucosan peak area (produced during pyrolysis of carbohydrates).

3.3 Results

3.3.1 Sulfurization solutions and reaction products

Each of the (poly)sulfide solutions displayed a range of color (light yellow – dark yellow/orange) upon mixing and the colors of the reaction products obtained from the solutions also varied with (poly)sulfide solution (Figure 8). The amount of sulfur (%TOS) incorporated into glucose depends on reaction conditions. Glucose sulfurized according to Method 1 had the greatest wt% TOS at 21.6%, then Method 2 (poly)sulfide solutions: NaHS at 12.4%, Na_2S at 11.2%, and lastly $(NH_4)_2S$ at 0.85% (Figure 9). The $(NH_4)_2S$ (poly)sulfide solution was the only solution where a small amount of glucose remained unsulfurized (2-5% of glucose was recovered) – in all other solutions 100% of glucose was sulfurized (no glucose was recovered upon derivatization of the reaction products). Pahokee Peat incorporated ca. 23x more sulfur compared to its initial sulfur content, going from 0.7 %TOS to 16.4 %TOS (Figure 9).

3.3.2 FT-IR – sulfurized reaction products

Peak center, identification and alternative identification for each of the reaction products spectra are given in Table 2.

3.3.2.1 Glucose

Overall, we observe a transformation from the glucose structure to a more constrained structure with the loss of major functional groups (Figure 10). The disappearance and appearance of bands largely depends on reaction conditions. In all reaction products there is a disappearance and/or broadening of hydroxyl (-OH) and C-H bands (3500 - 3000 cm^{-1} and just below 3000 cm^{-1}, respectively). In all reaction products, except $(NH_4)_2S$ reaction products, the appearance of strong peaks at 1400 and 880 cm^{-1} likely indicate sulfoxide (S=O) or thiocarbonyl (C=S) groups and CH_2-S-CH_2 bonds, respectively. Peaks at 1100 and 1000 cm^{-1} may be related to S-S=O and S-O bonded reaction products. The band at 1600 cm^{-1} likely results from either S-C=C groups or shifted carbonyl (C=O) groups. In Na_2S and NaHS reaction products the weak peak ca. 2600 cm^{-1} may be related to thiol (S-H) groups. $(NH_4)_2S$ reaction products lack strong absorbances in the mid-IR range, although weak absorbances are observed in the C-N region of amines.

Table 2. FT-IR peak functional group assignments

Peak center (cm^{-1})	Peak Intensity	Assignment	Alternative (intensity)
3500	variable & broad	-OH (hydroxyl)	
2600	weak	S-H (thiol)	
1600	weak	S-C=C	
1500	strong	Z-C=S (thiocarbonyl)	
1400	strong	S=O (sulfoxide)	Z-C=S (medium)
1200; 1100	strong	S-S=O	S=C-Z (medium)
1000	strong	S-O	Si-O (strong)
700-600	weak	C-S in S-S	

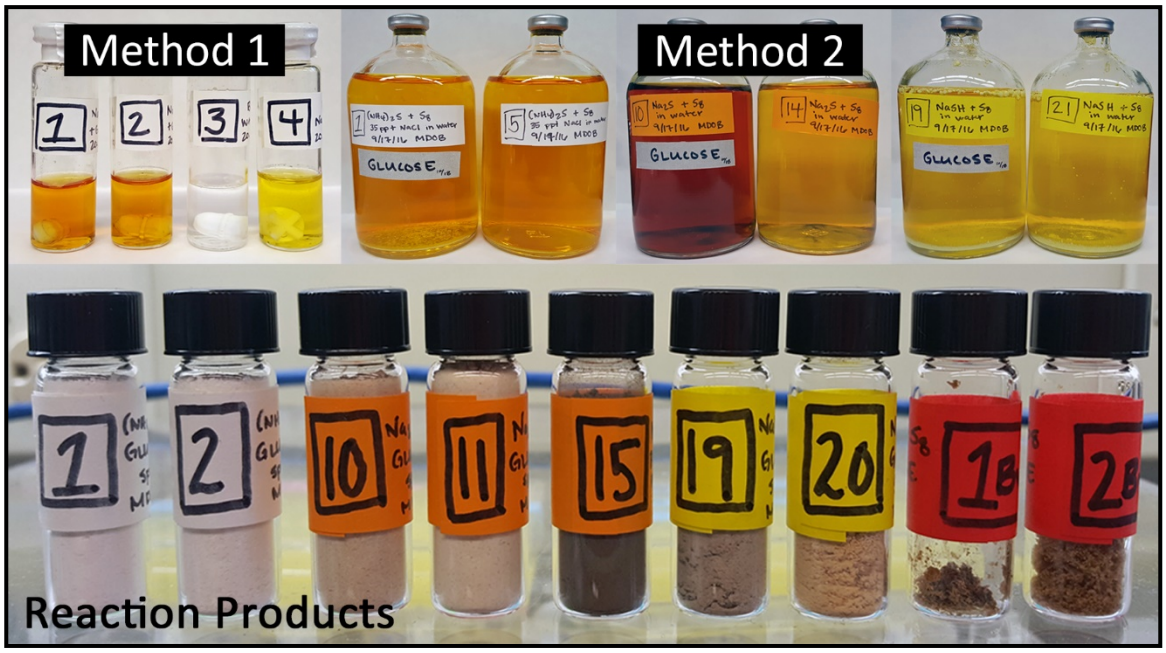

Figure 8. (Poly)sulfide solutions and reaction products. Upper left: Method 1 (poly)sulfide solutions after 4 weeks reaction time, in the following order - glucose addition, glucose addition, blank (water), blank (no glucose addition (poly)sulfide solution). **Upper right**: Method 2 (poly)sulfide solutions after 4 weeks reaction time, in the following order – $(NH_4)_2S$ (poly)sulfide solution with glucose addition and without, Na_2S (poly)sulfide solution with glucose addition and without, NaHS (poly)sulfide solution with glucose addition and without. **Bottom**: reaction products from both methods – the first seven vials are from Method 2 and the last two vials are from Method 1. White vial labels 1 and 2 are reaction products from $(NH_4)_2S$ (poly)sulfide solutions, orange labels 10 and 11 are reaction products from Na_2S (poly)sulfide solutions, orange label 15 is the reaction product of Pahokee Peat and Na_2S (poly)sulfide solution, yellow labels 19 and 20 are the reaction products from NaHS (poly)sulfide solutions. Red vial labels 1 and 2 are the reaction products from NaHS (poly)sulfide solutions using Method 1 conditions.

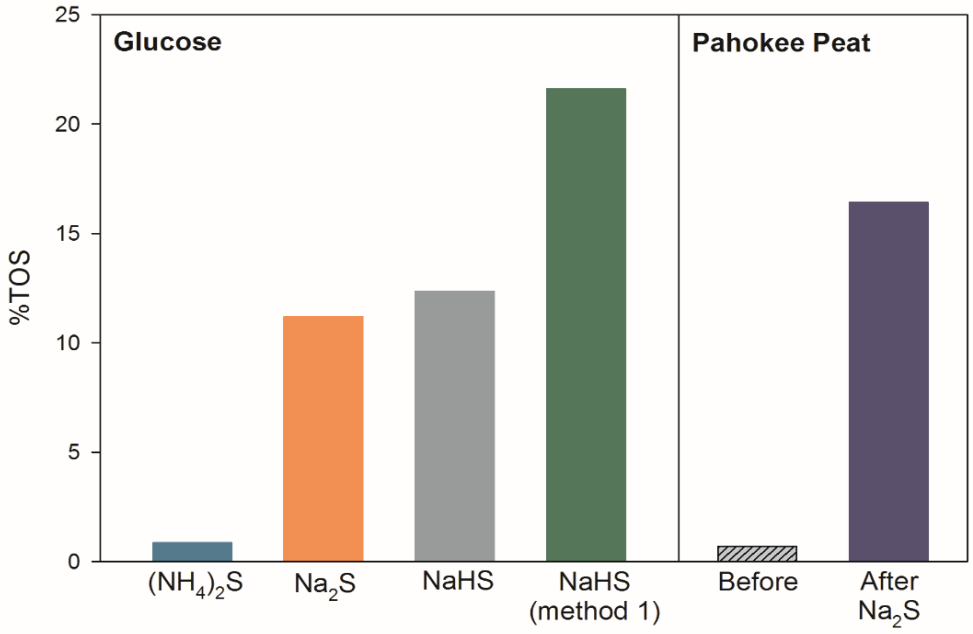

Figure 9. Weight % Total Organic Sulfur (%TOS) measurements. The amount of sulfur incorporated into glucose depends on reaction conditions. %TOS ranges from less than 1% to greater than 20% for glucose sulfurized using the various sulfide reactants. Pahokee Peat reacted with the Na_2S (poly)sulfide solution, incorporating ca. 20 times the amount of sulfur it originally contained.

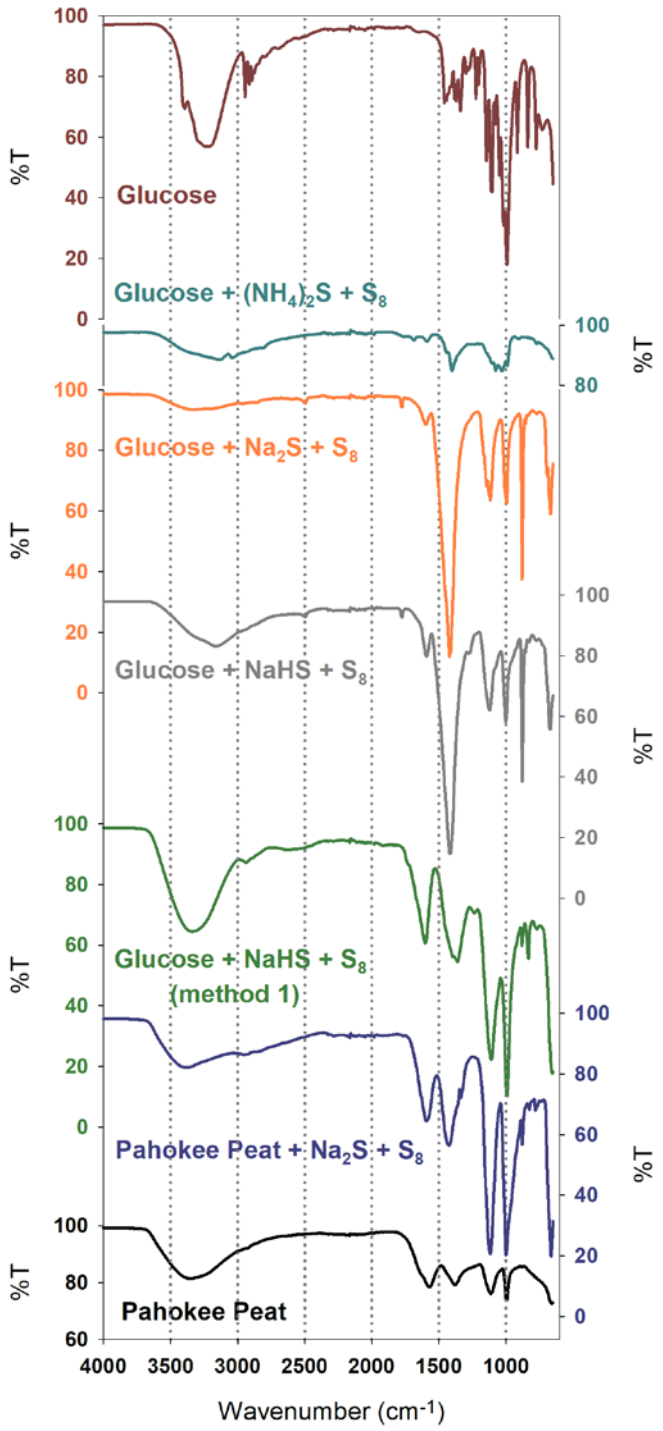

Figure 10. FT-IR spectra of the reaction products between glucose, Pahokee Peat, and various sulfides. Overall there is a disappearance and broadening of the hydroxyl (-OH) group bands and C-H bond peaks. Intensified peaks at 1400 cm^{-1} are indicative of sulfoxide (C=O) and/or thiocarbonyl (C=S) and at 880 cm^{-1} CH_2-S-CH_2 bonds. Peaks at ca. 1600 cm^{-1} likely indicate S-C=C groups. Strong peaks at 1100 and 1000 cm^{-1} are most related to S-S=O and S-O bonding, although strained CH_2-CHO bonds due to sulfur incorporation could also appear here.

3.3.2.2 Pahokee Peat

In sulfurized Pahokee Peat we observe broadening in the -OH band (3500 - 3000 cm^{-1}) region along with very weak peaks just below 3000 cm^{-1} suggestive of C-H bonds. The peak at 1600 cm^{-1} is likely related to S-C=C groups or possibly shifted C=O groups (Figure 10). Intensified peaks at 1400 cm^{-1} and below 1000 cm^{-1} are indicative of S=O or C=S groups and CH_2-S-CH_2 bonds, respectively, while intensified peaks between 1100 and 1000 cm^{-1} likely result from S-S=O and S-O bonds and are likely influenced by constrained CH_2-CHO groups in the macromolecular matrix due to S-bonding. These features are similar to sulfurized glucose – especially when compared to glucose sulfurized using Method 1 (Figure 10).

3.3.3 FT-IR – environmental samples

In both Mahoney Lake and Kimmeridge Clay Formation (KCF) residues there is a loss of the major functional groups as evidenced by the weakening and broadening of -OH and C-H bands (Figure 11). The peak at 1600 cm^{-1} is possibly from S-C=C groups or shifted C=O groups. In Mahoney Lake residues the peak just below 1500 cm^{-1} intensifies and shifts to ca. 1450 cm^{-1} as the sediment ages, this could be due to an increasing contribution of C=S and/or S=O groups through time. The peak at 880 cm^{-1}, indicative of CH_2-S-CH_2 bonding, also intensifies as the sediment ages. The peak just before 1000 cm^{-1} likely indicates complex intramolecular interactions resulting from S=O and/or S=C bonding coupled with straining of C-C and C-H bonds, as well as potential contributions from silicate (Si-O) bonding. In KCF residues, we observe similar features as those found in the sulfurized reaction products as well as in Mahoney Lake residues (Figures 10 and 11). KCF FT-IR spectra additionally show weak peaks above 3500 cm^{-1}, which indicate aromatic structures (Figure 11). Peak center and identification are given in Table 2.

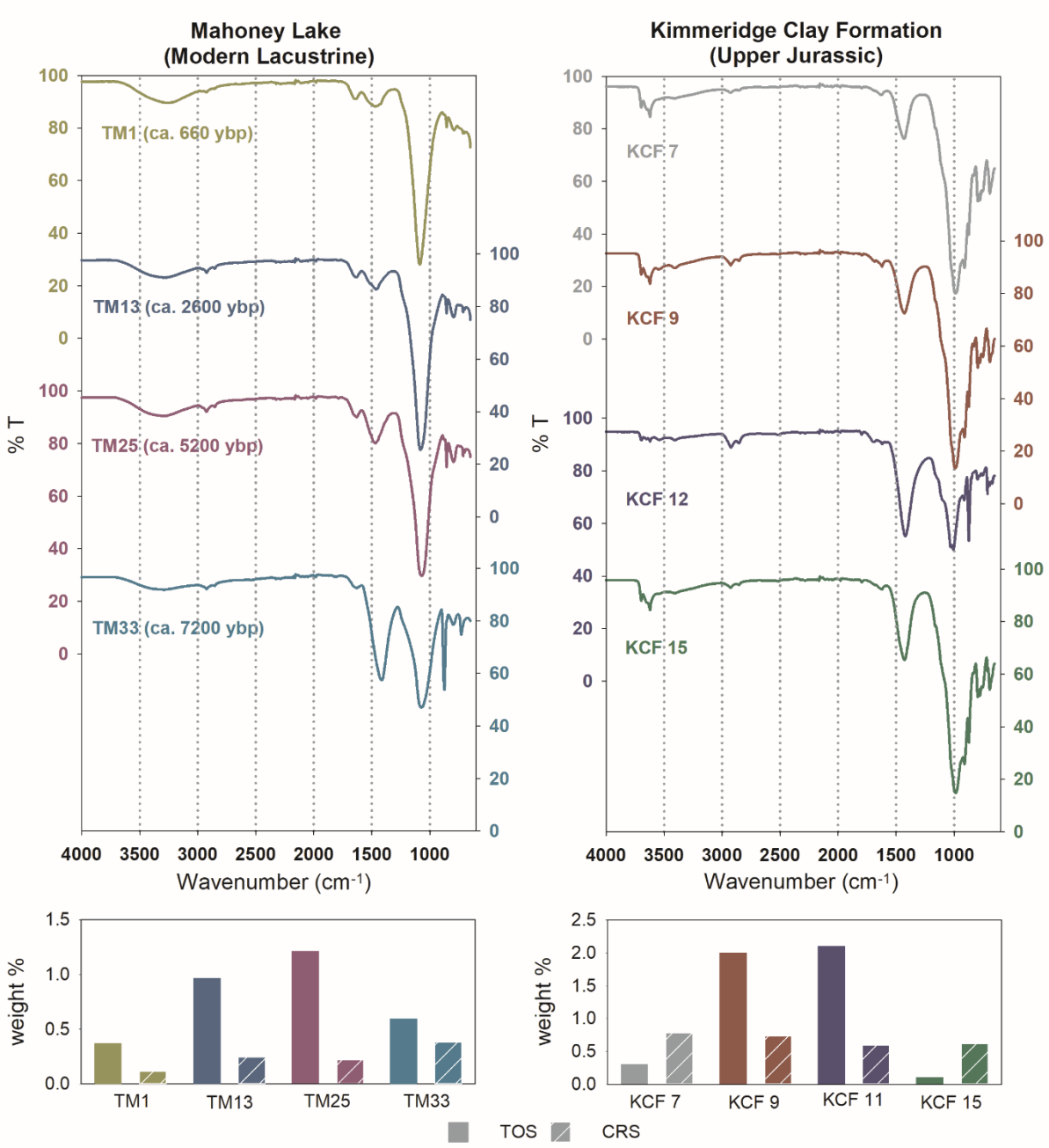

Figure 11. FT-IR spectra and weight % TOS and CRS of sediment and rock residues from modern and ancient euxinic systems. Top: Mahoney Lake and Kimmeridge Clay Formation (KCF) residues show similar structural features to laboratory sulfurized substrates. In Mahoney Lake residues, the peak at ca. 1500 cm^{-1} intensifies and shifts to ca. 1450 cm^{-1} as the sediment ages, this could be due to an increasing contribution of thiocarbonyl (C=S) groups through time. The peak at 880 cm^{-1}, indicative of CH_2-S-CH_2 bonding, also intensifies as the sediment ages. KCF residues are similar to Mahoney Lake residues, but show weak peaks above 3500 cm^{-1}, which indicate aromatic structures. The peaks at ca. 1000 cm^{-1} likely indicate complex intramolecular interactions resulting from straining of C-C and C-H bonds, as well as potential contributions from silicate (Si-O) bonding. **Bottom**: Total Organic Sulfur (TOS; solid bars) and Chromium Reducible Sulfur (CRS; patterned bars) for each of the samples, represented as weight percent dry sediment and rock.

3.3.4 Py-GC/MS

The (poly)sulfide solutions produced different flash pyrolysates (Figure 12). All pyrolysis-generated compounds are normalized to the levoglucosan peak area (which is also produced during pyrolysis). The $(NH_4)_2S$ reaction products formed few thiophenes, but did produce many nitrogen containing compounds. The Na_2S reaction products generated few S-containing pyrolysates (mostly consisting of methyl disulfide), whereas the NaHS reaction products generated several alkylthiophenes, along with thiiranes, and dithianes.

3.4 Discussion

3.4.1 Importance of reaction conditions – influence of (poly)sulfide cation, pH, temperature, and concentration

Since previous studies have shown the importance of reaction conditions on sulfur incorporation into functionalized lipids (de Graaf et al. 1992, Rowland et al. 1993, Krein and Aizenshtat 1993; 1994 Schouten et al. 1994) and relationship to natural sulfurization in marine sediments, we wanted to assess these same reaction conditions on carbohydrates and dissolved organic matter (DOM) sulfurization. The degree of sulfur incorporation and structural nature of the glucose reaction products is related to the reaction conditions. Reaction of glucose with the three (poly)sulfide solutions resulted in varying amounts of sulfur incorporation [12.4%, 11.2%, and 0.85% TOS for NaHS, Na_2S and $(NH_4)_2S$ (poly)sulfide solutions, respectively]. Thus, the sulfide cation exerts some control on the amount of sulfur incorporated into glucose. This finding is in contrast to (poly)sulfide reaction with functionalized lipids sulfurized under the same conditions – where it was found that Na_2S was less reactive towards lipids (less sulfur incorporated) than $(NH_4)_2S$ (Amrani and Aizenshtat, 2004), but is likely related to reaction mechanism(s) specific to the $(NH_4)_2S$ (poly)sulfide solutions (discussed below). Overall, we find that under the same

reaction conditions, glucose incorporates less sulfur than functionalized lipids (0.85 - 12.4% vs. 5.9 - 29.9%; Amrani and Aizenshtat, 2004) in the formation of macromolecular organic matter.

Additionally, each (poly)sulfide solution maintained a different pH related to the (poly)sulfide cation (buffer was not added to the solutions). pH exerts an important influence on the mechanism(s) of polysulfide incorporation into OM (Krein and Aizenshtat, 1993) and also determines the polysulfide speciation. The length of polysulfide sulfur chains decreases with increasing pH. At higher (more basic) pH, like those in Na_2S (pH 12-13) and (poly)sulfide solutions, the majority of polysulfide species are S_2^{2-} and S_3^{2-}, while at lower (but still basic) pH levels, such as those in $(NH_4)_2S$ solutions (pH 8-9), the longer chain lengths dominate (i.e. S_4^{2-}, S_5^{2-}, and S_6^{2-} species). It has additionally been shown that nucleophilicity, and thus reactivity, increases with increasing polysulfide sulfur chain length. Therefore, we may expect greater reactions and sulfur incorporation at lower pH where longer polysulfide chain lengths dominate, as was found in the reaction of functionalized lipids (Amrani and Aizenshtat, 2004). At first glance, sulfur incorporation into glucose is seemingly unrelated to pH – although we did not test the reaction for the same reactant sulfide at varying pH [e.g. Na_2S (poly)sulfide solutions at a lower pH than 12-13]. At the lowest pH [$(NH_4)_2S$; pH 8-9] little sulfur is incorporated, whereas at higher, more basic, pH (NaHS; (pH 10-11) incorporates slightly more (ca. 1%) than the most basic solution (Na_2S; pH 12-13). That said, the effect of pH may be masked by the reaction mechanism and competition between reactions of ammonia and polysulfide nucelophiles (discussed below and in section 3.4.2) at the lowest pH [i.e. the $(NH_4)_2S$ (poly)sulfide solution].

$(NH_4)_2S$ reaction products lack absorbance in the mid-IR range suggesting that the macromolecular structure lacks net dipole moments. This is possibly due to reaction with nitrogen – producing a product with weak absorbance (Figure 10). Mass spectra obtained from the online pyrolysis of the reaction products produced from $(NH_4)_2S$ (poly)sulfide solutions reveal several nitrogen-containing compounds. Along these same lines, bulk nitrogen analysis of the reaction products shows total nitrogen (%TN) to be 2 wt%, which is more than 2x the amount of %TOS.

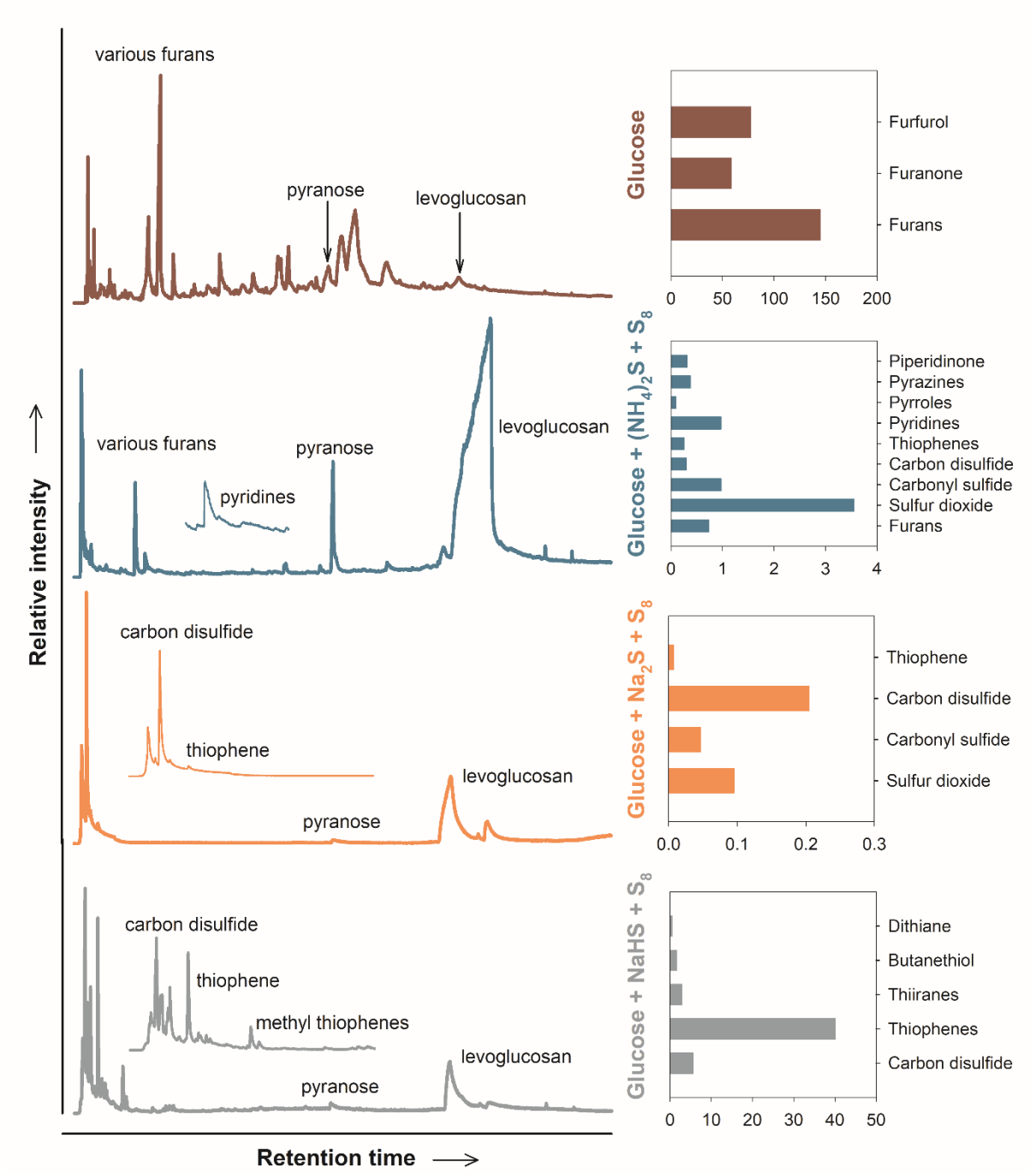

Figure 12. Mass spectra (total ion chromatograms – TIC) and normalized abundances of flash pyrolysates from sulfurized glucose. The compounds generated during online pyrolysis vary with reaction conditions. Pyrolysis generated compounds are normalized to the levoglucosan peak area (which is also produced during pyrolysis of carbohydrates). The $(NH_4)_2S$ reaction products formed myriad nitrogen-containing compounds and few sulfur-containing compounds. The Na_2S reaction products also produced few sulfur-containing compounds, whereas the NaHS reaction products generated the full suite of alkylthiophenes, along with thiiranes, and dithianes.

Thus, there is certainly competition between nitrogen and sulfur in the formation of macromolecules in this study and possibly of macromolecular organic matter in the environment, though this would highly depend on environmental conditions (discussed in the following sections).

Comparison of NaHS (poly)sulfide reactions with glucose at lower molar ratios of reactant and substrate (Method 2) to reaction of NaHS at higher temperature and molar ratio of reactants to substrate (Method 1) shows that a greater amount of sulfur is incorporated (Figure 9) under higher temperature and molar ratios (Method 1). This agrees with previous studies on lipids (Amrani and Aizenshtat 2004), where higher concentrations of polysulfides resulted in greater sulfur incorporation. Additionally, comparison of the FT-IR spectra of reaction products from the two methods (low/high temperature and polysulfide concentration) show that the structures of the reaction products differ (Figure 10). These observations suggest that the reaction mechanism(s) change as (poly)sulfide concentration and/or temperature increases (discussed in section 3.4.2).

3.4.2 Mechanisms of sulfurization reactions – reactivity of functional group(s)

In aqueous solutions of $(NH_4)_2S$, the hydrosulfide ion cannot be deprotonated to an appreciable amount by ammonia (NH_3^+). Accordingly, such solutions mainly consist of a mixture of NH_3^+ and $(NH_4)SH^-$. Reaction between amines and carbonyl compounds such as sugars has a long-standing interest in the food and medical fields because of its relevance to food flavor and coloring, the digestibility of food, and associated implications for several diseases due to the toxicity of some of the produced compounds. The complex set of chemical reactions that occurs between sugars and amino compounds (e.g. ammonia, amino acids, proteins or polypeptides) is collectively known as the Maillard reaction. In the presence of hydrogen sulfide and ammonia, the Maillard reaction will produce heterocyclic compounds (e.g. pyranones, pyrroles, and thiophenes; Nursten 2005), similar to the reaction products of glucose and $(NH_4)_2S$ observed in the current study. Therefore, we assume similar Maillard reaction occurs between glucose and the $(NH_4)_2S$ (poly)sulfide solution. A simplified Maillard reaction schematic with reactions pertinent to the current study is presented in Figure 13 and was modified from Hodge 1953 and Nursten 2005. Reaction with nitrogen in $(NH_4)_2S$ (poly)sulfide solutions was also observed in lipids (Amrani and

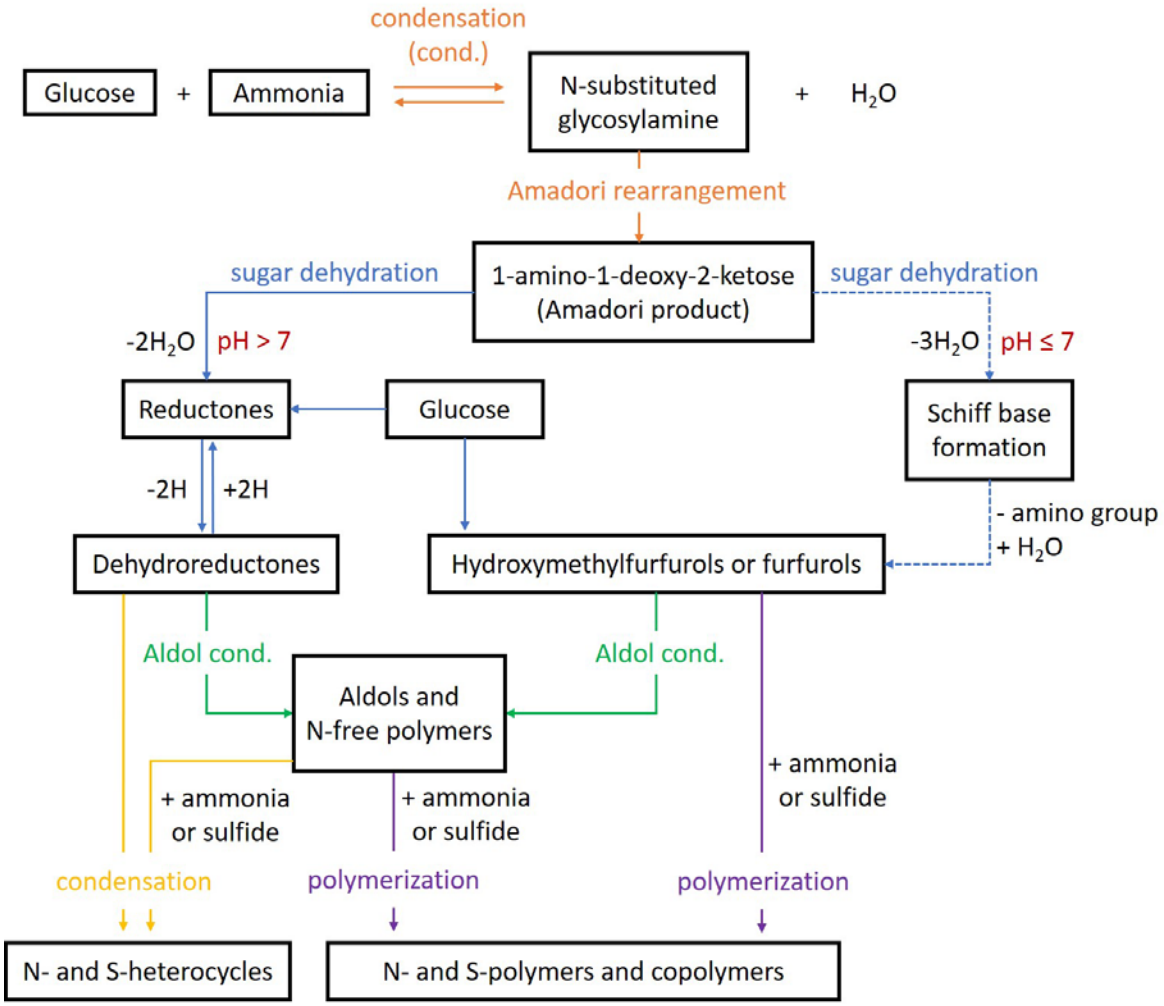

Figure 13. Simplified Maillard reaction schematic for the reaction between glucose and $(NH_4)_2S$ (poly)sulfide solution. Reactions may start with sugar-ammonia condensation, followed by Amadori rearrangement, then sugar dehydration producing reductones and dehydroreductones and possibly Schiff base formation, though Schiff base formation probably proceeds at a slower rate due to the basic pH of the solution. Aldol condensation from dehydroxyreductones and hydroxymethhylfurfurols/furfurols produces aldols and nitrogen-free polymers. Finally, polymerization of aldols and bydroxymethylfurols/furfurols in the presence of ammonia and sulfide produces N- and S-polymers and formation of heterocyclic nitrogen and sulfur compounds results from condensation of aldehyde-amines (-sulfides). Note that reductones and hydroxymethylfurfurols may also be produced directly from glucose under basic conditions and further react from there, which may explain the reaction mechanisms occurring in the other (poly)sulfide solutions not containing nitrogen. Not shown are glucose fragmentation products that may additionally react to form N- and S-compounds and (co)polymers under basic conditions.

Aizenshtat, 2004) where it was proposed that Michael addition forms the first C-S bond, followed by an intermediate attack of ammonia forming a Schiff base and subsequent elimination of the carbonyl oxygen. This is then followed by simultaneous attack of two polysulfide anions at the C-1 position and elimination of ammonia to produce polysulfide crosslinked oligo-polymers. This type of reaction mechanism may also occur here, but likely proceeds at a slower rate as Schiff base formation is less favored at basic pH. Expanding upon the previous study, Amrani et al. 2007 found that there is competition between ammonia/ammonium and polysulfide nucleophiles at the carbonyl position in functionalized lipids, forming N- and S-crosslinked oligo-polymers. Moreover, in the case of reaction of functionalized lipids, there was an observed synergistic effect between ammonia and polysulfides as reaction rates were very high (i.e. complete within 1h) in the presence of ammonia, while reaction rates slowed dramatically in the absence of ammonia (i.e. days to reaction completion). A synergistic effect is not observed in the current study, in fact, it appears that ammonia outcompetes polysulfide nucleophiles in reaction with glucose based on %TN vs. %TOS, FT-IR structures, and pyrolysates of reaction products. That said, nitrogen incorporation (N-crosslinking) may be an environmentally relevant process and could provide insight into past N-cycling (discussed in section 3.2.4).

Sodium hydrosulfide (NaHS) is the conjugate acid of sodium sulfide (Na_2S). It is perhaps unsurprising then, that reaction of glucose and (poly)sulfide solutions of Na_2S and NaHS produce such similar FT-IR spectra (Figure 10). Na_2S and NaHS reaction products show weakening of the –OH band and the appearance of a pronounced peak at 1400 cm^{-1}, indicating sulfur reaction with oxygen, forming sulfoxide groups (S=O). Because the peaks at 1100 and 1000 cm^{-1} are not as pronounced (of medium intensity), we attribute these to thiocarbonyl (S=C) groups. Thiocarbonyl groups suggest sulfur reaction and incorporation into carbonyl groups of glucose, which is in line with previous studies on lipids (Amrani and Aizenshtat 2004) and carbohydrates (van Dongen et al. 2003). What is more surprising is that the reaction products produce very different pyrolysates (Figure 12). The reasons for this remain unclear, but may be related to differences in the fragmentation of glucose under slightly different pH and subsequent reaction pathways (e.g. aldehyde-sulfide condensation versus polymerization).

Comparison of FT-IR spectra of the reaction products sulfurized via NaHS (poly)sulfides under different reaction conditions (Method 1 vs. Method 2) reveals that the mechanism(s) of sulfur incorporation are different (Figure 10). Under Method 1 conditions there is a greater contribution of S-C-C, S-S=O, and S-O, as indicated by the intensified peaks at 1600, 1100, and 1000 cm^{-1}, respectively. The peak at 1400 cm^{-1} is reduced (medium intensity) under Method 1 conditions and is likely indicative of thiocarbonyl (S=C) groups, rather than sulfoxide (S=O) groups, attributed to the strong intensity peak in NaHS reaction products under Method 2 conditions. Heating glucose with a basic solution (Method 1 conditions) likely leads to bond cleavage and/or fragmentation via retroaldol reactions and subsequent recombination followed by aldol reaction. This process generates two, three-carbon compounds from glucose with strong reductive properties (e.g. glycolic aldehyde, triose, tetrose, formaldehyde, glycolic acid) that may condense with each other producing resinous structures which give a dark brown color. This process may be the reason for the dark brown color (Figure 8) and resinous nature of reaction products sulfurized under Method 1 conditions. The reaction between sulfur and the three-carbon compounds (Method 1) may reflect the reactions occurring between sulfur and humic substances in Pahokee Peat (Method 2) giving rise to their similar FT-IR spectra (Figure 10). The reaction of Pahokee Peat with Na_2S (poly)sulfide solution produces a different structure from its reaction with gaseous H_2S (cf. Heitmann and Blodau 2006), highlighting the importance of reaction conditions when simulating environmental conditions. This additionally shows that dissolved organic matter may undergo similar reaction mechanisms during sulfurization to laboratory sulfurized glucose.

Overall, structural analysis via FT-IR shows that in addition to carbonyl (C=O) reactivity, hydroxyl (-OH) reactivity plays an important role in sulfur incorporation and S-crosslinking in the formation of macromolecular structures. The disappearance of the hydroxyl (-OH) band in the FT-IR spectra (Figure 10) confirms that the hydroxyl functional group is susceptible to sulfur attack and subsequent S-binding. This was originally suspected by van Dongen et al. (2003), as sulfurization of the hydroxyl group had to be invoked in order to account for the formation of sulfur-rich macromolecular material observed in their experiments.

3.4.3 Geochemical implications – kerogen formation and evolution

Our results provide further confirmation that sulfur incorporation into organic matter occurs under environmentally relevant conditions (e.g. aqueous mixtures of (poly)sulfides, under inert atmosphere, and at 24°C) forming sulfur-crosslinked macromolecular organic matter. Even though it has been previously demonstrated that under similar reaction conditions aldehyde and keto groups react much faster than alcohols with polysulfide ions (Schouten et al., 1993, 1994; Schneckenburger et al., 1998), it is clear from structural data presented here that hydroxyl groups can play a significant role in the formation of macromolecular material. This finding is not only important for understanding early diagenetic sulfurization mechanisms but also kerogen formation and maturation.

Environmental samples from Mahoney Lake (a permanently stratified euxinic basin; ca. 0.5 to 1.5 %TOS) and from the Jurassic aged Kimmeridge Clay Formation (epeiric sea with photic zone euxinia; ca. 0.3 to 2.5 %TOS) show pronounced peak stretches below 1500 cm^{-1} and loss of major functional groups, similar to what we observe in laboratory sulfurized glucose and Pahokee Peat (Figure 11). This observation provides evidence that sulfur incorporation into OM and formation of sulfur-rich kerogen may follow a similar reaction pathway.

As in previous studies (e.g. Amrani et al 2007), we find that the reaction of ammonia with organic matter is likely a significant process in the accumulation and preservation of organic nitrogen in the geologic record. This process may be especially important in anaerobic depositional environments where relatively high concentrations of ammonia and reactive organic matter are expected (e.g. high productivity marine shelves, restricted marine basins, anaerobic/euxinic lacustrine systems).

3.5 Conclusions

The present study demonstrates that sulfur incorporation into glucose and Pahokee Peat results in the formation of macromolecular structures. The sulfurization reaction happens on relatively fast

timescales and at low temperatures relevant to marine conditions. Structural analysis via FT-IR indicates that in addition to the carbonyl functionality, the hydroxyl group(s) has (have) a fundamental role in the formation of (poly)sulfide cross-linked carbohydrates and sulfur-rich macromolecular OM in the environment. As with functionalized lipids, controlling factors for sulfur incorporation into glucose and humic acid appear to be related to the molar ratio of (poly)sulfides to substrate, pH, sulfide cation, and functional group(s). Additionally, structural similarities among laboratory sulfurized glucose and Pahokee Peat and environmental samples demonstrates that similar reaction mechanisms occur during natural sulfurization processes, which is important for our understanding of kerogen formation and evolution, from early diagenesis to catagenesis.

Differences in the reaction products of glucose and various (poly)sulfide solutions highlight the importance of reaction conditions when simulating environmental conditions. Ammonia outcompetes polysulfide nucleophiles in the reactions presented here, the relative importance of which remains to be fully evaluated in the environment.

Results from this study will be useful for evaluating environmental samples, especially when combined with other measurements.

4.0 Laboratory low-temperature sulfurization of carbohydrates and dissolved organic matter using different sulfides. Part II: Sulfur isotope dynamics

4.1 Introduction

During early diagenesis, reaction of reduced sulfur species with reactive organic matter produces organic sulfur compounds (OSC) that are preserved through geologic time. This has led to myriad studies focused on understanding the origins, formation mechanisms, and isotopic composition of OSC (Sinninghe Damsté et al. 1989, Sinninghe Damsté and de Leeuw 1989, Aizenshtat et al. 1995, Krein and Aizenshtat 1995, Schouten et al. 1998, Werne et al. 2008, Amrani and Aizenshtat 2004, Amrani 2014, Greenwood et al. 2015, Raven et al. 2015;2016;2018). Up to now, much focus has been given to understanding the formation of low-molecular weight (LMW) compounds (i.e. the reaction products of reduced sulfur species and functionalized lipids), as laboratory experiments have shown that reactions between reduced sulfur species (e.g. polysulfides) and functionalized lipids (e.g. ketones, aldehydes, and compounds containing double bonds) yield OSC that are similar to those found in both recent and ancient marine sediments. More recently, the sulfur isotope compositions of such compounds have gained interest as new analytical advances have made their measurement possible (Amrani et al. 2009). Additionally, laboratory experiments have shown that the fractionation associated with sulfur incorporation into functionalized lipids is ca. 4-5‰ (Amrani and Aizenshtat, 2004), whereas reduced sulfur incorporation into organic matter was generally considered to have negligible $\delta^{34}S$ fractionation (e.g. Mossmann et al. 1991, Werne et al. 2003). Bearing in mind that LMW compounds constitute a minor fraction of bulk organic sulfur, there is still much to be explored in regards to bulk organic sulfur formation, occurrence, and isotopic composition.

Several studies have shown that in addition to the sulfurization of lipids, carbohydrates are also readily sulfurized (hours – weeks; Moers et al. 1998, Kok et al. 2000, van Dongen et al. 2003). Although carbohydrates are considered to be readily remineralized, reaction with sulfur acts to preserve carbohydrates over geologic timescales (Sinninghe Damsté et al. 1998, van Kaam-Peters

et al. 1998, van Dongen et al. 2006). The sulfurization of carbohydrates results in high-molecular weight (HMW) macromolecular organic matter which has been shown to be structurally similar to sulfur-rich kerogen – constituting the largest pool of bulk organic sulfur in the natural environment. Here, our focus is on understanding the sulfur isotopic fractionation associated with sulfur incorporation into carbohydrates and dissolved organic matter (humic acid) under conditions prevailing in marine environments (i.e. saline, aqueous, and low-temperature). We also study the effect of sulfide cation on polysulfide speciation and subsequent sulfur isotope fractionation upon sulfurization of carbohydrates. The results are then discussed in context with sulfur-rich macromolecular organic matter (i.e. kerogen) in the environment.

4.2 Experimental

4.2.1 Substrates, preparation of (poly)sulfide solutions, and sulfurization procedures

Glucose was obtained from Sigma-Aldrich as D-(+)-GLUCOSE. Pahokee Peat Humic Acid Standard (1S103H) was obtained from the International Humic Substances Society (IHSS). Procedures for the preparation of (poly)sulfide solutions and subsequent sulfurization reactions have been previously described in detail (see chapter 3). In short, (poly)sulfide solutions were prepared according to slight modifications of two different methods (briefly described below).

Method 1 conditions after van Dongen et al. 2003: ca. 1.6M sulfide solution; 10mmol:0.5mmol:1.0mmol sulfide:elemental sulfur:glucose; 50°C for 4 weeks

Method 2 conditions after Amrani and Aizenshtat 2004: ca. 0.3M sulfide solution; 29mmol:29mmol:1.6mmol sulfide:elemental sulfur:glucose; 24°C for 4 weeks

Glucose sulfurization took place according to both methods and Pahokee Peat was sulfurized under Method 2 conditions using sodium sulfide as the sulfide for the (poly)sulfide solution. After the reaction time was reached, aliquots of the (poly)sulfide solutions were taken for bulk inorganic sulfur isotope analysis (Figure 14). Elemental sulfur was removed from the remaining solution(s)

and the reaction products (sulfurized glucose and Pahokee Peat) were isolated by freeze drying. After freeze drying, the reaction products were homogenized and splits were taken for bulk sulfur stable isotope analysis. These splits allow for $\delta^{34}S$ measurements of total organic sulfur obtained from each (poly)sulfide solution.

4.2.2 Precipitation of (poly)sulfide solutions for total reactive sulfur (TRS) analysis

Duplicate aliquots (0.5ml) of each (poly)sulfide solution were taken from the sealed serum bottles with a gas tight syringe and immediately injected into a nitrogen purged, septum sealed vial containing 2ml of 3% silver nitrate ($AgNO_3$) – 10% ammonium hydroxide (NH_4OH) (wt./vol.) solution. This method precipitates reactive inorganic sulfur species as silver sulfide (Ag_2S) which then allows for the determination of the $\delta^{34}S$ of total inorganic sulfur in the (poly)sulfide solutions. The precipitated solutions were allowed to settle in the dark and overnight for complete conversion to Ag_2S. The solutions were then vacuum filtered through a 25mm, 0.2µm filter (Whatman® Nuclepore track-etched polycarbonate membrane filters) and rinsed several times with 18mΩ water. Residues were then oven dried overnight at 60°C and homogenized for sulfur stable isotope analysis. In addition, blank (no substrate addition) (poly)sulfide solutions were prepared for analysis in the same manner.

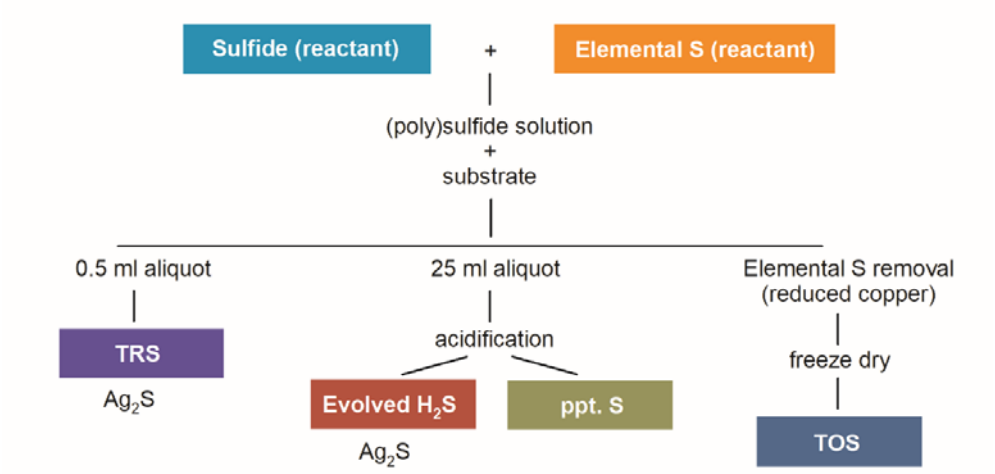

Figure 14. Analytical flowchart. Reactants were mixed under a nitrogen atmosphere (0.3% O_2). After initial mixing for complete isotopic mixing of the reactants, organic substrate was added. After four weeks, splits of the mixture were taken for sulfur isotope analysis of the various sulfur species.

4.2.3 Acidification of the (poly)sulfide solutions for polysulfide sulfur and elemental sulfur analysis

Duplicate aliquots (10ml) of each (poly)sulfide solution were taken from the sealed serum bottles with a gas tight syringe and immediately filtered through a 0.2µm regenerated cellulose syringe filter into a reaction tube purged with nitrogen. 6N HCl (ca. 20ml) was then added to decompose the (poly)sulfide solution (colorless solution, pH=0), releasing hydrogen sulfide gas (H_2S) and precipitating elemental sulfur (S^0). The reaction was allowed to proceed for 45 minutes. In addition, blank (no substrate addition) (poly)sulfide solutions were prepared for bulk sulfur stable isotope analysis in the same manner.

4.2.3.1 Evolved H_2S gas

Throughout the acidification reaction, evolved H_2S gas was bubbled through a trap containing 40ml of nitrogen purged (deaerated) 3% zinc acetate – 10% NH_4OH (wt./vol.) solution in order to precipitate it as zinc sulfide (ZnS). Once the reaction was complete, the precipitated ZnS was converted to silver sulfide (Ag_2S) by dropwise addition of 3% $AgNO_3$ – 10% NH_4OH (wt./vol.) solution to the trap until no additional color change was observed (milky white – black). The precipitated solutions were allowed to settle in the dark and overnight for complete conversion to Ag_2S. The solutions were then vacuum filtered through a 25mm, 0.2µm membrane filter (Whatman® Nuclepore track-etched polycarbonate membrane filters) and rinsed several times with 18mΩ water. The residues were then oven dried overnight at 60°C and homogenized for sulfur stable isotope analysis.

4.2.3.2 Precipitated S^0

Elemental sulfur precipitated during the acidification procedure (ppt. S) was vacuum filtered through a 25mm, 0.2µm membrane filter (Whatman® Nuclepore track-etched polycarbonate membrane filters) and rinsed several times with 18mΩ water. The residues were allowed to dry at room temperature for several days and then homogenized for sulfur stable isotope analysis.

4.2.4 Sulfur stable isotope ($\delta^{34}S$) analysis

Total reactive sulfur (TRS) and evolved H_2S silver sulfides, ppt. S, and total organic sulfur (TOS) splits were weighed (ca. 0.2mg) into tin capsules and analyzed for weight percent S (in the case of TOS) and S isotopic ratio determinations. Analyses were performed at Indiana University-Purdue University of Indianapolis (IUPUI) using a Thermo EAIsolink elemental analyzer coupled under continuous flow to a Thermo DeltaV Plus stable isotope ratio monitoring mass spectrometer. Sulfur isotope ($\delta^{34}S$) values are reported relative to Vienna Canyon Diablo Troilite (VCDT) by normalization to three international reference materials (IAEA S1=-0.3‰; IAEA S2=22.62‰; IAEA S3-32.49‰). Linear regression bracketed the full isotopic range of the samples and corrected for scale compression. All $\delta^{34}S$ values were calculated according to standard delta notation in per mil (‰) deviations from VCDT, where $\delta^{34}S=[(^{34}S/^{32}S_{sample})/(^{34}S/^{32}S_{VCDT})-1] \times 1000$. Samples were run in at least duplicate, with analytical precision of standards better than 0.2‰.

4.3 Results and discussion

4.3.1 Polysulfide solutions: chemical composition and isotope mixing

Polysulfides are the most reactive reduced sulfur species at conditions prevailing in marine sediments and euxinic environments (Krein, 1993; Lalonde et al., 1987; Vairavamurthy and Mopper, 1989; Loch et al., 2002). As such, polysulfides are considered to be among the most important species involved in diagenetic secondary sulfur enrichment (Aizenshtat et al., 1983; Francios, 1987; Mossmann et al., 1991; Vairavamurthy et al., 1992). Here, the polysulfide solutions are complex mixtures of sulfide (H_2S), bisulfide (HS^-), elemental sulfur (S_8^0), and polysulfides (S_x^{2-}). Polysulfides are instantly produced in the solution via the reaction of HS^- and S_8^0, according to equation 1.

$$nS^0 + xS^{2-} \leftrightarrow S^{2-}_{(n+x)}$$ Equation 1

In order to determine the extent of sulfur isotope fractionation during sulfur incorporation into organic matter, we need to know the isotope compositions of reactive reduced sulfur species involved in the reaction (i.e. polysulfides). As discussed in previous publications (Fossing and Jorgenson 1990, Krein and Aizenshtat 1993, Amrani and Aizenshtat, 2004, Amrani et al. 2006) the mixture of polysulfides is in isotopic mass balance between elemental sulfur and sulfide reactant. Here, we measured the sulfur isotope values of reactant sulfides and elemental sulfur (Tables 1 and 2). We also measured total reactive sulfur (TRS), in order to compare it to the calculated isotopic composition of polysulfides via isotopic mass balance of the reactant sulfides and elemental sulfur. Rayleigh isotope-mass balance for a closed-system dictates:

$$\delta_{TRS} = x\delta_{S^{2-}} + (1-x)\delta_{S^0}$$ Equation 2

where δ_{TRS} represents the stoichiometric $\delta^{34}S$ value of TRS, x represents the mole fraction of the reactants (sulfide and elemental sulfur) in solution for the formation of polysulfides, and $\delta_{S^{2-}}$ and δ_{S^0} are the measured isotope values of reactant sulfide and elemental sulfur, respectively. TRS measurements agree with our theoretical isotope calculations (Tables 3 and 4). Thus, there is complete isotopic mixing between the reactants in the formation of polysulfides (the inorganic sulfur pool is isotopically homogeneous) and supports previous studies (Fossing and Jørgensen, 1990; Krein and Aizenshtat, 1993; Amrani and Aizenshtat, 2004).

The process of acidification releases hydrogen sulfide gas and precipitates elemental sulfur, during which fractionation can occur. The process first requires the cleavage of a S–S bond and the formation of HS^-, and secondly the formation of H_2S gas. During the process of S-S bond cleavage and ultimately H_2S formation, isotopic discrimination against the heavy isotope (^{34}S) should result

in concentrating the lighter isotope (^{32}S) in the gas phase. This is because ^{32}S-^{32}S bonds require less energy to break, so will cleave first releasing isotopically light ^{32}S for subsequent formation of HS^- and H_2S gas, consequently leaving the precipitated elemental sulfur ^{34}S-enriched. Following previous studies (Amrani and Aizenshtat 2004), acidification of our (poly)sulfide solutions reveals a fractionation between 4 and 6.5‰, depending on reaction conditions, with evolved $H_2S_{(g)}$ ^{34}S-depleted relative to precipitated sulfur (Figure 15; Tables 3 and 4). This finding is similar to the 3-5‰ ^{34}S-depletion in evolved H_2S observed in previous studies (Amrani and Aizenshtat 2004). This finding also adds more to our understanding of the potential offsets in the traditional work-up of acid volatile sulfide (AVS) species from environmental samples, where isotopic bias between the $\delta^{34}S$ of AVS and elemental sulfur may be induced by methods (e.g. acidification) used to separate and differentiate inorganic sulfur species (Mossmann et al. 1991, Rozan et al. 2000, Neretin et al. 2003).

4.3.2 Isotopic fractionation associated with incorporation of reduced sulfur species into organic matter

Solutions were mixed to maximize the potential fractionation between reactive inorganic sulfur species and organic substrates (i.e. simulating open-system conditions in respect to polysulfides, with excess polysulfides relative to substrate – glucose and Pahokee Peat). Under such open-system conditions we would expect to see ^{34}S-enrichment of the substrate relative to the polysulfide if the reaction is reversible and equilibrium controlled. The X-^{34}S bond (X represents C, O, or S) is stronger than the X-^{32}S bond, so it requires higher bond cleavage energy. As such, the X-^{32}S bonds would be broken/cleaved first during reversible reactions at equilibrium, leaving the X-^{34}S bonds intact and causing ^{34}S-enrichment. Conversely, if the reaction mechanism is irreversible and kinetically controlled, we would expect to see ^{34}S-depletion of the substrate relative to the polysulfide, as the isotope fractionation is mass dependent and the lighter isotope (^{32}S) would react faster than the heavy isotope (^{34}S).

Isotopic fractionation associated with the reaction of polysulfides and organic substrates varies with reaction conditions (Figures 15 and 16; Table 3). We observe fractionations of -1.87 ± 1.63, +1.61 ± 0.64, and -0.19 ± 2.10‰ for $(NH_4)_2S$, Na_2S, NaHS (poly)sulfide solutions with glucose,

respectively under Method 2 conditions. Sulfur incorporation into glucose under Method 1 conditions results in a -2.05 ± 0.14‰ fractionation. The fractionation associated with sulfur incorporation into Pahokee Peat is -0.23 ± 0.01‰. The observed fractionations are within error of one another based on replicate measurements (Figure 16; Table 3). The negative fractionations suggest kinetic sulfur isotopic fractionation, while the positive fractionation may reflect equilibrium isotope effects. Any difference in isotope fractionations among the solutions likely has to do with the reaction mechanism(s) occurring during sulfur incorporation into organic matter (discussed in section 4.3.3). Fractionations associated with sulfur incorporation into carbohydrates and Pahokee Peat are in direct contrast with studies on lipids, where fractionations of +4-5‰ were observed (Amrani and Aizenshtat 2004) for sulfur incorporation to lipid carbonyl groups.

4.3.3 The influence of functional group and reaction mechanism(s) on the $\delta^{34}S$ of organic matter

It was previously recognized that the carbonyl functionality was one of the main determinants governing sulfur incorporation and S-isotopic fractionation into organic matter (Amrani and Aizenshtat 2004). The +4-5‰ fractionation associated with sulfur incorporation into carbonyl groups of lipids was presumed to be the same for sulfur incorporation into carbohydrates via reaction with its carbonyl group (Amrani and Aizenshtat 2004). Our results suggest otherwise. Structural analysis (Chapter 3) shows that in addition to the carbonyl functionality, the hydroxyl groups of glucose as well as those in Pahokee Peat react with sulfur, forming both C-S and S-O bonds. In order to determine meaning behind the isotope fractionations in the current results, we must consider the nature of chemical bonds as they relate to isotopic distribution. As discussed in the previous section, equilibrium S-isotope exchange results in ^{34}S-enrichment of the substrate relative to the reactant polysulfide because the X-^{34}S bond requires more energy to break than the X-^{32}S bond. Layered on top of this is the fact that C-S bonds are stronger than S-O bonds, which are stronger than S-S bonds (bond dissociation energies of 713.3, 517.90, and 425.30 kJ/mol at 298K, respectively). Accordingly, S-S and S-O bonds are more readily broken and formed, and the heavier isotope will preferentially accumulate where it is bound most strongly (S-S < S-O < C-S) during reversible, equilibrium reactions.

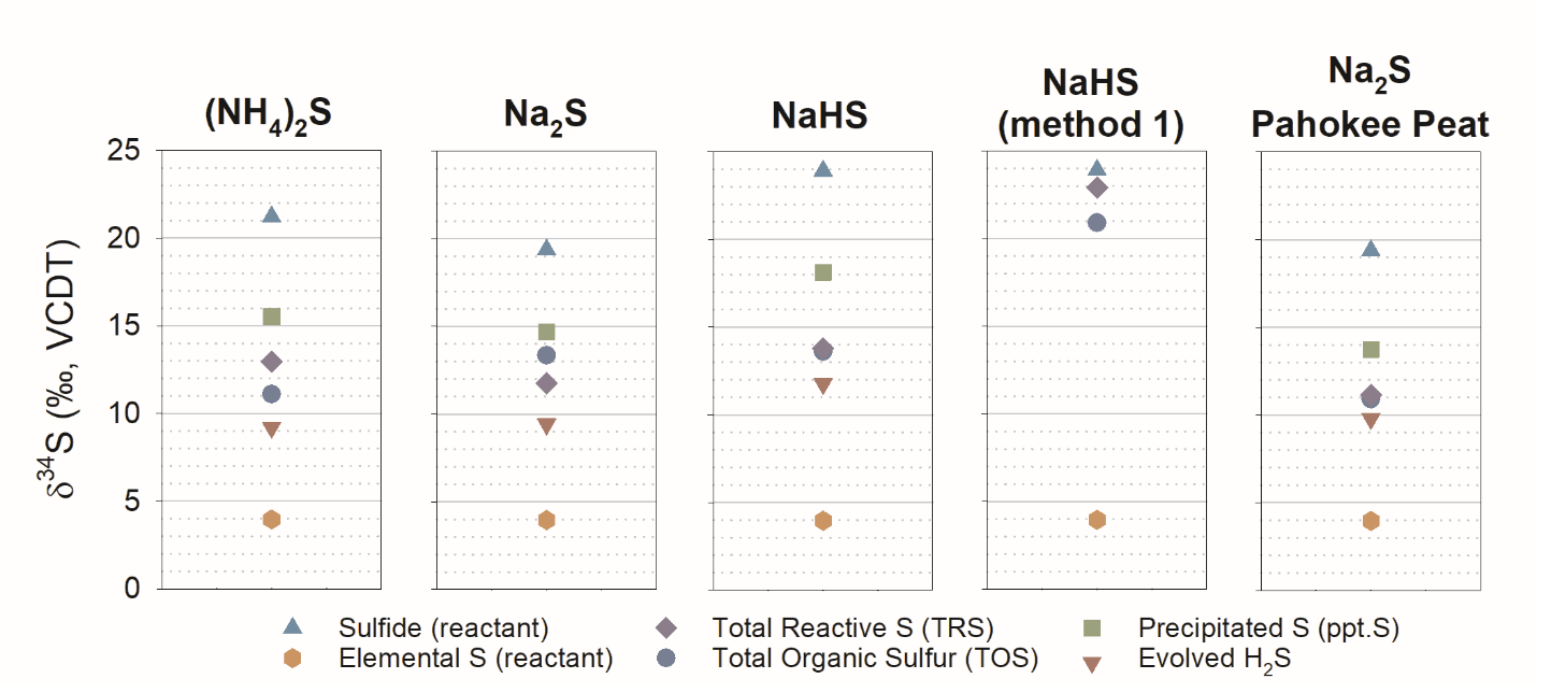

Figure 15. Bulk sulfur isotope composition of the (poly)sulfide solutions and reaction products. Depending on reaction conditions, the sulfur isotopic fractionation associated with sulfur incorporation into glucose and Pahokee Peat ranges from -2.05 to +1.61‰. Precipitated sulfur (polysulfide sulfur) is ^{34}S-enriched by avg. 5.5‰ relative to evolved H_2S gas. Precipitated sulfur and evolved H_2S were not measured for NaHS (Method 1).

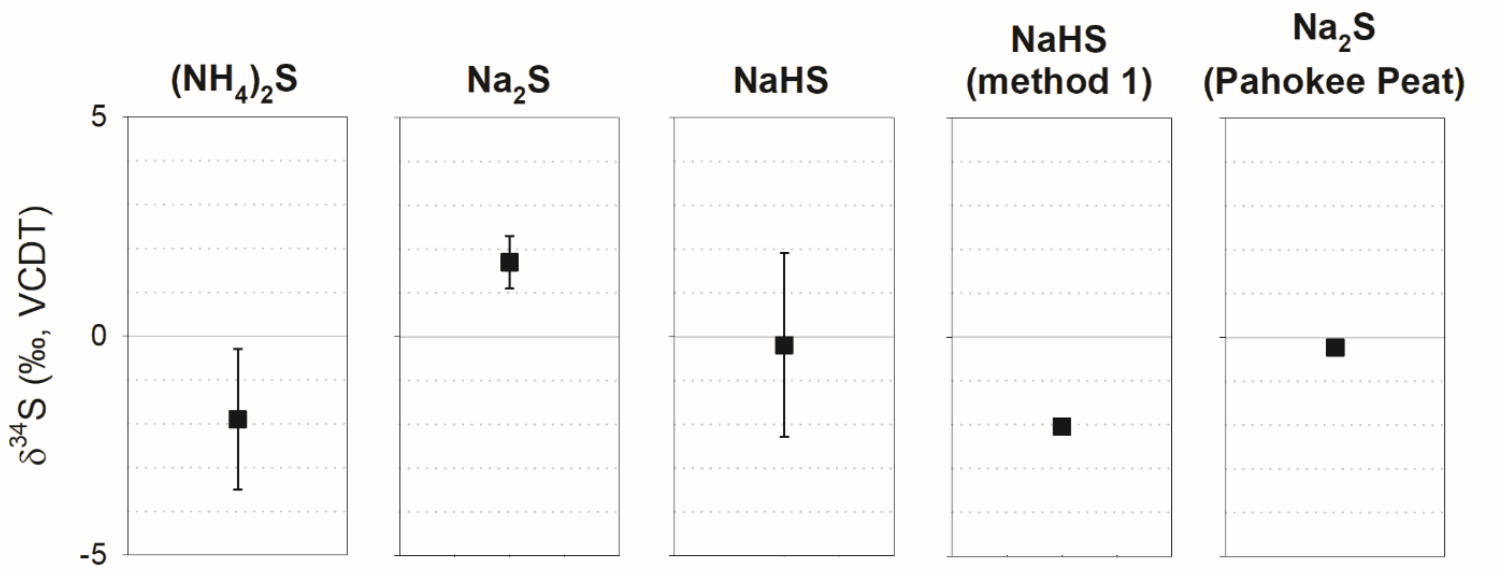

Figure 16. Sulfur isotope fractionation values associated with sulfur incorporation into organic matter for the laboratory experiments. The sulfur isotope fractionations observed in the experiments range from -2.05 to +1.61‰. The observed fractionations are within error of one another based on replicate measurements. Fractionations are calculated by subtraction of TRS values from the measured TOS values and include propagated error (Table 3). Where error bars cannot be seen, the error is less than the size of the symbol.

On the other hand, irreversible, kinetically controlled reactions result in ^{34}S-depletion of the substrate relative to the reactant polysulfide due to mass dependent effects [i.e. the light isotope (^{32}S) reacts faster than the heavy isotope (^{34}S)].

We propose here that C-S bond formation follows an irreversible, kinetic pathway (resulting in ^{34}S-depleted OSC), whereas S-O and S-S bond formation follow reversible, equilibrium pathways (leading to ^{34}S-enriched OSC). Therefore, the relative ratio of C-S to S-O and S-S bonds in a given macromolecular matrix is what governs the observed sulfur isotopic fractionation. For example, if there is a greater proportion of C-S bonds relative to S-O and S-S bonds in a given substrate, we would expect an overall ^{34}S-depletion (negative fractionation) of the substrate relative to the polysulfide reactant.

The S-isotopic fractionation (approximated as $\delta^{34}S_{TOS}$ - $\delta^{34}S_{TRS}$) associated with sulfur incorporation into $(NH_4)_2S$ sulfurized glucose is -1.87 ± 1.63‰ (Table 3). Pyrolysis of the sulfurized glucose shows that there are C-S bonds within the macromolecular matrix, but unfortunately the FT-IR data give no definitive indication of either C-S or S-O bonding (Chapter 3). We thus have insufficient data to satisfactorily explain the observed fractionation. If our model is true, the negative fractionation could indicate an irreversible kinetic isotope effect involving C-S bonding within the macromolecular matrix. Under Method 2 conditions, the S-isotopic fractionation of sulfur incorporation into Na_2S sulfurized glucose (+1.61 ± 0.64) is not significantly different from that of sulfur incorporation into NaHS sulfurized glucose (-0.19 ± 2.10‰), but is significantly different from S-isotopic fractionation of sulfur incorporation into Na_2S sulfurized Pahokee Peat (-0.23 ± 0.01‰) and Method 1 NaHS sulfurized glucose (-2.05 ± 0.15‰). Method 2 Na_2S sulfurized glucose results in more S-O bonding than C-S bonding as shown by FT-IR (loss of -OH band with an increase in S-O peak frequencies) and pyrolysis (low abundance of C-S bonded pyrolysates) when compared to the other reaction products (see Chapter 3). It appears that the reaction pathway taken in the formation of S-O bonds (keeping in mind that S-O bonds are weaker than C-S bonds) in Method 2 Na_2S glucose sulfurization is more favorable to reversible, equilibrium-type effects and results in ^{34}S-enrichment of the sulfurized glucose relative to the reactant polysulfide. This is not to say that C-S bonds are not formed or contribute to the observed

Table 3. Sulfur isotopes of the various sulfur species for each of the (poly)sulfide solutions and substrates – glucose and Pahokee Peat

$\delta^{34}S$ (‰, VCDT)	$(NH_4)_2S$[a]			Na_2S[a]			NaHS[a]			NaHS[b] (Method 1)			Na_2S[a] (Pahokee Peat)		
	average	**±**	**n**	**average**	**±**	**n**	**average**	**±**	**n**	**average**	**±**	**n**	**average**	**±**	**n**
Sulfide (reactant)	21.23		1	19.38		1	23.92			23.92			19.38		1
Elemental S (reactant)	3.96		1	3.96		1	3.96		1	3.96		1	3.96		1
Precipitated S (ppt. S)	15.53	1.09	6	14.70	1.73	4	18.13	0.38	6	N/A			13.75	0.15	2
Evolved H_2S	9.19	0.10	4	9.42	0.08	4	11.76	0.51	8	N/A			9.78	0.07	2
Offset H_2S – ppt. S	-6.34	1.09		-5.28	1.73		-6.37	0.97		N/A			-3.97	0.17	
Calculated TRS	12.59			11.67			13.94			22.92			11.67		
Total reactive S (TRS)	12.97	0.29	4	11.74	0.53	4	13.79	0.14	4	N/A			11.13	0.01	2
Total organic S (TOS)	11.10	1.60	2	13.35	0.35	2	13.60	2.10	2	20.87		1	10.89		1
Fractionation into OM (TOS – TRS)	-1.87	1.63		1.61	0.64		-0.19	2.10		-2.05	0.15		-0.23	0.01	

[a] 1:1 molar ratio sulfide:elemental sulfur

[b] 20:1 molar ratio sulfide:elemental sulfur

Table 4. Sulfur isotopes of the various sulfur species for blank mixtures (no substrate addition) of the various (poly)sulfide solutions

$\delta^{34}S$ (‰, VCDT)	$(NH_4)_2S$[a]			Na_2S[a]			NaHS[a]			NaHS[b] (method 1)		
	average	**±**	**n**	**average**	**±**	**n**	**average**	**±**	**n**	**average**	**±**	**n**
Sulfide (reactant)	21.23		1	19.38		1	23.92			23.92		
Elemental S (reactant)	3.96		1	3.96		1	3.96		1	3.96		1
Precipitated S (ppt. S)	14.85	0.05	2	14.57	0.59	4	18.68	1.13	4	23.71		1
Evolved H_2S	9.28	0.04	2	9.69	0.01	2	12.19	0.56	2			
Offset H_2S – ppt. S	-5.57	0.06		-4.87	0.59		-6.48	1.26				
Calculated TRS	12.59			11.67			13.94			22.92		
Total reactive S (TRS)	14.10	0.11	2	12.34	0.14	2	14.09	0.13	2	**15.88**		1

[a] 1:1 molar ratio sulfide:elemental s
[b] 20:1 molar ratio sulfide:elemental s

fractionation, but rather that the greater amount of S-O bonds dominates the overall isotopic fractionation we observe.

The negative fractionations of Pahokee Peat and Method 2 glucose experiments suggest that the reaction mechanism(s) follow irreversible, kinetic type effects and thus record ^{34}S-depletion of the sulfurized substrate relative to the polysulfide reactant (Figure 16 and Table 3). Indeed, structural analysis (FT-IR and pyrolysis) of the sulfurized reaction products reveals more C-S bonds relative to S-O bonds (Chapter 3). FT-IR analysis shows that the -OH band is still present and fairly unchanged with the appearance of peaks at frequencies that correspond to S=C bonding. Additionally, online pyrolysis of the reaction products shows an abundance of C-S bonded pyrolysates. Therefore, the observed ^{34}S-depletion of the substrates relative to the reactant polysulfides in these experiments is attributed to the greater proportion of C-S bonds relative to S-O bonds within the reaction products.

NaHS sulfurized glucose from Method 1 is ^{34}S-enriched relative to NaHS sulfurized glucose from Method 2 (Figure 16). The ^{34}S-enrichment is due to the 20:1 molar ratio of sulfide:elemental sulfur in Method 1, compared to the 1:1 molar ratio of sulfide:elemental sulfur in Method 2. Accordingly, theoretical isotopic mixing calculations (eq. 2) and measurements show that TRS lies closer to the ^{34}S-enriched sulfide end-member (Tables 3 and 4). Since TRS is what is reacting with the substrate, $\delta^{34}S_{TOS}$ should record a similar enrichment (Table 3) along with an associated isotopic offset due to potential fractionation during S-incorporation. The observed isotopic fractionation associated with sulfur incorporation into NaHS sulfurized glucose under Method 1 conditions is -2.05 ± 0.15‰ (Figures 15 and 16; Table 3). This fractionation is larger and more ^{34}S-depleted relative to the fractionation observed for Method 2 NaHS sulfurized glucose. This observation indicates that as temperature increases (24°C to 50°C) isotopic fractionation increases, which is contrary to the norm where isotopic fractionation decreases with increasing temperature. That said, the reaction mechanisms occurring at 50°C are likely not comparable to those at 24°C, as heating glucose under basic conditions results in a different molecular structure (see Chapter 3) and pyrolysates (van Dongen et al. 2003). In NaHS sulfurized glucose at 50°C there are many C-S bonded pyrolysates (van Dongen et al. 2003), including long-chain alkylthiophenes – which we do not observe in Method 2 NaHS sulfurized glucose pyrolysates. Additionally, comparison of FT-IR spectra from

Method 1 NaHS sulfurized glucose to Method 2 NaHS sulfurized glucose shows that the -OH band in Method 1 remains relatively unchanged, indicating fewer S-O bonds, along with the appearance of peaks at frequencies corresponding to C-S bonds. Thus, we suggest that the greater ^{34}S-depletion of the sulfurized product relative to the reactant polysulfides observed in Method 1 NaHS sulfurized glucose is related to the higher proportion of C-S bonds relative to S-O bonds.

Taking all of the above into account, we suggest that the relative proportion of S-O to C-S bonds may ultimately determine the δ^{34}S value of macromolecular organic matter – with C-S bonds exhibiting kinetic isotope effects and ^{34}S-depletion, whereas S-O bonds exhibit equilibrium effects and ^{34}S-enrichment of the substrate relative to the reduced sulfur reactant. Results from sulfurization of Pahokee Peat suggest that there is a negligible fractionation (-0.23 ± 0.01‰) associated with sulfur incorporation into natural dissolved organic matter, though different chemical compositions of dissolved organic matter under various natural conditions may give rise to different observed fractionations.

4.4 Conclusions

Results of the current study show varying sulfur isotopic fractionation (-2.05 to +1.61‰) between reduced sulfur species and organic substrates (i.e. glucose and Pahokee Peat) under different sulfurization reaction conditions. We propose that the variation in the observed fractionations may be related to the relative proportion of C-S to S-O bonds within a macromolecular matrix, though further study is needed to support this proposition. The -0.23 ± 0.01‰ fractionation of sulfur into Pahokee Peat, a dissolved organic matter standard, supports the general assumption that the incorporation of reduced sulfur species into organic matter has negligible net sulfur isotope fractionation (e.g. Mossmann et al. 1991, Werne et al. 2003).

5.0 Sulfur Stable Isotopic Analysis of the Blackstone Band of the Jurassic Kimmeridge Clay Formation

5.1 Introduction

Over geological timescales, biogeochemical cycling of sulfur is closely tied to the redox state of Earth's ocean-atmosphere system through the burial of oxidized (sulfate) and reduced (sulfide) sulfur species. Thus, the sulfur isotopic ($\delta^{34}S$) records of sulfate and pyrite are often used to reconstruct ocean chemistry at the time of deposition, constrain the activity of sulfur metabolizing organisms, as well as to determine diagenetic processes in marine depositional environments (Claypool et al. 1980, Canfield and Teske 1996, Canfield 2004, Johnston et al. 2005, Fike et al. 2006, Gill et al. 2007, Fike and Grotzinger, 2008, Hurtgen et al. 2009, Halevy et al. 2012, Jones and Fike 2013, Leavitt et al. 2013). The sulfur isotopic records preserved in sedimentary rocks are overwhelmingly dependent on sedimentological and geochemical conditions during deposition, thus the isotopic records need to be placed in a detailed context before variations can be understood.

Reconstruction of the sulfur isotopic values of ancient sulfide are derived from the analysis of pyrite (FeS_2). Since microbial sulfate reduction (MSR) generates the sulfide required for the formation of pyrite, the isotopes of pyrite should reflect the microbial fractionation(s) during MSR, which ultimately depends on the processes controlling the fractionation(s). Numerous studies have shown that there is an inverse correlation between the rate of MSR and the magnitude of MSR sulfur isotope fractionation. In general, large fractionations are observed during low rates of MSR and small fractionations are observed during high rates, reflecting a transition from equilibrium to kinetically controlled conditions at low and high rates, respectively (Chambers et al. 1975, Kaplan and Rittenberg 1964, Harrison and Thode 1958, Goldhaber and Kaplan 1975). In general, the rate of MSR is considered to be first order controlled with respect to the limiting reactant – either the electron acceptor (e.g. sulfate; Habicht et al. 2002) or the electron donor (e.g. organic carbon;

Chambers et al. 1975, Kaplan and Rittenberg 1964, Habicht and Canfield 1997, Sim et al. 2011, Leavitt et al. 2013, Wing and Halevy 2014).

Traditionally, the isotopic variations observed in the pyrite record are interpreted as changes in the "openness" of the system with respect to sulfate availability (the electron acceptor) during MSR. As sulfate is respired during MSR the residual sulfate pool shrinks, leading to ^{34}S-enrichment of sulfide, and therefore pyrite δ^{34}S values, according to typical Rayleigh-type distillation. The magnitude of the ^{34}S-enrichment according to the traditional scenario thus depends on sulfate concentration, where greater ^{34}S-enrichment of sulfide is observed under closed-system conditions relative to open-system conditions. ^{34}S-enriched pyrite values are typically interpreted as pyrite formation within sediments (i.e. diagenetic formation) where there is limited connectivity between the pore water sulfate pool and the overlying water column (closed-system conditions), whereas relatively ^{34}S-depleted pyrite values are interpreted as pyrite formation in the water column (i.e. syngenetic formation) where sulfate concentrations are not as limited (open-system conditions).

Alternatively, the isotopic variations observed in the pyrite record may be interpreted as changes in the availability of organic carbon used as the electron donor during MSR. Because microbial fractionations during MSR are not significantly affected by the concentration of sulfate until micromolar concentrations are reached (Leavitt et al. 2013, Wing and Halevy 2014), the rate of MSR and thus the observed microbial fractionation recorded by pyrite should mainly depend on the availability of metabolizable organic carbon. For example, under open-system conditions the formation of relatively ^{34}S-enriched pyrite is possible if abundant metabolizable organic carbon is available to support high rates of MSR (this is opposite of the expected ^{34}S-depletion of pyrite δ^{34}S values under traditional interpretations of open-system conditions related to sulfate concentration). The availability of metabolizable organic carbon would increase MSR rates with a consequent ^{34}S-enrichment of produced sulfide and thus pyrite δ^{34}S values. Indeed, variations in the pyrite δ^{34}S record over Phanerozoic time have been proposed as changes in MSR rates in response to organic matter availability, rather than sulfate concentrations (Leavitt et al. 2013). Therefore, not only understanding where pyrite forms within a depositional environment, but also understanding the controls on organic carbon availability are necessary for the interpretation of pyrite δ^{34}S values and reconstruction of past sulfur cycling.

Organic sulfur is usually thought to have played a minor role in the biogeochemical sulfur cycle and, as such, has often been overlooked in reconstructions of past environments. In addition to reaction with iron in the formation of pyrite, sulfide produced during MSR may react with labile organic matter (a process termed sulfurization) leading to a complex mixture of low and high molecular weight organic sulfur compounds (OSC) in the environment (Sinninghe Damsté et al. 1989, Sinninghe Damsté and de Leeuw 1989, Aizenshtat et al. 1995, Krein and Aizenshtat 1995, Sinninghe Damsté et al. 1998). In fact, organic sulfur represents the second largest pool of reduced sulfur in sediments, with pyrite being the largest. Sulfurization of organic matter often results in the formation of macromolecules (organic compounds bound via polysulfide crosslinking), which prevents or at least significantly hinders microbial attack and remineralization of labile organic matter. Such reactions may limit the availability of metabolizable organic carbon for MSR, which would act as a control on MSR rates and thus on the $\delta^{34}S$ values of produced sulfide. Accordingly, the $\delta^{34}S$ values of both pyrite and organic sulfur should also reflect this influence. That said, the processes leading to the $\delta^{34}S$ compositions of organic sulfur species must first be understood before we are able to deduce such valuable information from them.

Relative to the long-standing proxies and interpretive framework developed for pyrite formation and deposition, a major obstacle in the interpretation of the organic sulfur record is the uncertainty about the timing and pathway(s) of formation of organic sulfur, as well as how diagenetic alterations may affect the organic sulfur pool. Like pyrite, the sulfur isotopic composition of organic sulfur will reflect contributions from multiple factors, including the isotopic composition(s) of the sulfur source(s), which carries the isotopic history of MSR, sulfide oxidation, and disproportionation; the timing of sulfur incorporation (open- versus closed-system conditions); and diagenetic overprinting. Additionally, organic sulfur isotopes will be influenced by any isotopic fractionation(s) associated with sulfur incorporation into organic matter. The range of fractionations associated with said processes, as well as the isotopic relationship between organic sulfur and pyrite have yet to be fully evaluated in the environment.

The Kimmeridge Clay Formation (KCF) was deposited during the Late Jurassic (ca. 155 to 148 Ma) in a series of shallow marine basins in the epeiric Laurasian Seaway and represents one of the most prolonged periods of organic carbon accumulation during the Mesozoic (Hallam, 1987;

Jenkyns et al., 2002). Sediments constituting the KCF display a cyclic alternation of mudstones, bituminous shales, oil shales and carbonates, containing up to 60 wt% total organic carbon (TOC). The KCF has been the subject of numerous studies since the 1970s, as it is the presumed source rock of North Sea oils (e.g. *sedimentology and stratigraphy:* Irwin et al. 1977, Cox and Gallois, 1981, Tyson, 1989; 1996, Morgans – Bell et al. 2001, *environmental reconstruction:* Tyson et al. 1979, Oschmann 1988; 1991, Miller 1990, Bertrand and Lallier-Verges 1993, *geochemistry*: Farrimond et al. 1984, Tribovillard et al. 1994, van Kaam-Peters et al. 1997, *organic matter – preservation*: Demaison and Moore 1980, *organic matter – productivity*: Ramanampisoa and Disnar, 1994, Lallier-Verges et al. 1993; 1997, van Kaam-Peters et al. 1998, van Dongen et al. 2006).

The Blackstone Band (*wheatleyensis* zone) is one of the most organic-rich horizons in the KCF with a TOC content of up to 50 wt% (Coe 1992, Morgans-Bell et al. 2001, Tyson 2004). Previous studies (van Kaam-Peters et al. 1998, van Dongen et al. 2006) have shown that the high TOC content of the Blackstone Band is the result of the enhanced preservation of organic matter (especially carbohydrates) due to sulfurization. The enhanced preservation of carbohydrates via sulfurization results from more frequent or prolonged periods of photic zone euxinia (PZE) within the paleowater column (van Dongen et al. 2006). Such well-studied samples provide a unique opportunity to study the intricacies of sulfur cycling, with particular attention to organic sulfur formation and preservation on geologic timescales.

Here, we present results from the comprehensive analysis of bulk sulfur species from whole rock, kerogen, and pyrolyzed kerogen, including quantification of the abundance and sulfur isotope compositions of total sulfur (TS), chromium reducible sulfur (CRS; taken to represent pyrite), and total organic sulfur (TOS) from a complete total organic carbon (TOC) cycle in the Upper Jurassic Kimmeridge Clay Formation (KCF) comprising the extremely TOC-rich (34%) Blackstone Band. We also report abundance and compound-specific sulfur isotopes of benzothiophenes (BTs) and dibenzothiophenes (DBTs) from bitumen (solvent extractable organics) and kerogen (non-solvent extractable organics) pyrolysates. In light of our results, the relationship between the pyrite and organic sulfur records are discussed in terms of paleoenvironmental conditions and implications for the reconstruction of sulfur isotopic records are described.

5.2 Experimental

5.2.1 Rock samples and paleogeography

Rock samples presented here are from a core taken from the Swanworth Quarry 1 borehole [SY 9675 7823], South Dorset, UK, which was drilled as part of the UK Natural Environment Research Council's Rapid Global Geological Events special topic 'Anatomy of a Source Rock'. The samples in the current study are considered to be thermally immature and encompass a complete TOC cycle in the Upper Jurassic Kimmeridge Clay Formation comprising the organic-rich (34 wt% TOC) Blackstone Band (Bed group 42, *Pectinatites wheatleyenesis – Pectinatites hudlestoni* zones; Morgans-Bell et al. 2001). Deposition occurred during the Late Jurassic in a relatively shallow (max. depth 75m; Weedon et al. 2004) epeiric sea in what is now the southern coast of England. Lithologies include organic-rich shales and mudstones with pyritic nodules and shelly material. Samples in the current study constitute a sub-set of eight samples from van Dongen et al. (2006). The powdered rocks were stored frozen (-20°C) prior to analysis. Splits of the unextracted ("whole") powdered rock samples were taken for total sulfur (TS) measurements. The sample analytical scheme is shown in Figure 17.

5.2.2 Pyrite extraction as chromium reducible sulfur (CRS) and total organic sulfur (TOS) isolation

Into a reaction vessel, ca. 2 g of powdered rock sample was weighed and then purged with nitrogen. CRS species (i.e. pyrite) were liberated from the sediments as H_2S gas by addition of 20ml of 1M chromium (II) chloride ($CrCl_2$) solution, which was mixed with 7ml of 12N HCl directly before addition to the reaction vessel. The reaction vessel was heated until boiling and maintained for two hours to ensure quantitative recovery of the reduced sulfur species. Evolved H_2S gas was trapped as ZnS by bubbling through 25ml of nitrogen purged solution of 3% zinc acetate – 10% ammonium hydroxide (wt./vol.). Splits (1ml) of the trap solutions from the CRS extractions were taken for calorimetric determination of sulfide concentrations (Cline, 1969). The remaining trap solutions were precipitated as silver sulfide (Ag_2S), by dropwise addition of 3% silver nitrate - 10%

ammonium hydroxide (wt./vol.) solution until no color change was observed (milky white – black) and left to settle in the dark and overnight for complete conversion to Ag_2S. Precipitated Ag_2S was vacuum filtered through a 25mm, 0.2µm membrane filter (Whatman® Nuclepore track-etched polycarbonate membrane filter) and rinsed several times with 18mΩ water. The residues were then oven dried overnight at 40°C and homogenized for sulfur stable isotope analysis. Select residues were extracted a second time to ensure complete liberation of CRS species.

The residual rock/$CrCl_2$/HCl solution in the reaction vessel after chromium reduction was vacuum filtered through a 47 mm, 0.2 µm membrane filter (Whatman® Nuclepore track-etched polycarbonate membrane filter). The residue was rinsed several times with 18mΩ water and then oven dried overnight at 40°C. The dried residue was homogenized and analyzed as total organic sulfur (TOS).

5.2.3 Bulk sulfur stable isotope analysis

Homogenized samples for total sulfur (TS), chromium reducible sulfur (CRS), and total organic sulfur (TOS) were weighed (ca. 0.2mg) into tin capsules and analyzed for weight percent S (in the case of TS and TOS) and S isotopic ratio determinations. Analyses were performed at Indiana University-Purdue University of Indianapolis (IUPUI) using a Thermo EAIsolink elemental analyzer coupled under continuous flow to a Thermo DeltaV Plus stable isotope ratio monitoring mass spectrometer. Sulfur isotope ($\delta^{34}S$) values are reported relative to Vienna Canyon Diablo Troilite (VCDT) by normalization to three international reference materials (IAEA S1=−0.3‰; IAEA S2=22.62‰; IAEA S3=−32.49‰). Linear regression bracketed the full isotopic range of the samples and corrected for scale compression. All $\delta^{34}S$ values were calculated according to standard delta notation in per mil (‰) deviations from VCDT, where $\delta^{34}S=[(^{34}S/^{32}S_{sample})/(^{34}S/^{32}S_{VCDT})-1]\times1000$. Samples were run in at least duplicate, with analytical precision of standards better than 0.2‰.

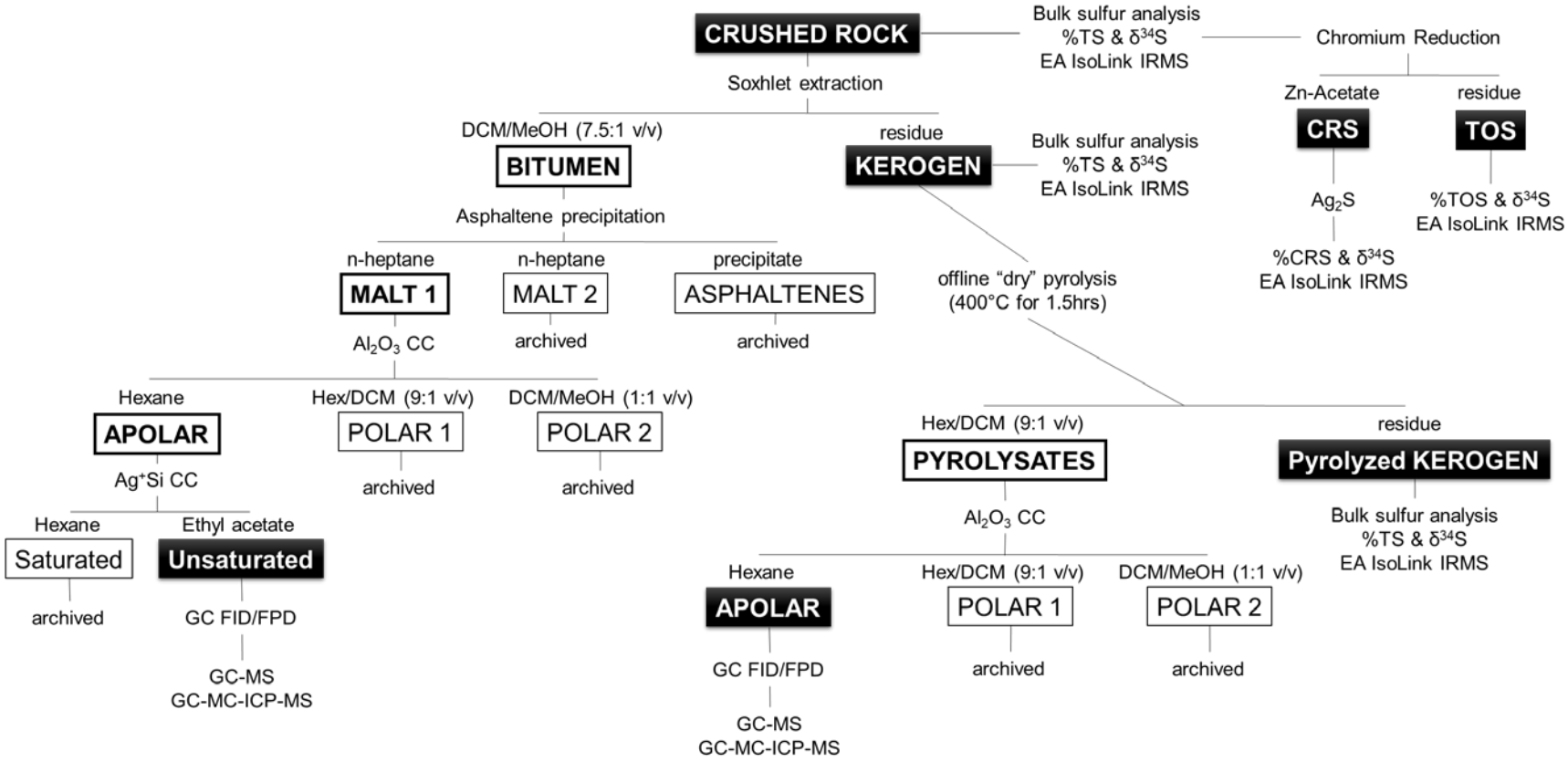

Figure 17. Analytical flowchart for KCF rock samples.

5.2.4 Solvent extraction and separation of bitumen

Extraction and separation of the bitumen fraction followed previously described procedures (van Kaam-Peters et al. 1998). In short, the total lipid extract (TLE) was obtained from powdered rock samples (ca. 50 g) via soxhlet extraction using 7.5:1 (vol./vol.) DCM/MeOH and refluxing for 24-48 hours. Splits of the TLEs were further separated into maltene (MALT 1 and MALT 2) and asphaltene fractions via sequential precipitation in *n*-heptane. After elemental sulfur removal by activated (reduced) copper beads, aliquots of the MALT 1 fractions (ca. 200 mg) were separated into individual hydrocarbon classes by alumina (activated at 150°C for 2 hrs) column (20 cm x 2 cm) chromatography using solvents of increasing polarity [150 mL of n-hexane; 150 mL of *n*-hexane/DCM 9:1 (vol./vol.), and 150 mL of DCM/MeOH 2:1 (vol./vol.) for aliphatic/apolar, aromatic, and polar compounds, respectively]. Aliphatic fractions were dissolved in hexane and analyzed directly. Aromatic fractions were derivatized prior to GC analysis.

5.2.5 Off-line "dry" pyrolysis of solvent extracted rock residues (kerogen) and separation of kerogen pyrolysates

Off-line pyrolysis was performed at the University of Manchester with a known amount (ca. 5 g) of dried, solvent extracted powdered rock sample using a Carbolite® Tube Furnace. Samples were heated (400°C) for 1.5 hr in a glass sample boat positioned in a glass tube within the cylindrical oven under a nitrogen flow. The volatile products (i.e. pyrolysates) generated during pyrolysis were flushed with N_2 into two successive traps containing hexane/DCM (9:1 vol./vol.). The first trap was kept at room temperature and the second trap was cooled with a slurry of liquid N_2 and acetone. The pyrolysates were combined from each trap and the solvent was removed via rotary evaporation. Pyrolysates were then transferred to pre-weighed vials and dried under a stream of N_2. After elemental sulfur removal, aliquots (ca. 200 mg) of the pyrolysates were subsequently fractionated by alumina column chromatography as described above.

5.2.6 Quantification and identification using gas chromatography flame ionization detection/flame photometric detection and mass spectrometry (GC-FID/FPD and GC/MS)

OSC were quantified using a Thermo Trace 1310 gas chromatograph with both flame ionization and flame photometric detectors. Aliquots (1 uL) of each fraction were introduced via a PTV injector operated in splitless mode held at 300°C. The gas chromatograph was programmed from 70°C (1 min) to 130°C at a rate of 10°C min^{-1}, and then to 320°C (15 min) at a rate of 4°C min^{-1}. Separation was achieved using an Agilent J&W DB-5 (30m x 0.32mm x 0.25µm) capillary column with a helium flowrate of 2 ml min^{-1}. OSC were identified using a Thermo ISQ QD single quadrupole mass spectrometer connected to a Thermo Trace 1310 gas chromatograph. Injector and GC operating conditions were the same as described above. The mass spectrometer transfer line was held at 320°C and ion source at 275°C. Compounds were ionized at 70 eV and mass analyzed over a range of m/z 50-600 with a scan rate of 4 scans per second. OSC were identified on the basis of relative retention time and on the basis of mass spectral data in comparison with literature data – BTs (m/z 134) and DBTs (m/z 184).

5.2.7 Compound-specific $\delta^{34}S$ analysis using coupled gas chromatography (GC) and multi-collector inductively coupled plasma mass spectrometry (GC/MC-ICP-MS)

OSC $\delta^{34}S$ values were measured at the California Institute of Technology with a Thermo Neptune Plus multi-collector ICP-MS coupled to either an Agilent 6890 or Thermo Trace 1310 GC inlet system (GC/MC-ICP-MS; Amrani et al. 2009 and Raven et al. 2015) and are reported in standard delta notation as per mil (‰) deviations from the standard Vienna Canyon Diablo Troilite (VCDT). Aliquots (1 uL) of each fraction were introduced via a SSL injector operated in splitless mode held at 320°C. The gas chromatograph was programmed from 50°C (1 min) to 320°C (15 min) at a rate of 20°C min^{-1}. Separation was achieved using a HP DB-5MS (30m x 0.32mm x 0.25µm) capillary column with a helium flowrate of 2 ml min^{-1}. The transfer line was held at 320°C. OSC $\delta^{34}S$ values reported for KCF rock samples represent the average of at least duplicate analyses. The precision of replicate sample measurements was generally better than ±2‰. Analytical precision was

assessed by daily replicate analysis of a mixture of five organic sulfur compounds (benzothiophene, 3-hexyl thiophene, hexyl sulfide, dibenzothiophene, 4-6-diethyl dibenzothiophene) with a standard deviation less than 1‰.

5.3 Results

5.3.1 Bulk analyses

The bulk concentrations of chromium reducible sulfur (CRS; represents pyrite), total sulfur (TS), and total organic sulfur (TOS) moving across the Blackstone Band are shown in Figure 18. Each shows a spike in concentrations at ca. 244.3 m level. TOS values are the calculated difference between TS and CRS values (bulk data are listed in Tables 5-8). To correct for dilution by inorganic minerals, Figure 18 also shows these same data normalized to Al content as per van Dongen et al. 2006. The Al ratio can also be used as a proxy for accumulation rates, but it is strongly dependent on the assumption that the Al flux remains constant over time, which is not necessarily realistic. That said, the proxy has shown good agreement with sedimentation rates in previous studies (c.f. Tyson 2004, van Dongen et al. 2006). Normalized values show similar trends to weight % values (Figure 18), but with sharper peaks centered at about 244.3 m and generally lower and more consistent background levels before and after these peaks.

The bulk $\delta^{34}S$ values for all sulfur species show an upcore trend of ^{34}S-enrichment that peaks around 244.3 m, followed by a period of ^{34}S-depletion, and then ^{34}S-enrichment through the 242 m level (Figure 19). The bulk $\delta^{34}S$ values are heavier in the organic sulfur (TOS) compared to the pyrite sulfur (CRS) in all of the samples analyzed (Figure 19). Notably, bulk TOS values remain relatively ^{34}S-enriched even as bulk CRS values trend back towards lower $\delta^{34}S$ values above the ca. 244.3m level.

5.3.2 Compound Specific Sulfur Isotope Analysis (CSSIA)

5.3.2.1 Bitumen

The abundance of benzothiophenes (BTs) and dibenzothiophenes (DBTs) varies with depth (Figure 20). Bitumen BTs and DBTs are the most abundant when TOS is also the most abundant. Note that bitumen BTs and DBTs were only in high enough abundance for CSSIA in five of the eight samples. $\delta^{34}S$ values of BTs and DBTs from bitumen range from -9 to -3‰. Weighted isotopic averages of the compounds show that BTs become slightly ^{34}S-enriched upcore, whereas DBTs show more variability (Figure 20). Cross-plots between $\delta^{34}S$ values of bitumen BTs, DBTs, and TOS show very low correlations (R^2 = 0.11 and 0.02 for BTs and DBTs versus TOS, respectively). Cross-plots of $\delta^{34}S$ values of BTs versus DBTs also shows a very low-correlation (R^2=0.17). Data are listed in Tables 9 and 10.

5.3.2.2 Kerogen

Overall, the abundance of kerogen BTs and DBTs are orders of magnitude greater than bitumen BTs and DBTs (Figures 20 and 21). Like bitumen BTs and DBTs, kerogen BTs and DBTs are in greatest abundance when TOS is most abundant. In contrast to bitumen BTs and DBTs $\delta^{34}S$ values, kerogen BTs and DBTs $\delta^{34}S$ values vary with depth and display similar trends to bulk TOS $\delta^{34}S$ values. $\delta^{34}S$ values of BTs and DBTs overlap, ranging from -16 to +4‰ (Figure 21). Cross-plots between $\delta^{34}S$ values of kerogen BTs, DBTs, and TOS show high correlations (R^2 = 0.84 and 0.88 for BTs and DBTs versus TOS, respectively). Cross-plots of $\delta^{34}S$ values of BTs versus DBTs also shows a high correlation (R^2=0.99). Data are listed in Tables 11 and 12.

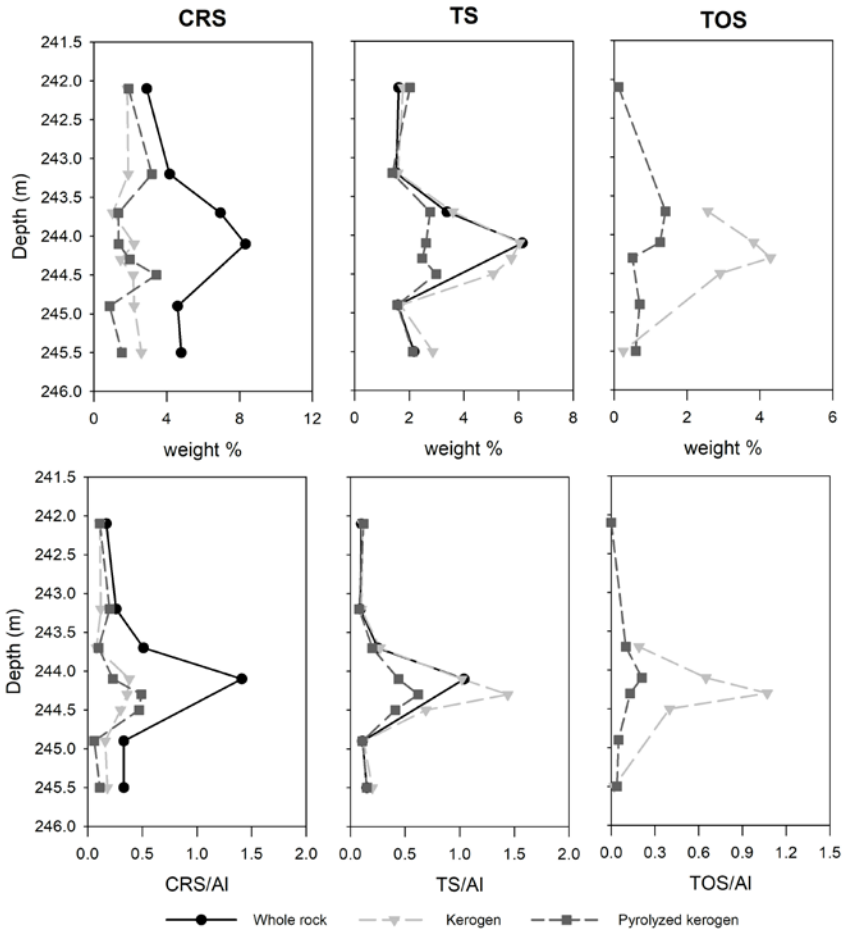

Figure 18. Weight percentages of bulk sulfur species (top panels) and Al-normalized values (bottom panels). Bulk sulfur species are shown as wt./wt. % (g sulfur species/g rock) as well as normalized values to the Al content (van Dongen et al. 2006). TOS values are the calculated difference between TS and CRS values. Normalized values show similar trends to weight % values. Both weight % and normalized values show an initial period of increase, before reaching a maximum at ca. 244.3m, and a decrease thereafter.

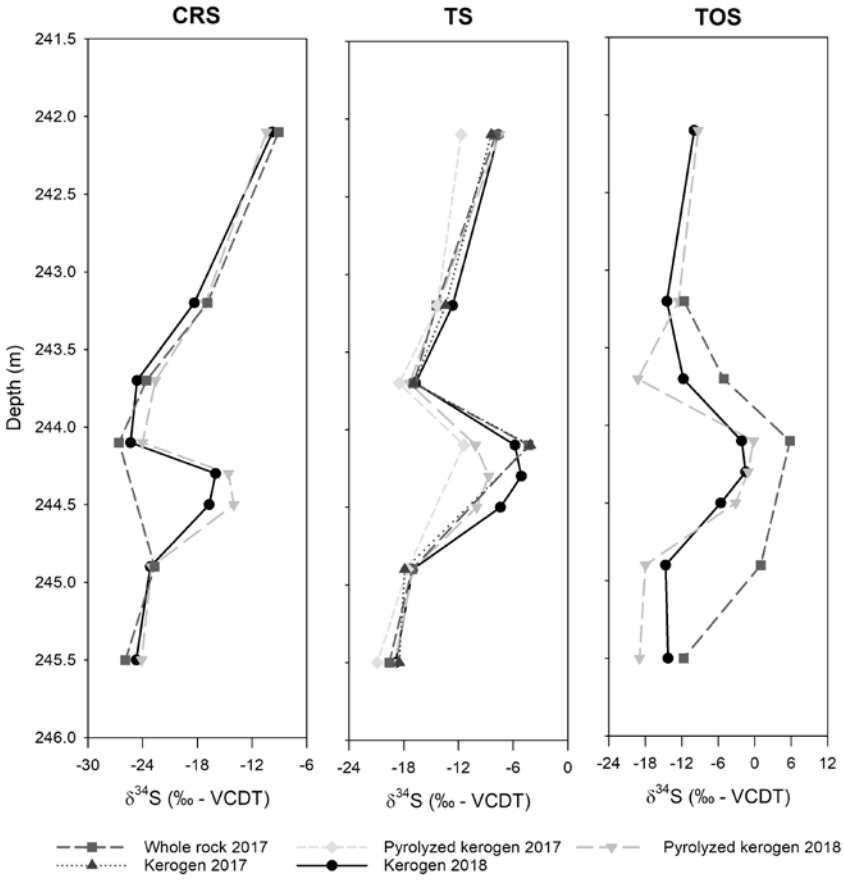

Figure 19. Sulfur isotopic measurements of bulk sulfur species. $\delta^{34}S$ values of bulk sulfur species are shown as per mil (‰) deviations from the standard Vienna Canyon Diablo Troilite (VCDT). Bulk $\delta^{34}S$ values for all sulfur species show an initial ^{34}S-enrichment, followed by a period of ^{34}S-depletion, and then additional ^{34}S-enrichment. Near 244.1m bulk TOS values remain ^{34}S-enriched, when bulk CRS values trend towards ^{34}S-depletion. Bulk $\delta^{34}S_{TOS}$ values are ^{34}S-enriched relative to bulk $\delta^{34}S_{CRS}$ values in all of the samples analyzed.

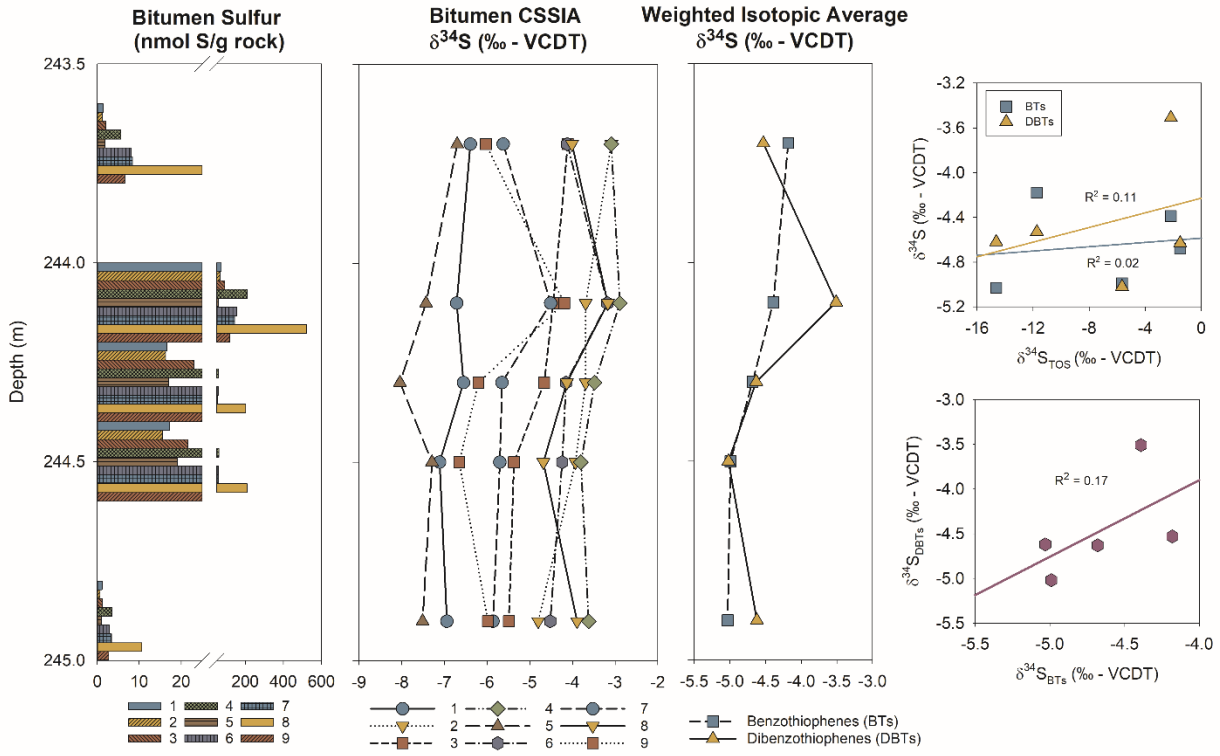

Figure 20. Bitumen compound abundance and compound-specific sulfur isotope analysis (CSSIA). Numbers 1-5 are benzothiophenes (BTs) and numbers 6-9 are dibenzothiophenes (DBTs). Compound abundance is displayed as nmol S/gram rock extracted – note break in scale from 50-100 nmol S/g rock. Compound-specific isotopes are shown as per mil (‰) deviations from the standard Vienna Canyon Diablo Troilite (VCDT). Bitumen BTs show a slight trend of ^{34}S-enrichment upcore, whereas bitumen DBTs are more variable. Cross-plots between δ^{34}S values of bitumen BTs, DBTs, and TOS show very low correlations [top right; y-axis displays both BTs (squares) and DBTs (triangles)]. Cross-plots of δ^{34}S values of BTs versus DBTs also shows a very low correlation (bottom right). NOTE: shown are the five samples which had high enough compound abundance for CSSIA.

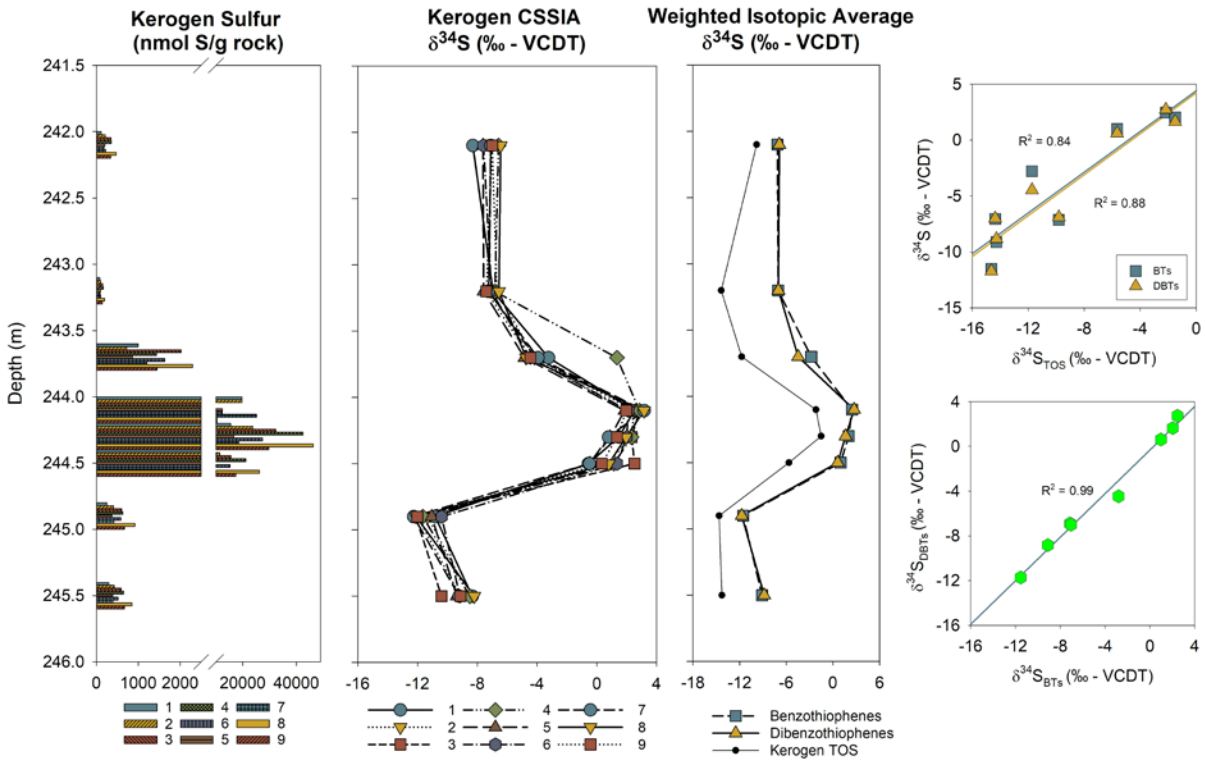

Figure 21. Kerogen pyrolysate compound abundance and compound-specific sulfur isotope analysis (CSSIA). Numbers 1-5 are benzothiophenes (BTs) and numbers 6-9 are dibenzothiophenes (DBTs). Compound abundance is displayed as nmol S/gram rock extracted – note break in scale from 2500-10000 nmol S/g rock. Compound-specific isotopes are shown as per mil (‰) deviations from the standard Vienna Canyon Diablo Troilite (VCDT). Kerogen BTs and DBTs are in greatest abundance when TOS is most abundant and are orders of magnitude greater than bitumen BT and DBT abundance. Kerogen BTs and DBTs $\delta^{34}S$ values vary with depth and display similar trends to bulk TOS $\delta^{34}S$ values. Cross-plots between $\delta^{34}S$ values of kerogen BTs, DBTs, and TOS show high correlations [top right; y-axis displays both BTs (squares) and DBTs (triangles)]. Cross-plots of $\delta^{34}S$ values of BTs versus DBTs also shows a high correlation (bottom right).

Table 5. Bulk data from van Dongen et al. 2006

Sample ID	Depth (m)	%TOC	TOC/Al	Σ Derivatives of isorenieratene/Al
KCF 3	242.1	3.8	0.23	1.73
KCF 7	243.2	4.7	0.29	0.64
KCF 9	243.7	15.9	1.18	2.42
KCF 11	244.1	33.1	5.61	31.53
KCF 12	244.3	33.6	8.40	46.7
KCF 13	244.5	28.7	3.93	12.25
KCF 15	244.9	5.5	0.40	4.43
KCF 17	245.5	9.7	0.67	0.39

Table 6. Whole rock bulk sulfur data

Sample ID	Depth (m)	%TS	%CRS	%TOS	TS/Al	CRS/Al	TOS/Al	δ^{34}S TS	δ^{34}S CRS	δ^{34}S TOS
KCF 3	242.1	1.61	2.90	-1.29	0.10	0.17	-0.08	-7.9	-9.1	
KCF 7	243.2	1.52	4.16	-2.64	0.09	0.26	-0.16	-14.4	-16.9	-11.6
KCF 9	243.7	3.38	6.95	-3.57	0.25	0.51	-0.26	-16.9	-23.6	-5.1
KCF 11	244.1	6.14	8.32	-2.18	1.04	1.41	-0.37	-4.3	-26.6	5.8
KCF 12	244.3	*N/A*	*N/A*	N/A	*N/A*	*N/A*	N/A	*N/A*	*N/A*	*N/A*
KCF 13	244.5	*N/A*	*N/A*	N/A	*N/A*	*N/A*	N/A	*N/A*	*N/A*	*N/A*
KCF 15	244.9	1.59	4.60	-3.02	0.11	0.33	-0.22	-17.1	-22.7	1.0
KCF 17	245.5	2.17	4.80	-2.63	0.15	0.33	-0.18	-19.6	-25.9	-11.7

Table 7. Kerogen bulk sulfur data

Sample ID	Depth (m)	%TS	%CRS	%TOS	TS/Al	CRS/Al	TOS/Al	$\delta^{34}S$ TS	$\delta^{34}S$ CRS	$\delta^{34}S$ TOS	$\Delta\delta^{34}S$ CRS-TOS	$\Delta\delta^{34}S$ Sulfate-CRS
KCF 3	242.1	1.77	1.83	-0.06	0.11	0.11	0.00	-7.44	-9.76	-9.81	0.05	27
KCF 7	243.2	1.58	1.89	-0.30	0.10	0.12	-0.02	-12.44	-18.33	-14.36	-3.97	35
KCF 9	243.7	3.60	1.03	2.57	0.27	0.08	0.19	-16.69	-24.62	-11.73	-12.88	42
KCF 11	244.1	6.04	2.21	3.83	1.02	0.38	0.65	-5.82	-25.31	-2.17	-23.14	42
KCF 12	244.3	5.74	1.46	4.29	1.44	0.36	1.07	-5.13	-16.00	-1.50	-14.50	33
KCF 13	244.5	5.07	2.16	2.91	0.69	0.30	0.40	-7.41	-16.70	-5.65	-11.06	34
KCF 15	244.9	1.68	2.21	-0.53	0.12	0.16	-0.04	-16.87	-23.15	-14.63	-8.52	40
KCF 17	245.5	2.86	2.61	0.25	0.20	0.18	0.02	-18.79	-24.72	-14.27	-10.45	42

Table 8. Pyrolyzed kerogen residue bulk sulfur data

Sample ID	Depth (m)	%TS	%CRS	%TOS	TS/Al	CRS/Al	TOS/Al	$\delta^{34}S$ TS	$\delta^{34}S$ CRS	$\delta^{34}S$ TOS
KCF 3	242.1	2.02	1.91	0.12	0.12	0.11	0.01	-7.31	-10.41	-9.01
KCF 7	243.2	1.38	3.18	-1.80	0.08	0.20	-0.11	-14.02	-17.14	-12.15
KCF 9	243.7	2.76	1.35	1.41	0.20	0.10	0.10	-17.31	-22.60	-19.26
KCF 11	244.1	2.61	1.36	1.26	0.44	0.23	0.21	-10.04	-24.01	-0.19
KCF 12	244.3	2.47	1.97	0.50	0.62	0.49	0.13	-8.61	-14.58	-1.07
KCF 13	244.5	2.98	3.42	-0.45	0.41	0.47	-0.06	-9.92	-14.03	-3.05
KCF 15	244.9	1.56	0.86	0.70	0.11	0.06	0.05	-16.83	-23.03	-17.85
KCF 17	245.5	2.13	1.54	0.59	0.15	0.11	0.04	-18.84	-24.11	-18.93

Table 9. Bitumen compound abundance (nmol S/g rock)

Sample ID	Depth (m)	Benzothiophenes					Dibenzothiophenes			
		1	2	3	4	5	6	7	8	9
KCF 9	243.7	1.35	1.18	1.97	5.62	1.82	8.03	8.40	29.81	6.51
KCF 11	244.1	74.96	66.67	93.01	211.17	60.04	157.36	143.73	521.21	118.97
KCF 12	244.3	16.66	16.28	22.99	60.27	17.06	57.06	54.31	203.18	46.98
KCF 13	244.5	17.29	15.51	21.61	61.19	19.11	59.10	57.91	209.27	48.81
KCF 15	244.9	1.11	0.63	1.16	3.50	0.98	2.83	3.36	10.64	2.76

Table 10. Bitumen compound-specific sulfur isotope data

Sample ID	Depth (m)	Benzothiophenes					Dibenzothiophenes				Weighted Isotopic Average	
		1	2	3	4	5	6	7	8	9	BTs	DBTs
KCF 9	243.7	-3.09	-4.11	-3.09	-6.70	-4.12	-5.62	-4.01	-6.03	-6.39	-4.18	-4.53
KCF 11	244.1	-3.69	-4.45	-2.89	-7.43	-3.18	-4.51	-3.17	-4.19	-6.71	-4.39	-3.51
KCF 12	244.3	-3.69	-4.66	-3.48	-8.04	-4.15	-5.65	-4.13	-6.20	-6.55	-4.68	-4.63
KCF 13	244.5	-3.93	-5.37	-3.80	-7.29	-4.24	-5.70	-4.68	-6.65	-7.11	-4.99	-5.02
KCF 15	244.9	-4.80	-5.49	-3.62	-7.51	-4.52	-5.86	-3.89	-5.98	-6.94	-5.03	-4.62

Table 11. Kerogen compound abundance (nmol S/g rock)

Sample ID	Depth (m)	Benzothiophenes					Dibenzothiophenes			
		1	2	3	4	5	6	7	8	9
KCF 3	242.1	112.75	207.48	345.71	353.87	197.51	182.10	224.89	474.18	339.98
KCF 7	243.2	76.39	101.12	153.21	162.18	94.56	87.34	100.64	194.19	139.76
KCF 9	243.7	997.69	719.82	2025.78	1435.34	862.09	1633.00	1207.05	2297.84	1446.24
KCF 11	244.1	19682.05	19682.05	6826.40	6826.40	12409.35	12409.35	25186.28	10413.05	10413.05
KCF 12	244.3	15487.54	23734.46	32377.83	42503.57	16729.48	27419.65	18500.03	46304.60	29717.23
KCF 13	244.5	7407.27	11383.68	15709.90	21124.33	8556.87	15188.67	9777.13	26323.02	17483.82
KCF 15	244.9	249.04	407.56	602.49	626.64	368.76	586.18	411.32	915.57	669.82
KCF 17	245.5	289.96	422.87	588.31	653.19	387.87	514.08	392.54	849.63	669.20

Table 12. Kerogen compound-specific sulfur isotope data

Sample ID	Depth (m)	Benzothiophenes					Dibenzothiophenes				Weighted Isotopic Average	
		1	2	3	4	5	6	7	8	9	BTs	DBTS
KCF 3	242.1	-8.30	-7.01	-7.10	-6.58	-7.62	-7.59	-7.10	-6.44	-7.00	-7.13	-6.89
KCF 7	243.2	-6.95	-6.69	-7.23	-6.83	-7.58	-7.06	-7.26	-6.55	-7.40	-7.04	-7.00
KCF 9	243.7	-3.23	-4.18	-4.14	1.35	-4.84	-4.45	-3.94	-4.73	-4.45	-2.79	-4.46
KCF 11	244.1	2.52	2.52	2.86	2.86	1.86	2.12	3.17	3.17	1.98	2.46	2.73
KCF 12	244.3	1.47	2.30	2.34	2.34	0.89	2.00	0.78	1.96	1.35	2.04	1.64
KCF 13	244.5	-0.56	0.70	2.53	1.14	-0.46	1.35	-0.49	0.81	0.34	0.99	0.62
KCF 15	244.9	-10.82	-11.33	-12.13	-11.65	-11.06	-10.40	-12.26	-12.10	-12.02	-11.53	-11.72
KCF 17	245.5	-8.34	-8.52	-10.40	-8.50	-9.38	-9.17	-9.22	-8.21	-9.13	-9.11	-8.83

5.4 Discussion

5.4.1 Bulk records of pyrite and organic sulfur

Pyrite and organic sulfur represent the two most abundant forms of reduced sulfur in sedimentary systems. Reconstructions of past sulfur cycling rely on accurate reconstructions and interpretations of the pyrite isotope record, with significantly less attention paid to the organic sulfur isotope record. The isotope compositions of both pyrite and organic sulfur will reflect contributions from several factors including the isotopic composition(s) of the sulfur source(s) – sulfide produced by MSR (which is ultimately governed by the availability of the limiting reactants, sulfate and organic matter); fractionations occurring during sulfide oxidation and disproportionation; the timing of sulfur incorporation (open- versus closed-system conditions); isotopic fractionations associated with sulfide reaction with iron during the formation of pyrite and with organic matter during the formation of organic sulfur; as well as diagenetic overprinting. Since the isotopic compositions of pyrite and organic sulfur reflect contributions from similar processes, reconstruction of both pyrite and organic sulfur isotopic compositions should provide complementary records and any discrepancies between the two should reveal processes unique to the formation of each.

The record presented here is divided into three stages: stage I – the earliest part of the record leading up to the period of photic zone euxinia (PZE); stage II – the period of photic zone euxinia, which is characterized by the increase in the diagenetic products of isorenieratene (a pigment of photosynthetic green sulfur bacteria; Sinninghe Damsté et al. 2001); and stage III – the later part of the record, after the period of PZE (Figure 22).

During stage I, pyrite and organic sulfur isotopes are relatively stable and display a consistent apparent fractionation ($\Delta\delta^{34}S_{TOS\text{-}CRS}$) of ca. 10‰ (Figure 22, Table 7), close to the global average offset (Anderson and Pratt 1995). Pyrite makes up the majority of the reduced sulfur pool, with minor contributions from organic sulfur [compare 0.16 - 0.18 CRS/Al to 0.02 TOS/Al (Figure 22, Table 7)]. The ^{34}S-enrichment of organic sulfur isotopes ($\delta^{34}S_{TOS}$) relative to pyrite isotopes

($\delta^{34}S_{CRS}$) during this stage may be explained by equilibrium isotopic exchange reactions during the formation of organic sulfur, which can cause ^{34}S-enrichments of up to 10‰ in organic sulfur relative to pyrite (Amrani and Aizenshtat 2004, Amrani et al. 2006; 2008). The $\delta^{34}S$ values of pyrite, on the other hand, likely reflect the isotopic composition of sulfide produced via MSR, as fractionation of sulfur isotopes during sulfide mineral precipitation is negligible (Berner and Westrich 1985, Hartgers et al. 1997, Butler et al. 2004). The apparent fractionation between the average Jurassic seawater sulfate $\delta^{34}S_{sulfate}$ value (17‰; Kampschulte and Strauss 2004) and pyrite $\delta^{34}S_{CRS}$ values ($\Delta\delta^{34}S_{Sulfate\text{-}CRS}$) is ca. 40‰ (Figure 22, Table 7), which is in the middle of the range of sulfur isotope fractionations by MSR observed within laboratory cultures and natural environments (19 to 66‰ range; Canfield et al. 2010, Sim et al. 2011, Leavitt et al. 2013, Wing and Halevy 2014). The $\Delta\delta^{34}S_{Sulfate\text{-}CRS}$ indicates that MSR rates are relatively low during this stage, likely limited by the availability of organic carbon rather than sulfate, as TOC/Al during this stage is comparatively low (0.40 - 0.67; Figure 22, Table 5). Most labile organic carbon would have been rapidly remineralized in a sub-oxic to oxic water column due to longer oxygen exposure times, with more refractory organic carbon deposited in the sediments which is not readily metabolizable to microbes during MSR. With the above considered, $\delta^{34}S$ values of pyrite and organic sulfur indicate that their formation likely takes place near the anoxic sediment-water interface (diagenetic formation), where the pore water sulfate pool is in connection with the water column – representing open-system conditions with respect to sulfate, where MSR may be limited by metabolizable organic carbon.

Moving into stage II and the period of PZE, we observe an initial shift in both pyrite and organic sulfur isotope composition towards ^{34}S-enrichment (Figure 22). This is followed by ^{34}S-depletion of pyrite isotope values at the end of the period of PZE, while TOS values remain ^{34}S-enriched. $\Delta\delta^{34}S_{TOS\text{-}CRS}$ values increase during this stage from ca. 11‰ to 23‰ (Figure 22, Table 7). Differing from stage I, organic sulfur makes up the majority of the sedimentary sulfur pool, 0.40 - 1.07 TOS/Al versus 0.30 - 0.38 CRS/Al (Figure 22, Table 7). Additionally, assuming seawater sulfate remains isotopically unchanged in this seaway due to the long residence time of

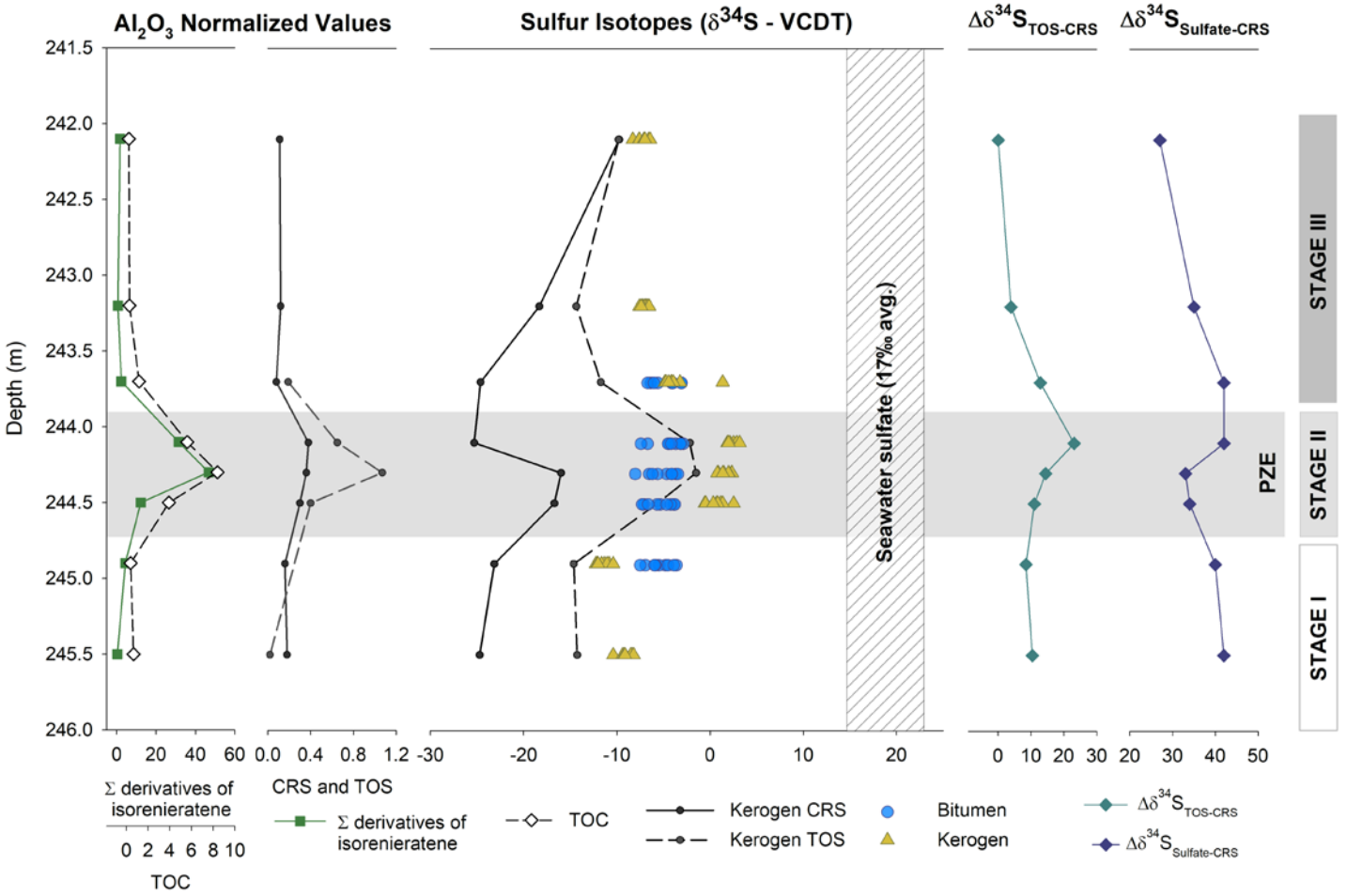

Figure 22. Sulfur isotopes in the context of environmental conditions during deposition of the Blackstone Band. Bulk CRS, TOS, TOC and Σ derivatives of isorenieratene are normalized to Al content as described in van Dongen et al. 2006. The period of photic zone euxinia (PZE) is represented by the increase in isorenieratene derivatives (biomarkers of photosynthetic green sulfur bacteria) and is bounded by the gray rectangle. The far-right shows the offset between pyrite (CRS) $\delta^{34}S$ values and the average Jurassic seawater sulfate $\delta^{34}S$ value. Sulfur isotopes are shown as per mil (‰) deviations from the standard Vienna Canyon Diablo Troilite (VCDT). Sulfur isotope composition of seawater sulfate is from Kampschulte and Strauss 2004.

sulfate, the $\Delta\delta^{34}S_{Sulfate\text{-}CRS}$ values shift between 33 and 42‰ (Figure 22, Table 7). Stage II also displays the highest TOC/Al values, ranging from 3.93 - 8.40 (Figure 22, Table 5).

The ^{34}S-enrichment of $\delta^{34}S_{TOS}$ values beyond the 10‰ accounted for by fractionations during formation and subsequent equilibrium sulfur isotope exchange reactions likely reflects contributions from primary biosulfur. Primary biosulfur refers to sulfur compounds synthesized by organisms (e.g. sulfolipids, proteins, and amino acids). Biosynthetic sulfur compounds are ^{34}S-enriched as there is only a small sulfur isotope fractionation (ca. -2‰; Canfield 2001) associated with assimilation from ^{34}S-enriched seawater sulfate (c.f. Kaplan et al. 1963, Goldhaber and Kaplan 1974, Rees et al. 1978, Chambers and Trudinger 1979, Canfield et al. 1998a, Bottcher et al. 2000). Although biosynthetic sulfur compounds are chemically and biologically labile, during the period of PZE biosulfur is more likely to be preserved due to limited oxygen exposure times in the euxinic water column, as well as possibly becoming crosslinked into organic matter creating macromolecules resistant to microbial degradation. Furthermore, contributions from ^{34}S-enriched biosulfur can make up 20-25% of total organic sulfur within sediments (Anderson and Pratt 1995, Canfield et al. 1998). If we assume that the isotope composition of primary biosulfur is +15 (based on the average Jurassic seawater sulfate $\delta^{34}S_{sulfate}$ values of 17‰; Kampschulte and Strauss 2004) it would only take a small proportion of biosulfur to shift $\delta^{34}S_{TOS}$ to more enriched values during the onset of the PZE. In fact, a simple mass balance calculation indicates that a 0-10% contribution of ^{34}S-enriched biosulfur to the total organic sulfur pool is needed to shift the isotope composition to values we observe leading up to the height of PZE (Figure 23). However, when $\Delta\delta^{34}S_{Sulfate\text{-}CRS}$ is at its maximum (42‰) after the height of PZE a ca. 35% contribution of ^{34}S-enriched biosulfur is needed. Better characterization of sulfur cycling dynamics during this stage may help our understanding of what sustains and, conversely, what leads to the collapse of PZE.

Water column conditions (i.e. PZE) during stage II are the most favorable for ^{34}S-depleted syngenetic pyrite formation. Measured $\delta^{34}S_{CRS}$ values, however, are relatively ^{34}S-enriched during the main part of stage II (Figure 22) which does not support a straightforward interpretation of syngenetic pyrite formation, and therefore other factors affecting the isotopic composition of pyrite must be considered. The variations in pyrite isotopes during stage II may be explained by the following scenarios.

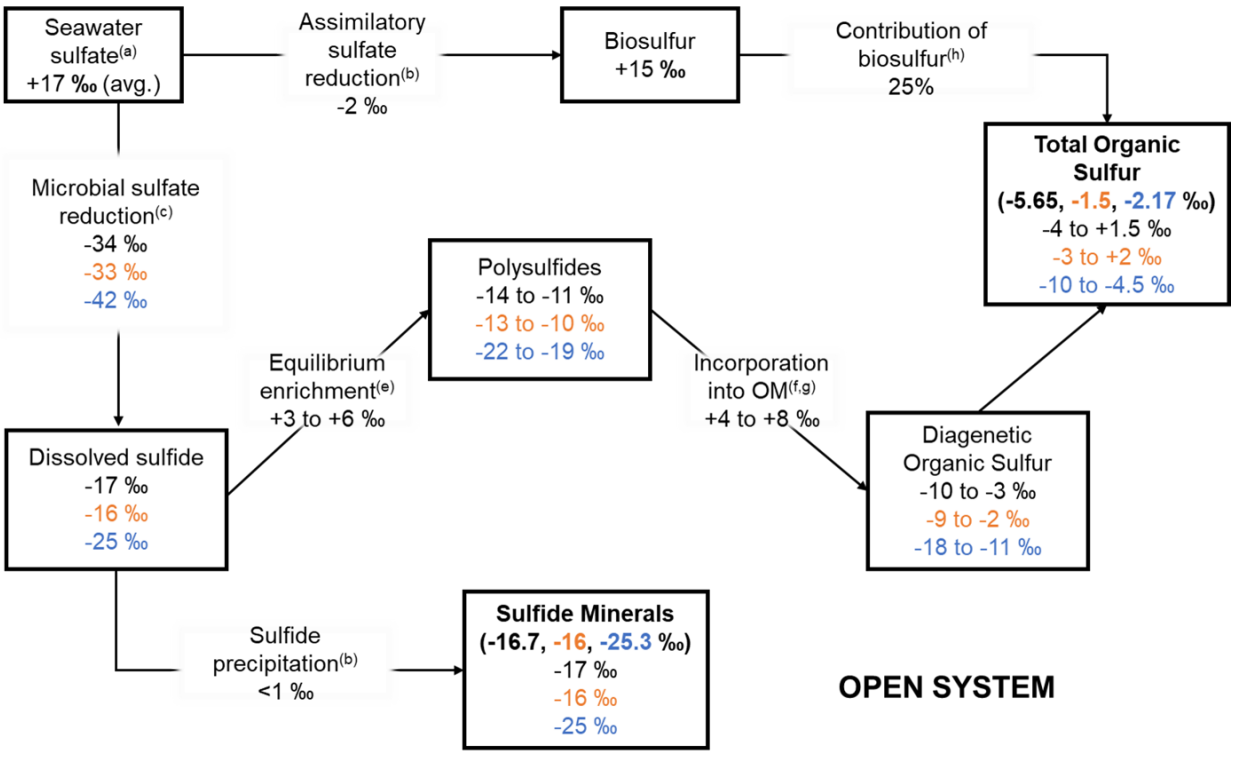

Figure 23. Sulfur isotope fractionation schematic during the period of photic zone euxinia (PZE). (a) Kampschulte and Strauss 2004, (b) Canfield 2001, (c) calculated $\Delta\delta^{34}S_{Sulfate\text{-}CRS}$ in the current study, (d) Zerkle et al. 2009, (e) Amrani et al. 2006, (f) Amrani and Aizenshtat 2004, (g) Amrani et al. 2008, (h) Anderson and Pratt 1995. At the beginning of the period of PZE, MSR rates are relatively high (calculated $\Delta\delta^{34}S_{Sulfate\text{-}CRS}$ = 34 and 33‰) and the measured $\delta^{34}S_{TOS}$ values are within the range of calculated diagenetic organic sulfur values, without contributions from biosulfur. After the height of the PZE, MSR rates are reduced (calculated $\Delta\delta^{34}S_{Sulfate\text{-}CRS}$ = 42‰) and a >25% contribution from ^{34}S-enriched biosulfur is needed to reach the measured $\delta^{34}S_{TOS}$ values at the maximum fractionation associated with sulfur incorporation into organic matter (OM). Inherent to our calculations are (1) the $\delta^{34}S$ values of CRS are recording the fractionation of MSR and (2) the $\delta^{34}S$ value of seawater sulfate doesn't change throughout the deposition of the Blackstone Band, which may not be entirely realistic.

Stage II, scenario I: Following traditional interpretations, the initial ^{34}S-enrichment of pyrite may indicate its formation under closed-system conditions, rather than in the euxinic water column (syngenetic formation). This would mean that pyrite formation would have to take place within the sediments (diagenetic formation) where there is limited connectivity between pore water sulfate and the water column. The ^{34}S-enrichment of pyrite may indicate its later diagenetic formation when the sedimentary sulfide pool has become ^{34}S-enriched. This would be possible if reactive iron became entrained by organic matter during deposition limiting its availability for pyrite formation within the water column. During later diagenesis, the iron may be released and subsequently react with a ^{34}S-enriched sulfide pool. Nearing the end of the period of PZE the shift to ^{34}S-depletion in pyrite isotopes would then indicate a transition to formation within the water column (syngenetic formation), representing open-system conditions. The extremely high TOC/Al values (3.93 - 8.40; Figure 22, Table 5) during this stage lends support to the hypothesis of iron entrainment and later pyrite formation. However, TOC/Al values remain high (5.61; Figure 22, Table 5) even when pyrite values shift to ^{34}S-depleted values, which seems to contradict the prior assertion.

Stage II, scenario II: Another possibility to consider is that the initial ^{34}S-enrichment of CRS values may indicate a change in MSR rates. At the beginning of the period of PZE, both sulfate and high amounts of labile organic carbon would have been available for MSR, which could drive high rates of MSR leading to the initially lower $\Delta\delta^{34}S_{CRS\text{-}sulfate}$ value (34‰; Figure 22, Table 7) and subsequent ^{34}S-enriched $\delta^{34}S_{CRS}$ values. Midway through this stage, $\delta^{34}S_{CRS}$ doesn't vary from its initial ^{34}S-enriched value and $\Delta\delta^{34}S_{CRS\text{-}sulfate}$ remains relatively low (33‰; Figure 22, Table 7) indicating a sustained relatively high rate of MSR. The ^{34}S-depletion of pyrite isotope values nearing the end of the period of PZE along with the ca. 10‰ shift to greater $\Delta\delta^{34}S_{CRS\text{-}sulfate}$ (42‰; Figure 22, Table 7) possibly reflects a shift to lower rates of MSR. Even though TOC/Al remains high (5.61; Figure 22, Table 5) during the period of ^{34}S-depletion of $\delta^{34}S_{CRS}$, the organic carbon during this particular time period (after the height of the period of PZE) may not have been readily available for use by microbes (water column reducing conditions may have limited the aerobic degradation of large, complex molecules to simple organic acids that are readily metabolized by

microbes). The formation of organic sulfur may compete with MSR for labile organic carbon, further limiting its availability for MSR, as TOS/Al also remains high (0.65; Figure 22, Table 7). Pyrite formation during stage II, scenario II, may have remained near the sediment water-interface or even taken place in the water column (open-system conditions with respect to sulfate and through time limited by metabolizable organic carbon), though we have no direct evidence for syngenetic pyrite formation, other than the locus of sulfide production moving into the photic zone.

With the present data we cannot conclusively rule out one scenario or the other. Even though the data indicate that water column conditions were conducive to syngenetic pyrite formation, pyrite isotopes do not necessarily reflect this in a forthright manner, which complicates reconstructions of paleoenvironmental conditions based on pyrite alone. That said, comparison with the TOS record indicates that scenario II may be more plausible. The parallel increase in pyrite and organic sulfur isotopes indicates that they likely form via similar pathways, once the ^{34}S-enrichment of organic sulfur relative to pyrite is accounted for. Since organic sulfur formation likely starts in the water column, preserving labile organic compounds (i.e. carbohydrates; van Dongen et al. 2006, Raven et al. 2016), it is likely that pyrite formation also begins in the water column where the ^{34}S-enriched isotopes reflect changes in MSR rates in relationship to metabolizable organic carbon availability rather than later diagenetic formation. However, analysis of additional proxies (e.g. iron speciation concentrations and isotopes, pyrite morphology, trace metal analysis etc.) are needed in order to confirm this proposition.

The transition out of the period of PZE during stage III brings a new set of conditions in which Al-normalized values of CRS and TOS are relatively low (0.08 - 0.12 CRS/Al and 0.19 TOS/Al; Figure 22, Table 7) and both CRS and organic sulfur δ^{34}S values become ^{34}S-enriched upcore (Figure 22). The progressive ^{34}S-enrichment of CRS and TOS δ^{34}S values during this time period likely reflect diagenetic formation of pyrite and organic sulfur deeper within the sediments (closed-system conditions), rather than an increase in MSR rates as was the case during the period of PZE. MSR rates are likely low and co-limited by the availability of sulfate and possibly metabolizable organic carbon (0.23 - 1.18 TOC/Al; Figure 22, Table 5). Limited exchange of sulfate between the water column and pore waters would shrink the pore water sulfate pool over time as sulfate is respired during MSR. This condition would lead to the ^{34}S-enrichment of sulfide, and therefore

CRS and TOS $\delta^{34}S$ values, according to typical Rayleigh-type distillation. This premise is supported by the surrounding stratigraphy where strata above and below the Blackstone Band are weakly laminated and sometimes bioturbated (Morgans-Bell at al. 2001). This indicates that occasional short-lived oxygenation events may have occurred outside of the period of PZE causing a shift in the locus of pyrite and organic sulfur formation to anoxic portions of the sediments.

As shown, the sulfur isotopic relationship between pyrite and organic sulfur may have important implications for reconstructing past environmental conditions from sedimentary sulfur isotope records (discussed in section 5.4.3.). A summary of the paleoenvironmental conditions necessary for the observed isotopic compositions of pyrite and organic sulfur throughout the three stages discussed herein is given in Figure 24.

5.4.2 Compound-specific sulfur isotope dynamics

Bitumen compounds do not display large $\delta^{34}S$ variations with depth, whereas kerogen compounds vary in similar ways to bulk TOS. The invariant $\delta^{34}S$ values of bitumen compounds indicates that they are not formed at the same time or via the same pathways as bulk sulfur species or kerogen compounds (Figure 20). This assertion is supported by the low correlations between $\delta^{34}S$ values of bitumen BTs, DBTs, and TOS (R^2 = 0.11 and 0.02 for BTs and DBTs versus TOS, respectively; Figure 20). Bitumen compounds may have formed from ^{32}S-depleted sulfide released from the sulfur-rich kerogen as it has matured, though the bitumen compounds are ^{34}S-enriched relative to bulk kerogen and the samples here are thermally immature, having undergone minimal catagenesis, so this seems unlikely. However, the $\delta^{34}S$ values of bitumen compounds suggest that they are formed from a sulfur source that doesn't vary isotopically through time or were formed during a single later digenetic event via water-rock interaction, for example.

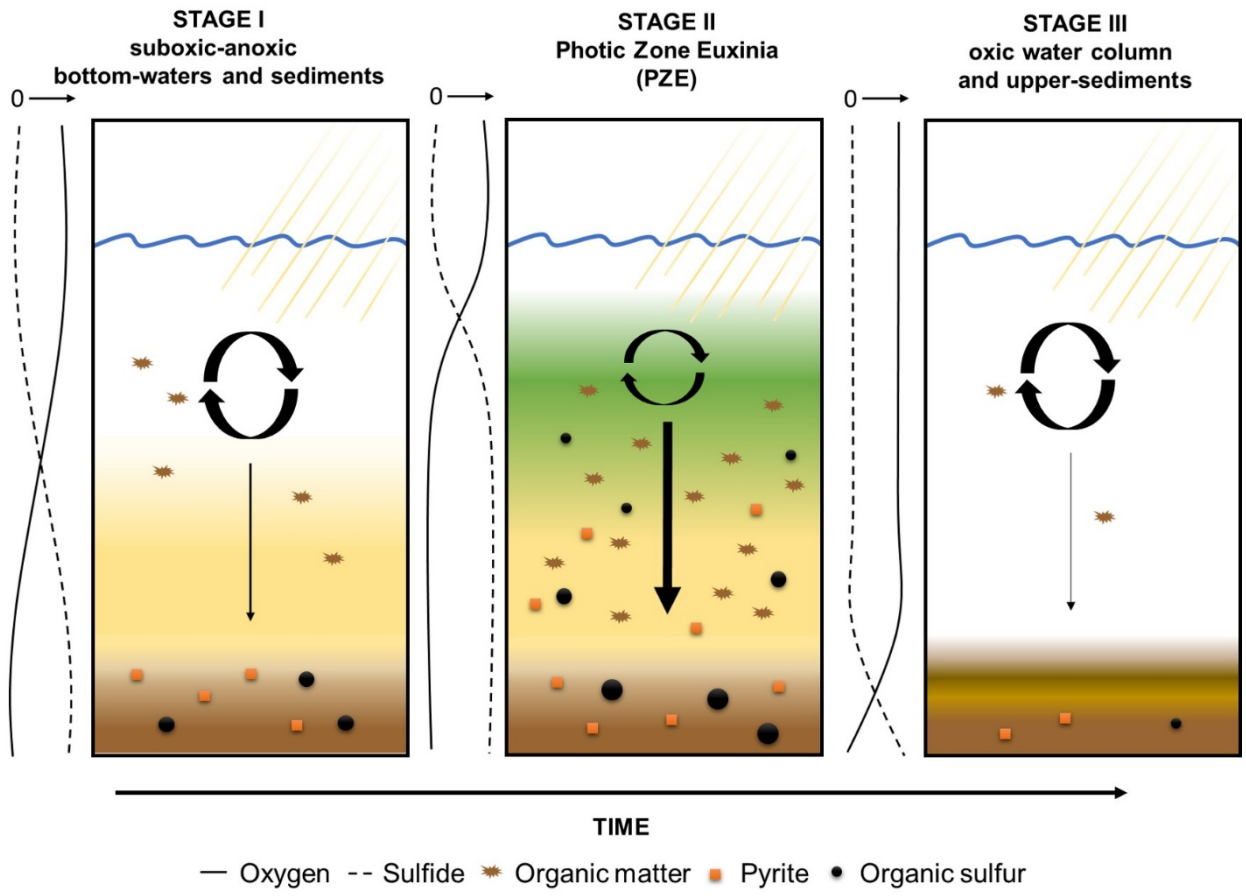

Figure 24. Schematic of paleoenvironmental conditions during deposition of the Blackstone Band. STAGE I: most organic matter is recycled within the water column, with slightly increased amounts of organic matter reaching the sediments with reduced oxygen exposure times. Pyrite formation and organic matter sulfurization are likely limited to the sediment-water interface and below. **STAGE II**: recycling of organic matter in the water column is relatively slow, allowing increased amounts of organic matter to reach the sediments. Pyrite formation may take place in the water column(?) and within the sediments. Organic matter sulfurization likely takes place in the water column and continues into the sediments. **STAGE III**: the majority of organic matter is recycled within the water column, with only small amounts of organic matter reaching the sediments due to lengthy oxygen exposure times. Pyrite formation and organic matter sulfurization are limited to the anoxic portions of the sediments.

Kerogen BTs and DBTs are highly correlated with each other (R^2 = 0.99; Figure 21) and with bulk TOS abundance and $\delta^{34}S$ values (R^2 = 0.84 and 0.88 for BTs and DBTs versus TOS, respectively; Figure 21), which likely indicates that they come from the same sulfur source, they were formed at the same time and by similar pathways (Figure 21). The overall ^{34}S-enrichment of kerogen compounds relative to bulk kerogen TOS indicates that they comprise the ^{34}S-enriched endmember of bulk TOS. Like TOS, the ^{34}S-enrichment of kerogen BTs and DBTs relative to pyrite reflects equilibrium exchange reactions with reduced sulfur species during diagenesis until kerogen BTs and DBTs form and lock-in their sulfur isotopic signature via ring formation (irreversible intramolecular sulfur addition). Outside of the period of PZE kerogen compounds are ^{34}S-depleted relative to compounds formed during the period of PZE (Figure 22). As with TOS, the further ^{34}S-enrichment of kerogen compounds during the period of PZE reflects the influence of ^{34}S-enriched biosulfur bound within the macromolecular matrix of kerogen during deposition and subsequent equilibrium sulfur isotope exchange reactions leading up to the formation of kerogen BTs and DBTs.

For kerogen compounds, we must also consider potential sulfur isotope exchange during pyrolysis as well as the possibility that BTs and DBTs were formed as reaction products during pyrolysis, instead of purely being released from kerogen. To our knowledge, there are no studies that show BTs and DBTs being formed during pyrolysis via secondary reaction with evolved H_2S and organic compounds in kerogen. In fact, BTs and DBTs have been identified in recent as well as ancient sedimentary environments (Sinninghe Damsté et al. 1989). Aizenshtat et al. (1995) discussed four possible pathways for BT and DBT formation and concluded that BTs and DBTs are formed in nature via cyclization and aromatization of alkyl sidechains of long chain alkylthiophenes. A recent study shows that there is no sulfur isotopic exchange with reduced sulfur species and BTs and DBTs during pyrolysis (Meshoulam and Amrani 2017). Thus, we are confident that the sulfur isotope values of kerogen BTs and DBTs reflect the $\delta^{34}S$ of the sulfur source at the time of formation.

Outside of the period of PZE, the trend of ^{34}S-depletion of kerogen compounds relative to bitumen compounds is consistent with previous studies. In Permian, Triassic, and Cretaceous shales, kerogen DBT $\delta^{34}S$ values were ^{34}S-depleted relative to bitumen DBT $\delta^{34}S$ values (Grotheer et al.

2017). Samples from the Miocene Monterey Formation also showed that bitumen released from kerogen during pyrolysis was ^{34}S-depleted relative to indigenous bitumen (Idiz et al. 1990). Despite the differences in age, depositional environments, and thermal maturity among the studies and samples presented here, it is apparent that native bitumen is likely not sourced from the same sulfur pool as kerogen, the timing and formation pathways differ between bitumen and kerogen organic sulfur pools, and that these differences persist on varying geologic timescales, where bitumen is more likely to be isotopically overprinted during later diagenesis when there is limited availability of sulfur, leading to ^{34}S-enriched values.

5.4.3 Implications for the geologic record

Results presented here show the utility of paired pyrite-organic sulfur records in interpreting past conditions and diagenetic processes. As discussed, the isotope records of pyrite and organic sulfur are primarily governed by the isotopic composition of sulfide produced from MSR. The isotopic composition of produced sulfide is, in turn, controlled by the rate of MSR where high rates produce relatively ^{34}S-enriched sulfide and low rates produce relatively ^{34}S-depleted sulfide. The rate of MSR and thus the isotopic composition of produced sulfide and by transferal the isotopic compositions of pyrite and organic sulfur is dependent on the availability of sulfate (as the electron acceptor) and organic carbon (the electron donor) during MSR. Therefore, factors affecting the availability of sulfate and organic carbon must be considered when reconstructing past MSR rates and hence the sulfur isotopic composition of reduced sulfur phases (i.e. pyrite). Because MSR fractionations are not significantly affected by the concentration of sulfate until micromolar concentrations are reached (Leavitt et al. 2013, Wing and Halevy 2014), the observed fractionation and rate of MSR is mostly dependent on the availability of metabolizable organic carbon. Results here show the importance of macromolecular organic sulfur in potentially limiting the availability of metabolizable carbon for MSR during times of increased organic carbon burial. The balance between reactive carbon uptake by microbes during MSR and reaction with sulfide in the formation of organic sulfur may have important implications for the interpretation of modern and ancient sedimentary sulfur isotopic records. Comparison of pyrite and organic sulfur isotopes can

provide a valuable insight into the processes that affect the sulfur isotopic records preserved in the geologic record and aide in the reconstruction of depositional conditions and sulfur cycling.

Kerogen pyrolysate sulfur isotope values mirror bulk $\delta^{34}S_{TOS}$ values, which may be useful for reconstructions of past sulfur cycling as $\delta^{34}S$ measurements of bulk TOS can be influenced by relict pyrite, whereas compound-specific isotopes are not. Additionally, CSSIA may be a useful tool for correlation between source rock and produced bitumen during petroleum genesis, as the pyrolysates (akin to produced bitumen) reflect the isotope composition of their parent material (source rock), at least in the current study. CSSIA of native bitumen compounds reveals that they are seemingly unrelated to bulk organic sulfur, as well as kerogen pyrolysates (produced bitumen), which leaves room for further investigation of their sulfur source, timing of formation, and relationship to petroleum genesis and (organic) sulfur cycling.

5.5 Conclusions

Sulfur isotopic records preserved in sedimentary rocks are critically dependent on sedimentological and geochemical conditions during deposition. In light of our current results, paired records of pyrite and organic sulfur isotopes will be useful in reconstructing past environmental conditions, including disentangling the potential causes of changes in MSR rates and consequent influence on the sulfur isotopic record of pyrite. Enhanced ^{34}S-enrichment of sedimentary organic sulfur, outside of what can be accounted for by known sulfur isotopic fractionation(s) associated with sulfur incorporation into organic matter and subsequent equilibrium isotope exchange, may best be explained by contributions from primary biosulfur. Increased amounts of biosulfur are more likely to be preserved by being bound into macromolecular organic sulfur matrices during times of water column anoxia/euxinia, thus allowing for correlation between ^{34}S-enrichment of the organic sulfur record and environmental conditions during deposition. Reconstructions will be especially robust when a multi-proxy approach is used, including both pyrite and organic sulfur, as well as biomarker proxies (e.g. derivatives of isorenieratene as an indicator of PZE) as shown in the current study.

References

Adam P., Schmid J.C., Mycke B., Strazielle C., Connan J., Huc A., Riva A., and Albrecht P. (1993) Structural investigation of nonpolar sulfur cross-linked macromolecules in petroleum. Geochimica et Cosmochimica Acta 57(14), 3395-3419.

Adam, P., E. Phillippe, and P. Albrecht (1998) Photochemical sulfurization of sedimentary organic matter: A widespread process occurring at early diagenesis in natural environments? Geochim. Cosmochim. Acta. 62:265-271.

Adam, P., Schneckenburger, P. Schaeffer, and P. Albrecht (2000) Clues to early diagenetic sulfurization processes from mild chemical cleavage of labile sulfur-rich geomacromolecules. Geochim. Cosmochim. Acta, 64:3485-3503.

Aizenshtat, Z., A. Stoler, Y. Cohen, and H. Nielsen (1983) The geochemical sulphur enrichment of recent organic matter by polysulfides in the Solar-Lake. in Bjorøy et al., eds., Advances in Organic Geochemistry 1981, John Wiley & Sons Limited, pp. 279-288.

Aizenshtat, Z., Krein, E., Vairavamurthy, M., and Goldstein, T. (1995) Role of sulfur in the transformations of sedimentary organic matter: A mechanistic overview, in Vairavamurthy, M.A., and Schoonen, M.A.A., eds., Geochemical transformations of sedimentary sulfur: Washington, D.C., American Chemical Society Symposium Series 612, p. 378–396.

Amrani A., Aizenshtat Z. (2004a) Mechanisms of sulfur introduction chemically controlled: □34S imprint. Org. Geochem. 35, 1319–1336.

Amrani A., Aizenshtat Z. (2004b) Reaction of polysulfide anions with α, β unsaturated isoprenoid aldehydes in aquatic media: simulation of oceanic conditions. Org. Geochem. 35, 909–921.

Amrani A., Lewan M. D., and Aizenshtat Z. (2005) Stable sulfur isotope partitioning during simulated petroleum formation as determined by hydrous pyrolysis of Ghareb Limestone, Israel. Geochimica et Cosmochimica Acta 69(22), 5317.

Amrani A., Said-Ahamed W., Lewan M. D., and Aizenshtat Z. (2006a) Experiments on delta S-34 mixing between organic and inorganic sulfur species during thermal maturation. Geochimica et Cosmochimica Acta 70(20), 5146-5161.

Amrani, A., Kamyshny, A., Lev, O., Aizenshtat, Z. (2006b) Sulfur stable isotope distribution of polysulfide anions in an (NH4)2Sn aqueous solution. Inorg. Chem. 45, 1427–1429.

Amrani A., Ma Q., Said-Ahmad W., Aizenshtat Z. and Tang Y. (2008) Sulfur isotope fractionation during incorporation of sulfur nucleophiles into organic compounds. Chem. Commun. 1356–1358.

Amrani A., Sessions A., Adkins J. (2009) Compound-specific δ34S analysis of volatile organics by coupled GC/multicollector-ICPMS. Anal. Chem. 81, 9027–9034.

Amrani, A., A. Deev, A. Sessions, Y. Tang, J. Adkins, R. Hill, J. Moldowan, Z. Wei (2012) The sulfur-isotopic compositions of benzothiophenes and dibenzothiophenes as a proxy for thermochemical sulfate reduction. Geochim. Cosmochim. Acta 84:152-164.

Anderson, T.F. and L.M. Pratt (1995) Isotope evidence for the origin of organic sulfur and elemental sulfur in marine sediments. in Vairavamurthy, M.A. and M.A.A. Schoonen, eds, Geochemical Transformations of Sedimentary Sulfur, ACS Symposium Series 612, Washington, D.C., pp. 378-396.

Arnosti, C. (1995) Measurement of depth- and site-related differences in polysaccharide hydrolysis rates in marine sediments. Geochim. Cosmochim. Acta 59, 4247–4257.

Arnosti, C., Repeta, D. (1994) Oligosaccharide degradation by anaerobic marine bacteria: characterization of an experimental system to study polymer degradation in sediments. Limnol. Oceanogr 39, 1865–1877.

Arnosti, C., Repeta, D.J., Blough, N.V. (1994) Rapid bacterial degradation of polysaccarides in anoxic marine systems. Geochim. Cosmochim. Acta 58, 2639–2652.

Aycard M., Derenne S., Largeau C., Mongenot T., Tribovillard N., Baudin F. (2003) Formation pathways of proto-kerogens in Holocene sediments of the upwelling influenced Cariaco Trench, Venezuela. Org. Geochem. 34, 701–718.

B. A. Wing, I. Halevy (2014) Intracellular metabolite levels shape sulfur isotope fractionation during microbial sulfate respiration. Proc. Natl. Acad. Sci. U.S.A. 111, 18116–18125.

Bates, A., E. Spiker, and C. Holmes (1998) Speciation and isotopic composition of sedimentary sulfur in the Everglades, Florida, USA. Chemical Geology. 146:155-170.

Beaudoin G, Taylor BE, Rumble D, Thiemens M (1994) Variations in the sulfur isotope composition of troilite from the Canyon Diablo iron meteorite. Geochim Cosmochim Acta 58:4253–4255

Berner, R.A. (1970) Sedimentary pyrite formation. American Journal of Science, 268: 1-23.

Bertrand, P. and Lallier-Verges, E. (1993) Past sedimentary organic matter accumulation and degradation controlled by productivity. Nature 364, 786-788.

Bigeleisen, J (1965) Chemistry of isotopes. Science 147:463–471

Bontognali, T., A. Sessions, A. Allwood, W. Fischer, J. Grotzinger, R. Summons, J. Eiler (2012) Sulfur isotopes of organic matter preserved in 3.45-billion-year-old stromatolites reveal microbial metabolism. Proceedings of the National Academy of Sciences 109:15146-15151.

Böttcher, M.E., B. Thamdrup, and T.W. Vennemann (2001) Oxygen and sulfur isotope fractionation during anaerobic bacterial disproportionation of elemental sulfur. Geochim. Cosmochim. Acta, v. 65, no. 10, pp. 1601-1609.

Brüchert, V. and L.M. Pratt (1996) Contemporaneous early diagenetic formation of organic and inorganic sulfur in estuarine sediments from St. Andrew Bay, Florida, USA. Geochim. Cosmochim. Acta, v. 60, no. 13, pp. 2325-2332.

Brüchert, V., C. Knoblauch, and B.B. Jørgensen (2001) Controls on stable sulfur isotope fractionation during bacterial sulfate reduction in Arctic sediments. Geochim. Cosmochim. Acta 65 763-776.

Bruno, T.J. and P.D.N. Svoronos (2005) CRC Handbook of Fundamental Spectroscopic Correlation Charts. Taylor and Francis CRC Press: Boca Raton, FL.

Burdige D. J. (2007) Preservation of organic matter in marine sediments: Controls, mechanisms, and an imbalance in sediment organic carbon budgets? Chemical Reviews 107(2), 467-485.

Cai, C., A. Amrani, R.H. Worden, Q. Xiao, T. Wang, Z. Gvirtzman, H. Li, W. Said-Ahmad, L. Jia (2016) Sulfur isotopic compositions of individual organosulfur compounds and their genetic links in the Lower Paleozoic petroleum pools of the Tarim Basin, NW China Geochimica et Cosmochimica Acta, 182, 88-108.

Canfield, D.E. and B. Thamdrup (1994) The production of 34S-depleted sulfide during bacterial disproportionation of elemental sulfur. Science, v. 266, pp. 1973-1975.

Canfield, D.E., B.P. Boudreau, A. Mucci, J.K. Gundersen (1998a) The early diagenetic formation of organic sulfur in the sediments of Mangrove Lake, Bermuda. Geochim. Cosmochim. Acta, v. 62, no, 5, pp. 767-781.

Canfield, D.E., B. Thamdrup, and S. Fleischer (1998b) Isotope fractionation and sulfur metabolism by pure and enrichment cultures of elemental sulfur-disproportionating bacteria. Limnol. Oceanogr., v. 43, pp. 253-264.

Canfield, D.E. (1998c) A new model for Proterozoic ocean chemistry. Nature, 396, 450-453.

Canfield, D.E. (2001a) Biogeochemistry of sulfur isotopes. Rev. Mineral. Geochem. 43, 607–636.

Canfield, D.E. (2001b) Isotope fractionation by natural populations of sulfate-reducing bacteria. Geochim. Cosmochim. Acta, v. 65, no. 7, pp. 1117-1124.

Canfield, D.E. (2004) The evolution of the Earth surface sulfur reservoir. Am. J. Sci. 304:839–61

Canfield, D.E., Teske, A. (1996) Late Proterozoic rise in atmospheric oxygen concentration inferred from phylogenetic and sulphur-isotope studies. Nature 382:127–32

Chadwell, S. J.; Rickard, D.; Luther, G. W., III. (1999) Electrochemical evidence for pentasulfide complexes with Mn2+, Fe2+,Co2+,Ni2+, Cu2+ and Zn2+. Aquat. Geochem. 5, 29-57.

Chambers LA, Trudinger PA, Smith JW, Burns MS (1975) Fractionation of sulfur isotopes by continuous cultures of Desulfovibrio desulfuricans. Can J Microbiol 21(10): 1602–1607.

Chambers, L.A. and P.A. Trudinger (1979) Microbiological fractionation of stable sulfur isotopes: a review and critique. Geomicrobiol. J., v. 1, pp. 249-293.

Clark, B.C. (1981) Sulfur: Fountainhead of Life in the Universe, in: Billingham, J. (Ed.), Life in the Universe. MIT Press, Cambridge, Massachussetts, NASA Ames Research Center, pp. 47-60.

Claypool, G.E., Holser, W.T., Kaplan, I.R., Sakai, H, Zak, I. (1980) The age curves of sulfur and oxygen isotopes in marine sulfate and their mutual interpretation. Chem. Geol. 28:199–260

Cline, J.D. (1969) Spectrophotometric Determination of Hydrogen Sulfide in Natural Waters. Limnology and Oceanography, 14, 454-458.

Cowie, G.L., Hedges, J.I., Prahl, F.G., and de Lange, G.J. (1995) Elemental and major biochemical changes across an oxidation front in a relict turbidite: an oxygen effect. Geochim. Cosmochim. Acta, 59:33−46.

Cox, B. M. and Gallois, R. W. (1981) The stratigraphy of the Kimmeridge Clay of the Dorset type area and its correlation with some other Kimmeridgian sequences. Reports of the Institute of Geological Science 80(4), 1-44.

Culver D. A. and Brunskill G. J. (1969) Fayetteville Green Lake, New York: V. Studies of primary production and zooplankton in a meromictic marl lake. Limnol. Oceanogr. 14, 862–873.

Cypionka, H., A. Smock, and M. Bøttcher (1998) A combined pathway of sulfur compound disproportionation in Desulfovivrio desulfuricans. FEMS Microbiol Lett. 166:181-186.

de Graaf, W., Sinninghe Damsté, J., and de Leeuw, J. (1992) Laboratory simulation of natural sulphurization: I. Formation of monomeric and oligomeric isoprenoid polysulphides by low-temperature reactions of inorganic polysulphides with phytol and phytadienes: Geochimica et Cosmochimica Acta, v. 56, p. 4321–4328

de Graaf, W., Sinninghe Damsté, J., and de Leeuw, J. (1995) Low-temperature addition of hydrogen polysulfides to olefins: Formation of 2.2′-dialkyl polysulfides from alk-1-enes and cyclic (poly)sulfides and polymeric organic sulfur compounds from α,ω-dienes: Journal of the Chemical Society, Perkin Transactions 1: Organic and Bio-Organic Chemistry, v. I, p. 634–640.

De Laeter JR, Böhlke JK, De Bièvre P, Hidaka H, Peiser HS, Rosman KJR, Taylor PD (2003) Atomic weights of the elements: review 2000 (IUPAC Technical Report). Pure Appl Chem 75:683–2000

Dean, W., M. Arthur (1998) Cretaceous Western Intior Seaway drilling project: An overview. In Stratigraphy and Paleoenvironments of the Cretaceous Western Interior Seaway, USA. SEPM concepts in sedimentology and paleontology No. 6, pp. 1-10.

Deevey, Jr., E. S., Nakai N. and Stuiver M. (1963) Fractionation of sulfur and carbon isotopes in a meromictic lake. Science 139, 407–408.

Demaison, G.J. and Moore, G.T. (1980) Anoxic Environments and Oil Source Rock Bed Genesis. American Association of Petroleum Geologists Bulletin, 64, 1179-1209.

Detmers, J., V. Brüchert, K.S. Habicht, and J. Kuever (2001) Diversity of sulfur isotope fractionations by sulfate-reducing prokaryotes. App. Env. Micro. v. 67, pp. 888-894.

Clarke ET, Solouki T, Russell DH, Martell A, McManus D. (1994) Transformation of polysulfidic sulfur to elemental sulfur in a chelatediron, hydrogen sulfide oxidation process. Anal Chim Acta 299:97–111

Farrimond, P., Comet, P., Eglinton, G., Evershed, R. P., Hall, M. A., Park, D. W. and Wardroper, A. M. K. (1984) Organic geochemical study of the Upper Kimmeridge Clay of the Dorset type area. Marine Petroleum Geology 1, 340-354.

Fike, D.A., Grotzinger, J.P., Pratt, L.M., Summons, R.E. (2006) Oxidation of the Ediacaran ocean. Nature 444:744–47

Fike, D.A., Grotzinger, J.P. (2008) A paired sulfate–pyrite δ34S approach to understanding the evolution of the Ediacaran–Cambrian sulfur cycle. Geochim. Cosmochim. Acta 72:2636–48

Fike DA, Bradley AS, Rose CV (2015) Rethinking the ancient sulfur cycle. Annu. Rev. Earth Planet. Sci. 43, 593–622.

Filley, T., K. Freeman, R. Wilkin, and P. Hatcher (2002) Biogeochemical controls on reaction of sedimentary organic matter and aqueous sulfides in Holocene sediments of Mud Lake, Florida. Geochim. Cosmochim. Acta. 66:937-954.

Fossing, H., Jørgensen, B.B. (1990) Isotope exchange reactions with radiolabeled sulfur compounds in anoxic seawater. Biogeochemistry 9, 223–245.

Francois, R. (1987) A study of sulphur enrichment in the humic fraction of marine sediments during early diagenesis: Geochimica et Cosmochimica Acta, v. 51, p. 17–27

Fry B. (1986) Sources of carbon and sulfur nutrition for consumers in three meromictic lakes of New York state. Limnol. Oceanogr. 31, 79–88.

Fry, B., J. Cox, H. Gest, and J. Hayes (1986) Discrimination between 34S and 32S during bacterial metabolism of inorganic sulfur compounds. J. Bact. 165:328-330.

Gelin, F., M. Kok, J. de Leeuw, and J. Sinninge Damsté (1998) Laboratory sulfurisation of the marine microalga Nannochloropsis salina. Org. Geochem. 29:1837-1848.

Giggenbach, W. (1996) Optical spectra and equlibrium distribution of polysulfide ions in aqueous solutions at 20 °C. Inorg. Chem. 1972, 11, 1201-1207.

Danielsson, L. G.; Chai, X. S.; Behm, M.; Renberg, L. (1996) UV characterization of sulphide-polysulphide solutions and its application for process monitoring in the electrochemical production of polysulphides. J. Pulp Pap. Sci. 22, J187-J191.

Gill, B.C., Lyons, T.W., Saltzman, M.R. (2007) Parallel, high-resolution carbon and sulfur isotope records of the evolving Paleozoic marine sulfur reservoir. Palaeogeogr. Palaeoclimatol. Palaeoecol. 256:156–73

Ginzburg, B.; Dor, I.; Chalifa, I.; Hadas, O.; Lev, O. (1999) Formation of dimethyloligosulfides in Lake Kinneret: biogenic formation of inorganic oligosulfide intermediates under oxic conditions. Environ. Sci. Technol. 33, 571-579.

Goldhaber MB, Kaplan IR (1975) Controls and consequences of sulfate reduction rates in recent marine sediments. Soil Sci 119(1):42–55.

Greenwood, P.F., Amrani, A., Sessions, A., Raven, M.R., Holman, A., Dror, G., Grice, K., McCulloch, M.T., Adkins, J.F. (2014) Development and initial biogeochemical applications of compound-specific sulfur isotope analysis. In: Grice, K. (Ed.), Principles and Practice of Analytical Techniques in Geosciences. Royal Society of Chemistry, UK, pp. 285–312.

Grotheer, H., Greenwood, P.F., McCulloch, M.T., Bottcher, M.E., Grice, K. (2017) d34S character of organosulfur compounds in kerogen and bitumen fractions of sedimentary rocks. Organic Geochemistry 110, 60-64.

Habicht KS, Canfield DE (1997) Sulfur isotope fractionation during bacterial sulfate reduction in organic-rich sediments. Geochim Cosmochim Acta 61(24):5351–5361.

Habicht, K.S., D.E. Canfield, and J. Rethmeier (1998) Sulfur isotope fractionation during bacterial reduction and disproportionation of thiosulfate and sulfite. Geochim. Cosmochim. Acta, v. 62, no. 15, pp. 2585-2595.

Habicht KS, Gade M, Thamdrup B, Berg P, Canfield DE (2002) Calibration of sulfate levels in the archean ocean. Science 298(5602):2372–2374.

Halevy, I., Peters, S.E., Fischer, W.W. (2012) Sulfate burial constraints on the Phanerozoic sulfur cycle. Science 337:331–34

Harrison AG, Thode HG (1958) Mechanism of the bacterial reduction of sulphate from isotope fractionation studies. Trans Faraday Soc 54:84–92.

Hartgers, W.A., J.F. Lopez, J.S. Sinninghe Damsté, C. Reiss, J.R. Maxwell, and J.O. Grimalt (1997) Sulfur-binding in recent environments: II. Speciation of sulfur andiron and implications for the occurrence of organo-sulfur compounds. Geochim. Cosmochim. Acta, v. 61, no. 22, pp. 4769-4788.

Hedges J. I. (1992) Global biogeochemical cycles – Progress and problems. Marine Chemistry 39(1-3), 67-93.

Hedges J. I. and Keil R. G. (1995) Sedimentary organic matter preservation – An assessment and speculative synthesis. Marine Chemistry 49(2-3), 81-115.

Heitmann, T., Blodau, C. (2006) Oxidation and incorporation of hydrogen sulfide by dissolved organic matter. Chem. Geol. 235, 12-20.

Heitz, A., Kagi, R.I., and Alexander, R. (2000) Polysulfide sulfur in pipewall biofilms: its role in the formation of swampy odour in distribution systems. Water Science and Technology, 41(4), 271 - 278

Henneke, E., G. Luther, G. de Lange, and J. Hoefs (1997) Sulphur speciation in anoxic hypersaline sediments from the eastern Mediterranean Sea. Geochim. Cosmochim. Acta. 61:307-321.

Hernes, P., Hedges, J.I., Peterson, M.L., Wakeham, S.G., Lee, C. (1996) Neutral carbohydrate geochemistry of particulate material in the central equatorial Pacific. Deep-Sea Res., Part 2, Top. Stud. Oceanogr. 43, 1181 – 1204.

Hodge, J.E. (1953) Dehydrated Foods, Chemistry of Browning Reactions in Model Systems. Journal of Agricultural and Food Chemistry 1(15): 928-943

Hurtgen, M.T., Pruss, SB.., Knoll, A.H. (2009) Evaluating the relationship between the carbon and sulfur cycles in the later Cambrian ocean: an example from the Port au Port Group, western Newfoundland, Canada. Earth Planet. Sci. Lett. 281:288–97

Idiz, E.F., Tannenbaum, E., Kaplan, I.R. (1990) Pyrolysis of high-sulfur Monterey kerogens. In: Orr, W.L., White, C.M. (Eds.), Geochemistry of Sulfur in Fossil Fuels. American Chemical Society, Washington D.C., pp. 575–591.

Irwin, H., Curtis, C. and Coleman, M. (1977) Isotopic evidence for source of diagenetic carbonates formed during burial of organic-rich sediments. Nature 269, 209-213.

Jensen, M.M., M. Holmer, B. Thamdrup (2005) Composition and diagenesis of neutral carbohydrates in sediments of the Baltic-North Sea transition Geochim. Cosmochim. Acta, 69, 4085-4099

Johnston, D.T., Farquhar, J., Wing, B.A., Kaufman, A.J., Canfield, D.E., Habicht, K.S. (2005) Multiple sulfur isotope fractionations in biological systems: a case study with sulfate reducers and sulfur disproportionators. Am. J. Sci. 305:645–60

Jones, D.S., Fike, D.A. (2013) Dynamic sulfur and carbon cycling through the end-Ordovician extinction revealed by paired sulfate–pyrite δ34S. Earth Planet. Sci. Lett. 363:144–55

Jørgensen, B.B. (1990) A thiosulfate shunt in the sulfur cycle of marine sediments. Science, 249: 152-154.

Jørgensen, B. B. and Nelson, D.C. (2004) Sulfide oxidation in marine sediments: Geochemistry meets microbiology. In Amend, J.P., Edwards, K.J. and Lyons, T.W. (eds), Sulfur Biogeochemistry – Past and Present. Geological Society of America, pp. 63-81.

Kampschulte, A., Strauss, H. (2004) The sulfur isotopic evolution of Phanerozoic seawater based on the analysis of structurally substituted sulfate in carbonates. Chem. Geol. 204, 255–286.

Kamyshny, A., Jr., Goifman, A., Gun, J., Rizkov, D., Lev, O. (2004) Equilibrium distribution of polysulfide ions in aqueous solutions at 25°C: a new approach for the study of polysulfides' equilibria. Environ. Sci. Technol. 38, 6633-6644.

Kamyshny, A., Jr., Ekeltchik, I., Gun, J., and Lev, O. (2006) Method for the determination of Inorganic Polysulfide Distribution in Aquatic Systems. Analytical Chemistry, 78(8), 2631 – 2639

Kamyshny, Jr., A., Borkenstein C. G. and Ferdelman T. G. (2009) Protocol for quantitative detection of elemental sulfur and polysulfide zero-valent sulfur distribution in natural aquatic samples. Geostand. Geoanal. Res. 33, 415–435.

Kaplan IR, Rittenberg SC (1964) Microbiological fractionation of sulphur isotopes. J Gen Microbiol 34(2):195–212.

Kiyosu Y. (1980) Chemical reduction and sulfur isotope effects of sulfate by organicmatter under hydrothermal conditions. Chem. Geol. 30:47–56

Kiyosu Y, Krouse HR. (1993) Thermochemical reduction and sulfur isotopic behavior of sulfate by acetic acid in the presence of native sulfur. Geochem. J. 27:49–57

Kohnen M.E.L., Sinninghe Damsté J.S., and de Leeuw J.W. (1991a) Biases from natural sulphurization in palaeoenvironmental reconstruction based on hydrocarbon biomarker distributions. Nature 349, 775-778.

Kohnen, M.E.L., J.S. Sinninghe Damsté, A.C. Kock-van Dalen, and J.W. de Leeuw (1991b) Di- or polysulphide-bound biomarkers in sulphur-rich geomacromolecules as revealed by selective chemolysis. Geochim. Cosmochim. Acta 55:1375-1394.

Kok, M.D., Schouten, S., Sinninghe Damste´, J.S. (2000) Formation of insoluble, nonhydrolyzable, sulfur-rich macromolecules via incorporation of inorganic sulfur species into algal carbohydrates. Geochim. Cosmochim. Acta 64, 2689– 2699.

Koopmans, M.P., J.W. de Leeuw, M.D. Lewan, and J.S. Sinninghe Damsté (1996) Impact of dia- and catagenesis on sulphur and oxygen sequestration of biomarkers as revealed by artificial maturation of an immature sedimentary rock. Org. Geochem. 25:391-426.

Krein, E.B., and Z. Aizenshtat (1995) Proposed thermal pathways for sulfur transformations in organic macromolecules: laboratory simulation experiments. in Vairavamurthy, M.A. and M.A.A. Schoonen, eds, Geochemical Transformations of Sedimentary Sulfur, ACS Symposium Series 612, Washington, D.C., pp. 110-137.

Kristiana I, Heitz A, Joll C, Sathasivan A (2010) Analysis of polysulfides in drinking water distribution systems using headspace solid-phase microextraction and gas chromatography-mass spectrometry. J Chromatogr A 1217(38):5995–6001

Krouse HR, Viau CA, Eliuk LS, Ueda A, Halas S (1988) Chemical and isotopic evidence of thermochemical sulfate reduction by light hydrocarbon gases in deep carbonate reservoirs. Nature 333:415–419

Lallier-Verges E., Bertrand P., Huc A. Y., Bückel D., and Tremblay P. (1993) Control of the preservation of organic matter by productivity and sulphate reduction in Kimmeridgian shales from Dorset (UK). Mar. Petr. Geol. 10, 600–605.

Lallier-Verges, E., Hayes, J.M., Boussafir, M., Zaback, D.A., Tribovillard, N.P., Connan, J., Bertrand, P., (1997) Productivity-induced sulphur enrichment of hydrocarbon-rich sediments from the Kimmeridge Clay Formation. Chemical Geology 134, 277–288.

LaLonde, R., L. Ferrara, and M. Hayes (1987) Low-temperature, polysulfide reactions of conjugated ene carbonyls: A reaction model for the geologic origin of S-heterocycles. Org. Geochem. 11:563-571.

Leavitt, W.D., Halevy, I., Bradley, A.S., Johnston, D.T. (2013) Influence of sulfate reduction rates on the Phanerozoic sulfur isotope record. PNAS 110:11244–49

Lewan, M.D. (1998) Sulphur-radical control on petroleum formation rates. Nature 391:164-166

Loch, A.R., Lippa, D.L., Carlson, D.L., Chin, Y.P., Trina, S.J., Roberts, A.L. (2002) Nucleophilic aliphtic sustitution reactions of propachlor, alachlor, and metolachlor with bisulfide (HS-) and polysulfides Sn2-. Environmental Science and Technology 36, 4065–4073.

Luther, G. W., III; Giblin, A. E.; Varsolona, R. (1985) Polarographic analysis of sulfur species in marine porewaters. Limnol. Oceanogr. 30, 727-736.

Luther, G. W., III. (1991) Pyrite synthesis via polysulfide compounds. Geochim. Cosmochim. Acta 55, 2839-2849.

Luther G W, Glazer B T, Hohmann L, Popp J I, Taillefert M, Rozan T F, Brendel P J, Theberge S M, Nuzzio D B (2001) Sulfur speciation monitored in situ with solid state gold amalgam voltammetric microelectrodes: polysulfides as a special case in sediments, microbial mats and hydrothermal vent waters. J Environ Manage. 20, 62:61–66.

Lyons TW, Severmann S. (2006) A critical look at iron paleoredox proxies based on new insights from modern euxinic marine basins. Geochim. Cosmochim. Acta 70:5698–722

Lyons TW. (2008) Ironing out ocean chemistry at the dawn of animal life. Science 321:923–24

Lyons TW, Anbar AD, Severmann S, Scott C, Gill BC (2009) Tracking euxinia in the ancient ocean: A multiproxy perspective and Proterozoic case study. Annu Rev Earth Planet Sci 37:507–534.

Mango, F. D. (1983) The diagenesis of carbohydrates by hydrogen sulfide. Geochimica et Cosmochimica Acta, 47, 1433-1442.

Menzel, D., E.C. Hopmans, P.F. van Bergen, J.W. de Leeuw, J.S. Sinninghe Damste (2002) Development of photic zone euxinia in the eastern Mediterranean Basin during deposition of Pliocene sapropels. Marine Geology 189: pp 215-226

Meshoulam, A., G.S. Ellis, W. Said Ahmad, A. Deev, A.L. Sessions, Y. Tang, J.F. Adkins, J. Liu, W.P. Gilhooly III, Z. Aizenshtat, A. Amrani (2016) Study of thermochemical sulfate reduction mechanism using compound specific sulfur isotope analysis. Geochimica et Cosmochimica Acta, 188, 73-92

Meshoulam, A., Amrani, A. (2017) Sulfur isotope exchange between thiophenes and inorganic sulfur compounds under hydrous pyrolysis conditions Organic Geochemistry, 103, 79-87.

Miller, R. G. (1990) A paleo-oceanographic approach to the Kimmeridge Clay Formation. In Deposition of Organic Facies, ed. A. Y. Huc, pp. 13-26. AAPG Studies in Geology 30, Amer. Assoc. of Petrol. Geol. Geological Society, London.

Moers, M.E.C., Boon, J.J., de Leeuw, J.W., Baas, M., Schenck, P.A. (1989) Carbohydrate speciation and Py-MS mapping of peat samples from a subtropical open marsh environment. Geochim. Cosmochim. Acta 53, 2011–2021.

Morgans-Bell, H.S., Coe, A.L., Hesselbo, S.P., Jenkyns, H.C., Weedon, G.P., Marshall, J.E.A., Tyson, R.V., Williams, C.J. (2001) Integrated stratigraphy of the Kimmeridge Clay Formation (Upper Jurassic) based on exposures and boreholes in south Dorset, UK. Geological Magazine 138, 511–539.

Mossman, J.R., A.C. Aplin, C.D. Curtis, and M.L. Coleman (1991) Geochemistry of inorganic and organic sulphur in organic-rich sediments from the Peru Margin. Geochim. Cosmochim. Acta, v. 55, pp. 3581-35-95.

Nelson B. C., Eglinton T. I., Seewald J. S., Vairavamurthy M. A., and Miknis F. P. (1995) Transformations in organic sulfur speciation during maturation of monetary shale: Constraints from laboratory experiments. In Geochemical Transformations of Sedimentary Sulfur, Vol. 612, pp. 138-166.

Neretin, L.N., Bottcher, M.E., Grinenko, V.A. (2003) Sulfur isotopes geochemistry of the Black Sea water column. Chemical Geology 200, 59–69.

Nursten, H. (2005). The Maillard Reaction: Chemistry, Biochemistry and Implications. The Royal Society ofChemistry.

O'Neil, J.R. (1986) Theoretical and experimental aspects of isotopic fractionation. In: Stable isotopes in high temperature geological processes. Rev Mineral 16:1–40

Oduro, Harry, Alexey Kamyshny Jr., Aubrey L. Zerkle, Yue Li, James Farquhar (2013) Quadruple sulfur isotope constraints on the origin and cycling of volatile organic sulfur compounds in a stratified sulfidic lake. Geochimica et Cosmochimica Acta 120, 251–262

Ohmoto H, Rye RO (1979) Isotopes of sulfur and carbon. In: Geochemistry of hydrothermal ore deposits, 2nd edn. Holt Rinehart and Winston, New York

Orr, W. (1978) Sulphur in heavy oils, oils sands and oil shales. in Strausz and Lown, eds., Oil sand and oil shale chemistry, p. 223-243. Verlag Chemie Int.

Orr, W.L., and Sinninghe Damsté, J.S. (1990) Geochemistry of sulfur in petroleum systems, in Orr, W.L., and C.M. White, eds., Geochemistry of sulfur in fossil fuels: Washington, D.C., American Chemical Society Symposium Series 429, p. 2–29.

Oschmann, W. (1988) Kimmeridge Clay sedimentation - new cyclic model. Palaeogeography, Palaeoclimatology, Palaeoecology 65, 217-251.

Oschmann, W. (1991) Distribution, dynamics and palaeoecology of Kimmeridgian (Upper Jurassic) shelf anoxia in western Europe. In Modern and Ancient Continental Shelf Anoxia, ed. R. V. Tyson and T. H. Pearson, pp. 381-395. Geological Society Special Publication 58. Geological Society, London.

Passier, H., M. Bottcher, G. de Lange (1999) Sulphur Enrichment in Organic Matter of Eastern Mediterranean Sapropels: A Study of Sulphur Isotope Partitioning. Aquatic Geochemistry 5(1):99-118.

Pearce C. R., Coe A. L. and Cohen A. S. (2010) Seawater redox variations during the deposition of the Kimmeridge Clay Formation, United Kingdom (Upper Jurassic): Evidence from molybdenum isotopes and trace metal ratios. Paleoceanography 25, PA4213.

Poulton S.W. and Canfield D.E. (2005) Development of a sequential extraction procedure for iron: implications for iron partitioning in continentally derived particulates. Chem. Geol. 214:209-221.

Putschew, A., C. Schaeffer-Reiss, P. Schaeffer, M.P. Koopmans, J.W. de Leeuw, M.D. Lewan, J.S. Sinninghe Damsté, and J.R. Maxwell (1998) Release of sulfur- and oxygen-bound components from a sulfur-rich kerogen during simulated maturation by hydrous pyrolysis. Org. Geochem., 29:1875-1998.

Steudel, R., G. Holdt, and T. Göbel. 1989. Ion-pair chromatographic separation of inorganic sulphur anions including polysulphide. J. Chromatogr. 475:442–446.

Raiswell, R., Buckley, F., Berner, R.A. and Anderson, T.F. (1988) Degree of pyritisation as a paleoenvironmental indicator of bottom water oxygenation. Journal of Sedimentary Petrology, 58: 812- 819.

Ramanampisoa, L. and Disnar, J. R. (1994) Primary control of paleoproduction on organic matter preservation and accumulation in the Kimmeridge rocks of Yorkshire (UK). Organic Geochemistry 21, 1153-1167.

Raven, M.R., A.L. Sessions, J.F. Adkins, J.P. Werne, T.W. Lyons. (2015) Sulfur-isotopic compositions of individual organic compounds from Cariaco Basin sediments Org. Geochem. 80:53–59.

Raven M. R., Sessions A. L., Adkins J. F. and Thunell R. C. (2016a) Rapid organic matter sulfurization in sinking particles from the Cariaco Basin water column. Geochimica et Cosmochimica Acta 190, 175–190.

Raven M. R., Sessions A. L., Fischer W. W. and Adkins J. F. (2016b) Sedimentary pyrite d34S differs from porewater sulfide in Santa Barbara Basin: proposed role of organic sulfur. Geochimica et Cosmochimica Acta 186, 120–134.

Raven, M.R., Fike, D.A., Gomes, M.L., Webb, S.M., Bradley, A.S., McClelland, H.-L.O. (2018) Organic carbon burial during OAE2 driven by changes in the locus of organic matter sulfurization. Nature Communications 9, 3409

Rees, C.E., Jenkins, W.J., Monster, J. (1978) The sulphur isotopic composition of ocean water sulphate. Geochimica et Cosmochimica Acta 42, 377-381.

Reinhard, C. (2008) Controls on authigenic sequestration of molybdenum in the sediments of meromictic Mahoney Lake, British Columbia. Unpublished M.S. Thesis, University of California, Riverside, 101 pp.

Riccardi, A. L., Arthur, M. A. & Kump, L. R. (2006) Sulfur isotopic evidence for chemocline upward excursions during the end-Permian mass extinction. Geochim. Cosmochim. Acta 70, 5740–5752.

Rowland, S., Rockey, C., al-Lihaibi, S.S., and Wolff, G.A. (1993) Incorporation of sulphur into phytol derivatives during simulated early diagenesis: Organic Geochemistry, v. 20, p. 1–5

Rozan T.F., Theberge S.M. and Luther III G.W. (2000) Quantifying elemental sulphur (S0), bisulfide (HS-) and polysulfides (Sx 2-) using a voltametric method. Analytica Chimica Acta, 415, 175-184.

Schneckenburger, P., Adam, P., and Albrecht, P. (1998) Thioketones as key intermediates in the reduction of ketones to thiols by HS– in natural environments: Tetrahedron Letters, v. 39, p. 447–450

Schouten, S., de Graaf, W., Sinninghe Damsté, J.S., van Driel, B.G., de Leeuw, J.W. (1993) Natural sulphurization of ketones and aldehydes: a key reaction in the formation of organic sulfur compounds. Geochimica et Cosmochimica Acta 57, 5111–5116.

Schouten S., de Graaf W., Sinninghe Damsté, J., van Driel G., De Leeuw J. (1994) Laboratory simulation of natural sulphurization: II. Reaction of multi-functionalized lipids with inorganic polysulphides at low temperatures. Org. Geochem. 22, 825–834.

Schouten, S., Sinninghe Damsté, J.S., Baas, M., Kock-van Dalen, A.C., Kohnen, M.E.L., de Leeuw, J.W., (1995) Quantitative assessment of mono and polysulphide-linked carbon skeletons in sulphur-rich macromolecular aggregates present in bitumens and oils. Organic Geochemistry 23, 765–775.

Schouten, S., de Loureiro, M.R.B., Sinninghe Damsté, J.S., and de Leeuw, J.W. (2001) Molecular biogeochemistry of Monterey sediments (Naples Beach, USA). I. distributions of hydrocarbons and organic sulphur compounds, in Isaacs, C.M., and Rullkötter, J., eds., The Monterey Formation: From rocks to molecule: Columbia University Press, p. 150–174.

Shawar, Lubna, Itay Halevy, Ward Said-Ahmad, Shimon Feinstein, Valeria Boyko, Alexey Kamyshny, and Alon Amrani. (2018). Dynamics of Pyrite Formation and Organic Matter Sulfurization in Organic-Rich Carbonate Sediments. Geochimica et Cosmochimica Acta 241, 219–39.

Sim, M., Bosak, T., Ono, S. (2011) Large Sulfur Isotope Fractionation Does Not Require Disproportionation. Science, 333, 74-77.

Sim, M., S. Ono, K. Donovan, S. P. Templer, T. Bosak (2011) Effect of electron donors on the fractionation of sulfur isotopes by a marine Desulfovibrio sp. Geochimica et Cosmochimica Acta 75, 4244-4259.

Sinninghe Damsté J.S., and de Leeuw J.W. (1990) Analysis, structure and geochemical significance of organically-bound sulphur in the geosphere: State of the art and future research. In Advances in Organic Geochemistry 1989 (ed. B. Durand and F. Behar); Org. Geochem. 16, 1077-1101.

Sinninghe Damsté, J. S.; Eglinton, T. I.; Rijpstra, W. I. C.; de Leeuw, J. (1989) In Geochemistry of sulfur in fossil fuels; W. L. Orr and C. M. White, Eds.; Am. Chem. Soc.: Washington, D.C. Vol. 429; pp 486

Sinninghe Damsté, J.S., M.E.L. Kohnen, and B. Horsfield (1998a) Origin of low-molecular-weight alkylthiophenes in pyrolysates of sulphur-rich kerogens as revealed by micro-scale sealed vessel pyrolysis. Org. Geochem. 29:1891-1903.

Sinninghe Damsté, J.S., Kok, M.D., Koster, J., Schouten, S. (1998b) Sulfurized carbohydrates and important sedimentary sink for organic carbon? Earth and Planetary Science Letters 164, 7–13.

Sinninghe Damste´, J.S., Schouten, S., van Duin, A.C.T. (2001) Isorenieratene derivatives in sediments: possible controls on their distribution. Geochimica et Cosmochimica Acta 65, 1557–1571.

Steudel, R. (1996) Mechanism for the formation of elemental sulfur from aqueous sulfide in chemical and microbiological desulfurization processes. Ind. Eng. Chem. Res. 35, 1417- 1423.

Suits N. S. and Wilkin R. T. (1998) Pyrite formation in the water column and sediments of a meromictic lake. Geology 26, 1099–1102.

Suits, N., and M. Arthur (2000) Sulfur diagenesis and partitioning in Holocene Peru shelf and upper slope sediments. Chemical Geology 163:219-234.

Swain F.M. (1969) Fossil Carbohydrates. In: Eglinton G., Murphy M.T.J. (eds) Organic Geochemistry. Springer, Berlin, Heidelberg

Thamdrup, B., Fossing, H. and Jørgensen, B.B. (1994) Manganese, iron, and sulfur cycling in a coastal marine sediment, Aarhus Bay, Denmark. Geochimica et Cosmochimica Acta, 58: 5115-5129.

Tissot, B., and D. Welte (1984) Petroleum Formation and Occurrence, 2nd ed, Springer, Heidelberg.

Tomic, J., F. Behar, M. Vandenbrouke, and Y. Tang (1995) Artificial maturation of Monterey kerogen (Type II-S) in a closed system and comparison with Type II kerogen: implications on the fate of sulfur. Org. Geochem. 23:647-660.

Tonolla, M., Demarta, A., Peduzzi, R., and Hahn, D. (1999) In Situ Analysis of Phototrophic Sulfur Bacteria in the Chemocline of Meromictic Lake Cadagno (Switzerland): Applied and Environmental Microbiology, v. 65, no. 3, p. 1325-1330.

Tonolla, M., Demarta, A., Peduzzi, R., Hahn, D., and Peduzzi, R. (2000) In Situ Analysis of Sulfate Reducing Bacteria Related to Desulfocapsa thiozymogenes in the Chemocline of Meromictic

Lake Cadagno (Switzerland): Applied and Environmental Microbiology, v. 66, no.2, p. 820-824.

Tribovillard, N., Desprairies, A., Lallier-Verges, E., Bertrand, P., Moureau, N., Ramdani, A. and Ramanampisoa, L. (1994) Geochemical study of organic-matter rich cycles from the Kimmeridge Clay Formation of Yorkshire (UK): productivity versus anoxia. Palaeogeography, Palaeoclimatology, Palaeoecology 108, 165-181.

Trudinger PA, Chambers LA, Smith JW (1985) Low temperature sulphate reduction: biological versus abiological. Can J Earth Sci 22:1910–1918

Tyson, R. V., Wilson, R. C. L. and Downie, C. (1979) A stratified water column environmental model for the type Kimmeridge Clay. Nature 277, 377-380.

Tyson, R. V. (1989) Late Jurassic palynofacies trends, Piper and Kimmeridge Clay Formations, UK onshore and northern North Sea. In Northwestern European Micropalaeontology and Palynology, ed. D. J. Batten and M. C. Keen, pp. 135-172. British Micropalaeontological Society Series. Ellis Horwood, Chichester.

Tyson, R. V. (1996) Sequence stratigraphical interpretation of organic facies variations in marine siliciclastic systems: general principles and application to the onshore Kimmeridge Clay Formation, UK. In Sequence Stratigraphy in British Geology, ed. S. Hesselbo and N. Parkinson, pp. 75-96. Geol. Soc. Lond. Spec. Publ. 103.

Tyson, R.V. (2004) Variation in marine total organic carbon through the type Kimmeridge Clay Formation (Late Jurassic), Dorset, UK. Journal of the Geological Society 161, 667–673.

Vairavamurthy, A., and K. Mopper (1987) Geochemical formation of organic sulphur compounds (thiols) by addition of H2S to sedimentary organic matter. Nature. 329:623-625.

Vairavamurthy, M.A., Mopper, K. (1989) Mechanistic studies of organo-sulphur (thiol) formation in coastal marine sediments. In: Saltzman, E.S., Cooper, W.J. (Eds.), Biogenic Sulfur in the Environment. American Chemical Society, Washington, DC, pp. 231–242.

Vairavamurthy, M., W. Orr, and B. Manowitz (1995) Geochemical transformations of sedimentary sulfur: An introduction. in Vairavamurthy and Schoonen, eds. Geochemical transformations of sedimentary sulfur. ACS Symposium Series 612:1-15. American Chemical Society, Washingon D.C.

van Dongen, B., S. Schouten, J.S. Sinninghe Damsté (2006) Preservation of carbohydrates through sulfurization in a Jurassic euxinic shelf sea: Examination of the Blackstone Band TOC cycle in the Kimmeridge Clay Formation, UK. Org. Geochem. 37:1052-1073.

van Dongen, B.E., S. Schouten, and J.S. Sinninghe Damsté (2003b) Sulfurization of carbohydrates results in S-rich, unresolved complex mixture in kerogen pyrolysates. Energy & Fuels. 17:1109-1118.

van Dongen, B.E., S. Schouten, M. Baas, J.A.J. Geenevasen, and J.S. Sinninghe Damsté (2003a) An experimental study of the low-temperature sulfurization of carbohydrates. Org. Geochem. 34, 1129-1144.

van Kaam-Peters, H. M. E., and Sinninghe Damsté, J. S. (1997) Characterisation of an extremely organic sulfur-rich, 150 Ma old carbonaceous rock: palaeoenvironmental implications. Organic Geochemistry 27, 371-397.

van Kaam-Peters, S. Schouten, J. Köster, and J. Sinninghe Damsté (1998) Controls on the molecular and carbon isotopic composition of organic matter deposited in a Kimmeridgian euxinic shelf sea: Evidence for preservation of carbohydrates through sulfurisation. Geochim. Cosochim. Acta. 62:3259-3283.

Vandenbroucke, M. and Largeau, C. (2007) Kerogen origin, evolution and structure. Organic Geochemistry 38, 719–833.

Wakeham, S.G., and Pease, T.K. (1992) Lipid Analysis in Marine Particle and Sediment Samples, A Laboratory Handbook: Unpublished manuscript, Skidaway Institute of Oceanography, Savannah Georgia, pp. 8-10.

Wakeham, S.G., J.S. Sinninghe Damsté, M.E.L. Kohnen, and J.W. de Leeuw (1995) Organic sulfur compounds formed during early diagenesis in Black Sea sediments. Geochim. Cosmochim. Acta, v. 59, no. 3, pp. 521-533.

Weedon, G.P., Coe, A.L., Gallois, R.W. (2004) Cyclostratigraphy, orbital tuning and inferred productivity for the type Kimmeridge Clay (Late Jurassic), Southern England. Journal of the Geological Society 161, 655–666.

Werne, J.P., D.J. Hollander, A. Behrens, P. Schaeffer, p. Albrecht, and J.S.S. Sinninghe Damsté (2000) Timing of early diagenetic sulfurization of organic matter: A precursor-product

relationship in Holocene sediments of the anoxic Cariaco Basin, Venezuela. Geochim. Cosmochim. Acta, v. 64(10):1741-1751

Werne, J.P., Lyons, T.W., Hollander, D.J., Formolo, M., and Sinninghe Damsté, J.S. (2003) Reduced sulfur in euxinic sediments of the Cariaco Basin: Sulfur isotope constraints on organic sulfur formation. Chemical Geology, v. 195, p. 159-179

Werne, J.P., T.W. Lyons, D.J. Hollander, S. Schouten, E.C. Hopmans, and J.S. Sinninghe Damsté (2008) Investigating pathways of diagenetic organic matter sulfurization using compound-specific sulfur isotope analysis. Geochimica et Cosmochimica Acta, v. 72, pp. 3489-3502.

Zaback, D.A. and L.M. Pratt (1992) Isotope composition and speciation of sulfur in the Miocene Monterey Formation: Reevaluation of sulfur reactions during early diagenesis in marine environments. Geochim. Cosmochim. Acta, v. 56, pp. 763-774.

Zerkle, A.L., Farquhar, J., Johnston, D.T., Cox, R.P., Canfield, D.E. (2009) Fractionation of multiple sulfur isotopes during phototrophic oxidation of sulfide and elemental sulfur by a green sulfur bacterium. Geochim. Cosmochim. Acta 73, 291–306.

Zerkle. A.L., A. Kamyshyny Jr., L.R. Kump, J. Farquhar, H. Oduro, and M.A. Arthur (2010) Sulfur cycling in a stratified euxinic lake with moderately high sulfate: Constraints from quadruple S isotopes Geochim. Cosmochim. Acta. 74:4953-4970.